

1 **Anthropogenic CO<sub>2</sub>, air-sea CO<sub>2</sub> fluxes and acidification in the Southern**  
2 **Ocean: results from a time-series analysis at station OISO-KERFIX (51°S-**  
3 **68°E).**

4  
5 Nicolas Metzl<sup>1</sup>, Claire Lo Monaco<sup>1</sup>, Coraline Leseurre<sup>1,2</sup>, Céline Ridame<sup>1</sup>, Gilles Reverdin<sup>1</sup>,  
6 Thi Tuyet Trang Chau<sup>3</sup>, Frédéric Chevallier<sup>3</sup>, Marion Gehlen<sup>3</sup>

7  
8 <sup>1</sup> Laboratoire LOCEAN/IPSL, Sorbonne Université-CNRS-IRD-MNHN, Paris, 75005, France

9 <sup>2</sup> Flanders Marine Institute (VLIZ), 8400 Ostend, Belgium

10 <sup>3</sup> Laboratoire LSCE/IPSL, CEA-CNRS-UVSQ, Université Paris-Saclay Gif-sur-Yvette, 91191, France

11  
12 *Correspondence to:* Nicolas Metzl (nicolas.metzl@locean.ipsl.fr)

13  
14  
15 **Abstract:** The temporal variation of the carbonate system, air-sea CO<sub>2</sub> fluxes and pH is analyzed in the Southern  
16 Indian Ocean, south of the Polar Front, based on in-situ data obtained from 1985 to 2021 at a fixed station  
17 (50°40'S-68°25'E) and results from a neural network model that reconstructs the fugacity of CO<sub>2</sub> (fCO<sub>2</sub>) and  
18 fluxes at monthly scale. Anthropogenic CO<sub>2</sub> (C<sub>ant</sub>) ~~was~~is estimated in the water column and is detected down to  
19 the bottom (1600m) in 1985 resulting in an aragonite saturation horizon at 600m that migrated up to 400m in  
20 2021 due to the accumulation of C<sub>ant</sub>. ~~In~~At subsurface, the trend of C<sub>ant</sub> is estimated at +0.53 (~~±±~~±±0.01) μmol.kg<sup>-1</sup>.  
21 yr<sup>-1</sup> with a detectable increase in the trend in recent years. At the surface during austral winter the oceanic fCO<sub>2</sub>  
22 increased at a rate close or slightly lower than in the atmosphere. To the contrary, in summer, we observed  
23 contrasting fCO<sub>2</sub> and dissolved inorganic carbon (C<sub>T</sub>) trends depending on the decade and emphasizing the role  
24 of biological drivers on air-sea CO<sub>2</sub> fluxes and pH inter-annual variability. The ~~region-moved~~regional air-sea  
25 CO<sub>2</sub> fluxes evolved from an annual source to the atmosphere of 0.8 molC.m<sup>-2</sup>.yr<sup>-1</sup> in 1985 to a sink of -0.5  
26 molC.m<sup>-2</sup>.yr<sup>-1</sup> in 2020. ~~In~~Over 1985-2020, the annual pH trend in surface waters of -0.0165 (~~±±~~±±0.0040).decade<sup>-1</sup>  
27 was mainly controlled by the accumulation of anthropogenic CO<sub>2</sub>, but the ~~trend-was~~summer pH trends were  
28 modulated by natural processes that reduced the acidification rate in the last decade. Using historical data from  
29 November 1962 we estimated the long-term trend for fCO<sub>2</sub>, C<sub>T</sub> and pH confirming that the progressive  
30 acidification was driven by the atmospheric CO<sub>2</sub> increase. In 59 years this ~~leads~~led to a diminution of 11% for  
31 both aragonite and calcite saturation state. As atmospheric CO<sub>2</sub> ~~will desperately continue rising~~is expected to  
32 increase in the future, the pH and carbonate saturation state will decrease at a faster rate than observed in recent  
33 years. A projection of future C<sub>T</sub> concentrations for a high emission scenario (SSP5-8.5) indicates that the surface  
34 pH in 2100 would decrease to 7.32 in winter. This is up to -0.86 lower than pre-industrial pH and -0.71 lower  
35 than pH observed in 2020. The aragonite under-saturation in surface waters would be reached as soon as 2050  
36 (scenario SSP5-8.5) and 20 years later for a stabilization scenario (SSP2-4.5) with potential impacts on  
37 phytoplankton species and higher trophic levels in the rich ecosystems of the Kerguelen Island area.

38  
39 **Keywords:** Ocean Carbonate System, Ocean acidification, anthropogenic CO<sub>2</sub>, air-sea CO<sub>2</sub> fluxes, Southern  
40 Ocean, Time-series station

42

## 43 1 Introduction

44 The ocean plays an important role in mitigating climate change by taking up ~~since decades~~ a large part  
45 of the excess of heat (Cheng et al., 2020; Fox-Kemper et al., 2021) and of CO<sub>2</sub> released by human activities  
46 (Sabine et al., 2004; Gruber et al., 2019a; Canadell et al., 2021). Since 1750, the global ocean ~~has~~ captured 185  
47 (~~±35~~) PgC (Petagram of Carbon) from a total of 700 (~~±75~~) PgC of anthropogenic carbon emissions from  
48 fossils fuels and land ~~used use~~ changes (Friedlingstein et al., 2022). ~~From year to year, the ocean~~ The oceanic sink  
49 for anthropogenic CO<sub>2</sub> ~~sink~~ increased progressively from 1.1 (~~±0.4~~) PgC.yr<sup>-1</sup> in the 1960s to 2.3 (~~±0.4~~)  
50 PgC.yr<sup>-1</sup> in the 2000s. Over the decade 2012-2021, the partitioning of the anthropogenic CO<sub>2</sub> ~~sinks~~ suptake was  
51 roughly equal between the ocean (2.9 ± 0.4 PgC.yr<sup>-1</sup>) and the land (3.1 ± 0.6 PgC.yr<sup>-1</sup>) (Friedlingstein et al.,  
52 2022). This partitioning has been confirmed for the decade 2013-2022 (Friedlingstein et al., 2023).

53 Ocean observations indicate that ~~since the 1990s~~ the Southern Ocean (SO) south of 45°S has been  
54 accumulating each year about 0.5 PgC.yr<sup>-1</sup> since the 1990s (e.g. Takahashi et al., 2009; Lenton et al., 2013;  
55 Rödenbeck et al., 2013; Long et al., 2021; Fay et al, 2023; Gray, 2024). Results based on BGC-Argo floats  
56 (Southern Ocean Carbon and Climate Observations and Modeling project, SOCCOM) suggest that the CO<sub>2</sub> sink  
57 in the SO might be much lower (0.16 PgC.yr<sup>-1</sup> south of 44°S for the period 2015-2017, Gray et al. 2018;  
58 Bushinsky et al., 2019) but there is an ongoing debate on the size of the carbon sink in this region depending the  
59 periods and methods (Long et al., 2021; Sutton et al., 2021; Hauck et al. 2023b; Gray, 2024). It is also well  
60 established that the CO<sub>2</sub> sink in the SO undergoes substantial decadal variability first documented for the 1990s  
61 (Le Quéré et al., 2007; Metzl, 2009; Lenton et al., 2013) and subsequently identified for the period 1982-2018  
62 (Landschützer et al., 2015; Keppler and Landschützer, 2019; Mackay et al., 2022; Hauck et al., 2023;2023a, b),  
63 However as for the mean state, there are also uncertainties on both the magnitude and phasing of decadal  
64 variability in the SO carbon sink mainly due to insufficient sampling (Gloege et al. 2021; Hauck et al. 2023a, b).  
65 A recent extension of the period to 1957-2020 suggests that the inter-annual to decadal variability of the SO CO<sub>2</sub>  
66 sink was most pronounced after the 1980s (Rödenbeck et al., 2022; Bennington et al., 2022). Whatever the  
67 variability of the SO CO<sub>2</sub> sink since the 1960s, the ocean continuously absorbs atmospheric CO<sub>2</sub> and the  
68 distribution of anthropogenic CO<sub>2</sub> (C<sub>ant</sub>) in the SO is now relatively well documented (e.g. Pardo et al., 2014;  
69 Gruber et al., 2019a) thanks to the GLODAP data synthesis effort for the global ocean (Global Ocean Data  
70 Analysis Project, Olsen et al., 2016, 2019, 2020). The SO takes up about 40% of the total anthropogenic carbon  
71 that enters the ocean (Khatiwala et al., 2013; Gruber et al., 2019a).

Mis en forme : Police : +Corps  
(Calibri), 11 pt, Français (France)

72 The anthropogenic CO<sub>2</sub> uptake in the ocean results ~~is in~~ lowering carbonate ion concentrations and pH, a  
73 chemical process termed “ocean acidification” (OA) (Caldeira and Wickett 2003; Doney et al., 2009). This  
74 decreases the saturation state with respect to carbonate minerals (aragonite, Ω<sub>ar</sub> and calcite, Ω<sub>ca</sub>), a process most  
75 pronounced in the cold ~~and naturally at a low saturation state~~ waters ~~in at~~ high latitudes where the saturation state  
76 is naturally low (Orr et al., 2005; Takahashi et al., 2014; Jiang et al., 2015). The first estimate of C<sub>ant</sub> distribution  
77 in the global ocean (for a nominal year 1994, Sabine et al., 2004) shows that the accumulation of C<sub>ant</sub> uptake led  
78 to an upward migration of the Ω<sub>ar</sub> and Ω<sub>ca</sub> saturation horizon in all ocean basins (Feely et al., 2004). This  
79 change is particularly pronounced south of the Polar Front (PF) in the SO ~~linked due~~ to both C<sub>ant</sub> uptake and the  
80 enhanced upwelling of ~~dissolved inorganic carbon (C<sub>d</sub>)~~ C<sub>d</sub>-rich deep waters (e.g. Hauck et al., 2010; Pardo et al.,  
81 2017). It has been suggested, through numerical studies, that depending on future CO<sub>2</sub> emission levels, surface  
82 waters in the SO could reach under-saturation state for aragonite by 2030-2050 ~~in the SO~~ (Orr et al., 2005;

Mis en forme : Couleur de police :  
Rouge foncé

83 Gangstø et al., 2008; McNeil and Matear, 2008; Negrete-Garcia et al., 2019). Such a change would have multiple  
84 and detrimental impacts on marine ecosystems (Fabry et al., 2008; Doney et al., 2012; Bopp et al., 2013), in  
85 particular calcifying marine organisms, and especially aragonite producers such as pteropods (Hunt et al., 2008;  
86 Gardner et al., 2023), but also calcite producing planktonic foraminifera (Moy et al., 2009), coccolithophorids  
87 (Beaufort et al., 2011), and non-calcifying species such as the abundant SO diatoms (e.g. Benoiston et al., 2017;  
88 Petrou et al., 2019; Weir et al., 2020; Duncan et al., 2022) and krill (Kawaguchi et al., 2013).

89 Hindcast simulations with Global Ocean Biogeochemical Models (GOBM), as well as projections with  
90 Earth System Models (ESM) have been used to evaluate the ocean carbon cycle over the past decades and future  
91 changes in  $C_{\text{ant}}$  storage, ocean acidification or impacts of global changechanges on marine ecosystems. However,  
92 current model-based estimates of the contemporary SO  $\text{CO}_2$  sink are subject to relatively large uncertainties (e.g.  
93 Long et al., 2013; Hauck et al., 2020; Gooya et al., 2023; Hauck et al., 20232023a, b; Mayot et al., 2023;  
94 DeVries et al., 2023). Difference between GOBM models can reach up to 0.7  $\text{PgC.yr}^{-1}$  in the SO (Hauck et al.,  
95 2020), which is roughly equivalent to the mean climatological flux of 0.5  $\text{PgC.yr}^{-1}$  (McNeil et al., 2007;  
96 Takahashi et al., 2009; Lenton et al., 2013). InAt the high latitudes of the SO (> 50°S) for the 2010s, ESMESMs  
97 from the Coupled Model Intercomparison Project Phase 6 (CMIP6) simulated either a large sink or a modest  
98 source of  $\text{CO}_2$  (McKinley et al., 2023). This is mainly due to incorrect or missing physical and/or biological  
99 processes in the models (e.g. Pilcher et al., 2015; Kessler and Tjiputra, 2016; Mongwe et al., 2018; Lerner et al.,  
100 2021) leading to biases in the seasonality of temperature, dissolved inorganic carbon  $C_T$ , partial pressure of  $\text{CO}_2$   
101 ( $p\text{CO}_2$ ), air-sea  $\text{CO}_2$  fluxes, pH or  $\Omega$  (e.g. McNeil and Sasse 2016; Rodgers et al., 2023; Rustogi et al., 2023;  
102 Joos et al., 2023). Such model imperfections should be resolved to havegain reliability in future projections of  
103  $\text{CO}_2$  uptake, OA, productivity and the responses of the marine ecosystems, gain in reliability (Frölicher et al.,  
104 2015; Hauck et al., 2015; Sasse et al., 2015; Kessler and Tjiputra, 2016; McNeil and Sasse 2016; Kwiatkowski  
105 and Orr, 2018; Negrete-Garcia et al., 2019; Burger et al., 2020; Terharr et al., 2021; Krumhardt et al., 2022;  
106 Jiang et al., 2023; Mongwe et al., 2023). In this context, as often concluded in modeling studies (e.g. Kessler and  
107 Tjiputra, 2016; Gooya et al., 2023; Wright et al., 2023; Hauck et al., 2023; Mayot et al., 2023; Rodgers et al.,  
108 2023), long-term biogeochemical observations are particularly valuable to quantify and understand recent past  
109 and current changes, and ultimately evaluate model simulations, as often concluded in modeling studies (e.g.  
110 Kessler and Tjiputra, 2016; Gooya et al., 2023; Wright et al., 2023; Hauck et al., 2023a; Mayot et al., 2023;  
111 Rodgers et al., 2023).

112 Although the SO south of the Polar Front remains much less observed than other oceanic regions,  
113 several observations-based studies have allowed to estimateestimated the decrease in pH in the surface waters in  
114 response to the increase in oceanic  $\text{CO}_2$  fugacity,  $f\text{CO}_2$  (Mirodikwa et al., 2012; Takahashi et al., 2014; Lauvset  
115 et al., 2015; Munro et al., 2015; Xue et al., 2018; Iida et al., 2021; Leseurre et al., 2022; Brandon et al., 2022).  
116 Results showed a large range ofin the pH trends from  $-0.008.\text{decade}^{-1}$  to  $-0.035.\text{decade}^{-1}$  depending on the period  
117 and regionsthe region of interest. Most of these analyses were based on summer observations (Table 1) and some  
118 studies highlighted contrasting pH trends on a 5-10 yearyears time probably linked to large scale climate  
119 variability such as the Southern Annular Mode (SAM) (e.g. Xue et al., 2018). Given such variability, it is  
120 important to continue monitoring  $f\text{CO}_2$  and pH trendtrends and, if possible, at different seasons as future change  
121 in  $\text{CO}_2$  uptake and potential tipping points of thatthe carbonate saturation state also dependsdepend on  
122 seasonality (Sasse et al., 2015). The above observational studies were dedicated to pH changes in surface waters.  
123 In contrast to Northern high latitudes (e.g. Olafsson et al., 2009, 2010; Franco et al., 2021; Skjelvan et al.,

124 | 2022)), few studies in the SO ~~attempted to evaluate~~evaluated decadal changes of carbonate system properties and  
125 | acidification in the water column based on time-series stations. These changes in the SO water column were  
126 | investigated from data collected during cruises generally 3 to 15 years apart (e.g., Hauck et al., 2010; Van  
127 | Heuven et al., 2011; Pardo et al., 2017; Tanhua et al., 2017; Carter et al., 2019).  
128 |

Mis en forme : Couleur de police :  
Automatique

129

130 Table 1: Trends of oceanic fCO<sub>2</sub> (µatm.yr<sup>-1</sup>) and pH (decade<sup>-1</sup>) in the Southern Ocean south of the Polar Front  
 131 based on observations ~~and from this study.~~ IO: Indian Ocean sector. PO: Pacific Ocean sector. AO: Atlantic  
 132 Ocean sector. SO SPSS: Southern Ocean SubPolar Seasonally Stratified biome (around 50-60°S). PZ: Polar  
 133 Zone. NR: Not Reported. Standard-deviations when available are given in brackets.

134

135

136

137

138

139

140

141

142

143

144

145

146

147

148

149

150

151

152

153

154

155

156

157

158

159

160

161

162

163

164

165

166

167

168

169

170

171

172

173

174

175

176

177

178

179

180

181

182

183

184

185

186

187

188

189

Mis en forme : Gauche, Espace Après  
: 10 pt

Mis en forme : Police : +Corps  
(Calibri), 11 pt

Period	Season	Zone	Trend fCO <sub>2</sub> µatm.yr <sup>-1</sup>	Trend pH decade <sup>-1</sup>	Reference
1991-2000	Summer	IO PZ 55-60°S	2.93	-0.035	Xue et al (2018)
2001-2011	Summer	IO PZ 55-60°S	1.41	-0.016	Xue et al (2018)
2005-2019	Summer	IO PZ 54-64°S	NR	-0.026(0.003)	Brandon et al (2022)
1998-2019	Summer	IO 50°S-68°E	1.9 (0.3)	-0.019 (0.004)	Leseurre et al (2022)
1998-2019	Summer	IO 55°S-63°E	2.1 (0.3)	-0.022 (0.003)	Leseurre et al (2022)
1998-2007	Summer	IO 55°S-63°E	5.3 (0.4)	-0.050 (0.016)	Leseurre et al (2022)
2006-2019	Summer	IO 55°S-63°E	0.3 (0.2)	no trend	Leseurre et al (2022)
1969-2003	Summer	PO 55-62°S	1.7 (0.2)	-0.020 (0.003)	Midorikawa (2012)
2002-2012	Annual	Drake North	2.21 (0.55)	-0.023 (0.007)	Takahashi (2014)
2002-2012	Annual	Drake South	1.50 (0.65)	-0.015 (0.008)	Takahashi (2014)
2002-2015	Summer	Drake North	1.95 (0.55)	-0.021 (0.006)	Munro et al (2015)
2002-2015	Winter	Drake North	1.92 (0.24)	-0.018 (0.003)	Munro et al (2015)
2002-2015	Summer	Drake South	1.30 (0.85)	-0.017 (0.010)	Munro et al (2015)
2002-2015	Winter	Drake South	0.67 (0.39)	-0.008 (0.004)	Munro et al (2015)
2002-2015	Annual	Drake North	1.74 (0.15)	-0.019 (0.002)	Munro et al (2015)
2002-2015	Annual	Drake South	1.16 (0.27)	-0.015 (0.003)	Munro et al (2015)
1981-2011	Annual	SO SPSS	1.44 (0.10)	-0.020 (0.002)	Lauvset et al (2015)
1991-2011	Annual	SO SPSS	1.46 (0.11)	-0.021 (0.002)	Lauvset et al (2015)
1993-2018	Annual	SO 44-75°S	NR	-0.0165 (0.0001)	Iida et al (2021)
1962-2016	November	IO 50°S-68°E	1.31 (0.20)	-0.014 (0.002)	This study, Obs.
1991-2021	Summer	IO 50°S-68°E	2.10 (0.22)	-0.022 (0.002)	This study, Obs.
1991-2001	Summer	IO 50°S-68°E	0.76 (0.90)	0.009 (0.010)	This study, Obs.
2001-2010	Summer	IO 50°S-68°E	3.23 (1.07)	0.035 (0.011)	This study, Obs.
2010-2020	Summer	IO 50°S-68°E	0.84 (0.77)	-0.008 (0.008)	This study, Obs.
1985-2020	Summer	IO 50°S-68°E	1.71 (0.08)	-0.018 (0.001)	This study, FFNN
1991-2020	Summer	IO 50°S-68°E	1.85 (0.11)	0.020 (0.001)	This study, FFNN
1991-2001	Summer	IO 50°S-68°E	1.18 (0.26)	0.013 (0.004)	This study, FFNN
2001-2010	Summer	IO 50°S-68°E	2.87 (0.25)	-0.030 (0.003)	This study, FFNN
2010-2020	Summer	IO 50°S-68°E	0.98 (0.40)	0.010 (0.004)	This study, FFNN
1991-2001	Winter	IO 50°S-68°E	0.98 (0.09)	-0.010 (0.001)	This study, FFNN
2001-2010	Winter	IO 50°S-68°E	1.99 (0.10)	-0.021 (0.001)	This study, FFNN
2010-2020	Winter	IO 50°S-68°E	2.21 (0.17)	0.022 (0.002)	This study, FFNN
1985-2020	Annual	IO 50°S-68°E	1.57 (0.03)	0.0165(0.0004)	This study, FFNN

Mis en forme : Police : 10 pt

Mis en forme : Interligne : Multiple  
1,15 li

The present study complements in time, seasons, and in the water column, the surface fCO<sub>2</sub> and pH trends investigated by Leseurre et al., (2022) in different regions of the Southern Indian Ocean for the period 1998-2019 during austral summer. South of the PF around 50°S, Leseurre et al. (2022) showed that in summer the surface fCO<sub>2</sub> increase and pH decrease over 20 years were mainly driven by the increase in accumulation of anthropogenic CO<sub>2</sub> sequestration by about +0.6 ( $\pm \pm 0.2$ ) µmol.kg<sup>-1</sup>.yr<sup>-1</sup> and by a small warming of +0.03 ( $\pm \pm 0.02$ ) °C.yr<sup>-1</sup>. In addition Leseurre et al. (2022) showed that in the recent decade, 2007-2019, the fCO<sub>2</sub> trend

190 | was low  $+0.3 (\pm 0.2) \mu\text{atm yr}^{-1}$  compared to ~~the previous decade~~  $+5.3 (\pm 0.4) \mu\text{atm yr}^{-1}$  ~~in over~~ 1998-  
191 | 2007), highlighting the sensitivity of the fCO<sub>2</sub> and pH trends to the selected time period (especially during  
192 | summer). In particular, they observed relatively stable pH values over 2010-2019 (i.e. no decrease in pH) with  
193 | no clear explanation on the origin of the slow-down of the fCO<sub>2</sub> and pH trends in surface waters south of the PF  
194 | in recent years. To complement the analysis by Leseurre et al. (2022) based on summer observations ~~in over the~~  
195 | ~~period~~ 1998-2019 this study ~~foeusses~~~~focuses~~ on one location regularly visited south of the Polar Front (around  
196 | 50°S-68°E south-west of Kerguelen Island, Figure 1). The analysis period is ~~first~~ extended back to 1985 and  
197 | forward to 2021 to investigate the recent status of fCO<sub>2</sub> and pH. We also evaluate the trends ~~for different seasons~~  
198 | ~~during late winter~~ using sparse ~~spring/winter~~ data ~~in October/November~~. The combination of in situ observations  
199 | and monthly estimates from a neural network model over the period 1985-2020 (Chau et al., 2022) enables to  
200 | assess potential changes in seasonality of the surface ocean carbonates system (including fCO<sub>2</sub>, C<sub>T</sub>, pH, Ω) as  
201 | suggested in recent decades or in future scenarios (Hauck and Völker, 2015; Gallego et al., 2018; Landschützer  
202 | et al., 2018; Kwiatkowski and Orr, 2018; Kwiatkowski et al., 2020; Lerner et al., 2021; Fassbender et al., 2022;  
203 | Yun et al., 2022; Rodgers et al., 2023; Joos et al., 2023). The ~~variability changes observed~~ in surface waters will  
204 | be related to changes in C<sub>ant</sub> concentrations ~~observed~~~~estimated~~ in the water column and will be complemented by  
205 | an analysis of OA at depth between 1985 and 2021. Finally we will explore the long-term ~~variability change~~ of  
206 | ~~surface~~ fCO<sub>2</sub> and pH since ~~the~~ 1960s and potential future changes of the carbonate system at this time-~~series~~  
207 | site.

208

## 209 | 2 Data selection, methods and quality control

210

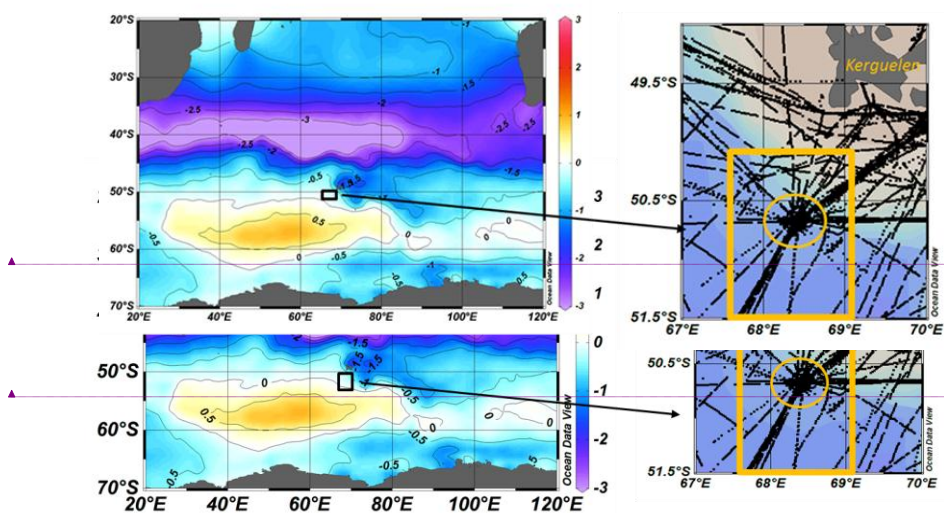
### 211 | 2.1 Study area and data selection

212

213 | This study ~~foeused~~~~focuses~~ on a High Nutrients Low Chlorophyll area (HNLC, Minas and Minas, 1992)  
214 | ~~of in~~ the Indian sector of the Southern ocean (SO) in the Permanent Open Ocean Zone (POOZ) south of the Polar  
215 | Front (PF) and south-west of Kerguelen Islands (around 50°S-68°E, Figure 1). The Kerguelen Plateau is an  
216 | extended topographic feature that controls part of the Antarctic Circumpolar Current (ACC), generates eddies  
217 | (Daniault and Ménard, 1985) and the northward deflection of the PF ~~near~~~~just east of~~ the Island (Pauthenet et al.,  
218 | 2018). The Plateau is also a region of relatively high ~~chlorophyll-a (Chl-a) concentration~~ (Moore and Abbott,  
219 | 2000; Mongin et al., 2008) and strong CO<sub>2</sub> uptake during austral spring-summer that contrasts with the weaker  
220 | sink over the POOZ/HNLC (Metzl et al., 2006; Jouandet et al., 2008, 2011; Lo Monaco et al., 2014; Leseurre et  
221 | al., 2022). The POOZ/HNLC region west (upstream) of the Kerguelen Plateau is characterized by rather stable  
222 | water mass properties (temperature, salinity, oxygen or nutrients) over time and low eddy activity compared to  
223 | the Plateau (Daniault and Ménard, 1985; Chapman et al., 2015; Dove et al., 2022). In this region, located in the  
224 | deep Enderby Basin, the flow is not constrained by topography and there is no local upwelling that would import  
225 | C<sub>T</sub>-rich ~~water~~~~waters~~ to ~~the~~ surface layers as observed on the eastern side of the Kerguelen Plateau (Brady et al.,  
226 | 2021).

227 | The Indian ~~austral~~ sector ~~of the SO~~ is also recognized to host the strongest winds in the SO leading to  
228 | year-round high gas transfer coefficients (Wanninkhof and Trinanes 2017). As a result, and in contrast to the  
229 | Atlantic ~~seetors~~~~sector~~ of the SO, the Indian region south of 45°S was a periodic ~~annual~~ CO<sub>2</sub> source, especially in  
230 | the 1960s to the 1980s (Rödenbeck et al., 2022; Bennington et al., 2022; Prend et al., 2022; Gray, 2024). In the

231 POOZ-HNLC region, high winter wind speed (monthly average up to  $16 \text{ m}\cdot\text{s}^{-1}$ ) and associated heat loss drive  
 232 deep mixing. Deep winter mixing entrains subsurface properties to the surface layer, increases surface  $C_T$   
 233 concentrations leading to wintertime outgassing of  $\text{CO}_2$  (Metzl et al., 2006). This combination of characteristics  
 234 makes the region an ideal test-bed for 1-D modeling studies investigating the temporal dynamics and drivers of  
 235 biogeochemical processes including nutrients, iron, phytoplankton and carbon (Pondaven et al., 1998, 2000;  
 236 Louanchi et al., 1999, 2001; Jabaud-Jan et al., 2004; Metzl et al., 2006; Mongin et al., 2006, 2007; Kane et al.,  
 237 2011; Pasquer et al., 2015; Demuyne et al., 2020).



Mis en forme : Police :10 pt  
 Mis en forme : Retrait : Première ligne : 0 cm, Interligne : simple  
 Mis en forme : Interligne : simple  
 Mis en forme : Police :Times New Roman, 9 pt, Couleur de police : Rouge foncé

259 Figure 1: Left: Annual air-sea  $\text{CO}_2$  flux ( $\text{molC}\cdot\text{m}^{-2}\cdot\text{yr}^{-1}$ ) in the South Indian Ocean for year 2020 from the FFNN model  
 260 (negative flux for ocean sink, positive flux for ocean source). The black box identified the location of the study south-west of  
 261 Kerguelen Islands. Right: Track of cruises with underway  $f\text{CO}_2$  data South-West of Kerguelen Islands. The  
 262 station at  $50^\circ40'S$ - $68^\circ25'E$  occupied in 1985, 1992-1993 and 1998-2021 is indicated by a yellow circle. The yellow square is  
 263 the region selected to calculate the mean values from the underway surface observations and from the FFNN model. Figures  
 264 produced with ODV (Schlitzer, 2018).  
 265

266 Here we used surface and water-column observations around location  $50^\circ40'S$ - $68^\circ25'E$  (Figure 1, Table  
 267 S1), historically called KERFIX station (KERguelen FIXed station) sampled infrom 1990- to 1995 in the  
 268 framework of the WOCE/JGOFS programs (Jeandel et al., 1998). The station was first occupied in March 1985  
 269 during the INDIGO-1 cruise (Indian Ocean Geochemistry, Poisson, 1985; Poisson et al., 1988) and since 1998 it  
 270 is regularly visited during the OISO cruises (Océan Indien Service d'Observations, Metzl and Lo Monaco, 1998,  
 271 <https://doi.org/10.18142/228>). The regular occupation from 1985 to 2021 makes it the longest time-series station  
 272 in the Southern Ocean POOZ/HNLC area allowingfor investigating the inter-annual to decadal trends of  
 273 carbonate properties in surface waters and across the water-column (0-1600m). Despite the occasional  
 274 variabilitylarge anomalies in surface waters properties (e.g. lower surface Salinitytemperature in 2011-December  
 275 1998, lower salinity in February 2013) we consider all observations selected for this study both in surface waters  
 276 and the water-column to be representative of the water masses in this POOZ/HNLC region upstream of the  
 277 Kerguelen Plateau.

278 Data for the period 1985-2011 were extracted from the GLODAP data-product, version V2.2021  
 279 (Lauvset et al., 2021 a, b; Table S1a). Observations collected during OISO cruises infrom 2012- to 2021-(Lø

280 | [Monaco, 2020; Lo Monaco et al., 2021](#)) will be included in GLODAP-V3. For the surface water properties, all  
281 | available underway fCO<sub>2</sub> data were selected (Figure 1). This includes one cruise in November 1962 (Keeling and  
282 | Waterman, 1968) and 41 cruises [infrom 1991- to 2021](#) (Table S1b). All surface temperature, salinity and fCO<sub>2</sub>  
283 | data were extracted from the SOCAT data-product version v2022 (Surface Ocean CO<sub>2</sub> Atlas, Bakker et al., 2016,  
284 | [2022-\)](#) and have an accuracy for fCO<sub>2</sub> between 2 to 5  $\mu$ atm.  
285 |



286  
287  
288  
289  
290  
291  
292  
293  
294  
295  
296  
297  
298  
299  
300  
301  
302  
303  
304  
305  
306  
307  
308  
309  
310  
311  
312  
313  
314  
315  
316  
317  
318  
319  
320  
321  
322  
323  
324  
325  
326

## 2.2 Methods

The methods for surface underway  $f\text{CO}_2$  and biogeochemical properties (~~Oxygen-oxygen~~,  $C_T$ , total alkalinity  $A_T$ ,  $C_T$ , nutrients) in the water-column for the INDIGO-1, KERFIX and OISO cruises were described in previous studies (e.g. Poisson et al., 1993; Louanchi et al., 2001; Metzl et al., 2006; Metzl, 2009; Mahieu et al., 2020; Leseurre et al., 2022). Here we briefly recall the methods for underway  $f\text{CO}_2$  and water-column observations.

### 2.2.1 Surface $f\text{CO}_2$ data

For  $f\text{CO}_2$  measurements in 1991-2021, sea-surface water was continuously equilibrated with a "thin film" type equilibrator thermostated with surface seawater (Poisson et al., 1993). The  $x\text{CO}_2$  in the dried gas was measured with a non-dispersive infrared analyser (NDIR, Siemens Ultramat 5F or 6F). Standard gases for calibration (around 270, 350 and 490 ppm) were measured every 6 hours. To correct  $x\text{CO}_2$  dry measurements to  $f\text{CO}_2$  *in situ* data, we used polynomials from Weiss and Price (1980) for vapour pressure and from Copin-Montégut (1988, 1989) for temperature. Note that when incorporated in the SOCAT data-base, the original  $f\text{CO}_2$  data are recomputed (Pfeil et al., 2013) using temperature correction from Takahashi et al. (1993). Given the small difference between equilibrium temperature and sea surface temperature ( $+0.56 \pm 0.30$  °C on average for the cruises in 1998-2021), the  $f\text{CO}_2$  data from SOCAT used in this analysis (Bakker et al., 2022) are almost identical (within 1  $\mu\text{atm}$ ) to the original  $f\text{CO}_2$  values from our cruises ([www.ncei.noaa.gov/access/ocean-carbon-data-system/oceans/VOS\\_Program/OISO.html](http://www.ncei.noaa.gov/access/ocean-carbon-data-system/oceans/VOS_Program/OISO.html)).

### 2.2.2 Water column data

~~In~~Over the period 1990-1995, water samples were collected during the KERFIX program on the ship *La Curieuse* at standard depths using 8 L Niskin bottles mounted on a stainless steel cable and equipped with reversing SIS pressure and temperature probes. Methods and accuracy for the geochemical measurements used in this analysis ( $A_T$ ,  $C_T$ , oxygen, nutrients) are detailed by Jeandel et al. (1998) and by Louanchi et al. (2001). From 1998 onwards, the station was occupied within the framework of the OISO long-term monitoring program onboard the *R.V. Marion-Dufresne*. We used Conductivity-Temperature-Depth (CTD) sensors mounted on a 24 bottles rosette equipped with 12 L Niskin bottles. Temperature and salinity measurements have an accuracy of 0.002 °C and 0.005 respectively (Mahieu et al., 2020). Samples for  $A_T$  and  $C_T$  were filled in 500 mL glass bottles and poisoned with ~~400~~300  $\mu\text{L}$  of saturated mercuric chloride solution to halt biological activity. Discrete  $C_T$  and  $A_T$  samples were analyzed onboard by potentiometric titration derived from the method developed by Edmond (1970) using a closed cell. Based on replicate samples from the surface or depth, the repeatability for  $A_T$  and  $C_T$  varies from 1 to 3.5  $\mu\text{mol.kg}^{-1}$  depending on the cruise. The accuracy of  $\pm 3$   $\mu\text{mol.kg}^{-1}$  was ensured by daily analyses of Certified Reference Materials (CRMs) provided by Andrew Dickson's laboratory (Scripps Institute of Oceanography).

Dissolved oxygen ( $\text{O}_2$ ) concentration was determined by a sensor fixed on the rosette and values were adjusted based on discrete measurements (Winkler method, Carpenter, 1965) using a potentiometric titration

Mis en forme : Justifié

Mis en forme : Police :Non Gras

Mis en forme : Justifié, Retrait :  
Première ligne : 1,25 cm

327 system. Accuracy for O<sub>2</sub> is  $\pm 2 \mu\text{mol.kg}^{-1}$  (Mahieu et al., 2020). Although long-term deoxygenation in the  
328 Southern ocean has been suggested (Ito et al., 2017; Schmidtko et al., 2017; Oschlies et al., 2018), no significant  
329 trend in O<sub>2</sub> was identified over 1985-2021 at this station around 50°S in both ~~the surface or in~~ and the subsurface  
330 ~~waters (e.g. in the~~ layer (at the depth of the temperature minimum representing winter water, a layer used for C<sub>ant</sub>  
331 calculations as described later). However, in the station data a small O<sub>2</sub> decrease was detected around 800m in  
332 the O<sub>2</sub> minimum layer over 36 years ( $-0.22 \pm 0.07 \mu\text{mol.kg}^{-1}.\text{yr}^{-1}$ ). As this has no impact on the interpretation for  
333 pH and  $\Omega$  trends for this analysis, the observed change of O<sub>2</sub> at depth will ~~be not~~ be discussed further. Here the  
334 O<sub>2</sub> data are mainly used for the calculation of anthropogenic CO<sub>2</sub> concentrations and the observed O<sub>2</sub> change at  
335 depth is too small to have an impact on temporal variations of C<sub>ant</sub> concentrations given the uncertainty of the  
336 calculation.

337 Nitrate (NO<sub>3</sub>) and silicate (DSi) were analyzed on board or at LOCEAN/Paris by colorimetry following  
338 the methods described by Tréguer and Le Corre (1975) for 1998-2008 or from Coverly et al. (2009) for 2009-  
339 2021. The uncertainty of NO<sub>3</sub> and DSi measurements is  $\pm 0.1 \mu\text{mol.kg}^{-1}$ . Based on replicate measurements ~~for on~~  
340 deep samples, we estimate an error of about 0.3 % for both nutrients. Phosphate (PO<sub>4</sub>) samples were analyzed ~~in~~  
341 ~~samples~~ from a few cruises following the method of Murphy and Riley (1962) revised by Strickland and Parsons  
342 (1972) with an uncertainty of  $\pm 0.02 \mu\text{mol.kg}^{-1}$ . When ~~nutrient~~ nutrients data are not available for a cruise, we  
343 used climatological values based on the seasonal nutrients cycles inferred from data from 1990 to 2021. This  
344 method has a very small impact on the carbonate system calculations and the trend analysis as we did not detect  
345 any significant trends in nutrients in surface or at depth since 1985 (not shown) as opposed to what has been  
346 observed at higher ~~latitude~~ latitudes of the SO (Iida et al., 2013; Hoppema et al., 2015). However, we will see in  
347 section 3.1 that the inter-annual variability of nutrients (especially DSi in the HNLC region) might inform on  
348 potential changes in biological processes.

349 ~~For Chlorophyll-a (Chl-a), samples~~ Samples were ~~taken~~ collected in the top layers (0-150m). ~~One~~ for  
350 chlorophyll-a (Chl-a). For that, one to two liters of seawater were filtered onto 0.7  $\mu\text{m}$  glass microfiber filters  
351 (GF/F, Whatman) and filters were stored at -80°C onboard. Back at the LOCEAN/Paris laboratory, samples were  
352 extracted in 90% acetone (Strickland and Parsons, 1972) and the fluorescence of Chl-a was measured on a  
353 Turner Type 450 fluorometer ~~in for the period~~ 1998-2007 and since 2009 at 670 nm on a Hitachi F-4500  
354 spectrofluorometer (Neveux and Lantoine, 1993).

355

### 356 2.2.3 Data quality-control and data consistency

357

358 When exploring the trends of ocean properties based on different cruises more than 35 years apart, it is  
359 important to first verify the consistency of the data and if there is correct for any bias or drift. The INDIGO  
360 data from 1985 (i.e. prior to CRM available for A<sub>T</sub> and C<sub>T</sub>) were first controlled prior to their incorporation into  
361 the original GLODAP product (Sabine et al., 1999; Key et al., 2004) and corrections for A<sub>T</sub> and C<sub>T</sub> were  
362 revisited within the framework of the CARINA project (CARbon IN the Atlantic, Lo Monaco et al., 2010) and  
363 the GLODAPv2 synthesis (Olsen et al., 2016). A secondary quality control was performed on the data from the  
364 OISO cruises collected between 1998 and 2011 within the CARINA and GLODAP-v2 initiatives (Lo Monaco et  
365 al., 2010; Olsen et al., 2016). Significant off-sets were identified for A<sub>T</sub> and C<sub>T</sub> in samples from the KERFIX  
366 cruises (1990-1993) compared to INDIGO and OISO data and it was proposed to correct the original values by -  
367  $35 \mu\text{mol.kg}^{-1}$  for C<sub>T</sub> and  $-49 \mu\text{mol.kg}^{-1}$  for A<sub>T</sub> (Metzl et al., 2006). These corrections were applied in GLODAP

368 version v2.2019 (Olsen et al., 2019) and resulted in coherent  $A_T$  and  $C_T$  concentrations for KERFIX in the deep  
369 layers compared to other cruises (Supp. Mat., Table S2, Figure S1). The same data quality control protocol as for  
370 GLODAP-v2 was applied to data from OISO cruises for the yearsperiod 2012-2021 (Mahieu et al., 2020). Given  
371 the accuracy of the data no systematic bias (~~exeepted~~except in 2014) was found for the properties measured in  
372 2012-2021. The time-series of  $A_T$  and  $C_T$  at depthdepths below 1450 m for all cruises in 1985-2021 show some  
373 variability but no trend over 36 years as expected in the bottom waters in this region (Supp. Mat., Figure S1).  
374 However, we identified a small bias for  $C_T$  in 2014 (cruise OISO-23) where  $C_T$  concentrations in the deep water  
375 appeared slightly lower (2228-2234  $\mu\text{mol.kg}^{-1}$  in 2014 compared to the mean value of 2240.7 ( $\pm 3.7$ )  $\mu\text{mol.kg}^{-1}$ ,  
376 Table S2, Figure S1). When compared to  $f\text{CO}_2$  in surface waters, we also suspect the  $C_T$  data in the mixed-layer  
377 in 2014 to be too low by about 10  $\mu\text{mol.kg}^{-1}$  (Figures S2, S3). Therefore we applied a WOCE/GLODAP flag 3  
378 for  $C_T$  data of this cruise and will not use the station data in 2014 for the  $C_{\text{ant}}$  calculations and the trend analysis  
379 described in this study.

380

#### 381 2.2.4 CMEMS-LSCE-FFNN model

382

Mis en forme : Police :Gras

383

As most of the cruises took place during austral summer and data are not available each year, we  
384 completed the observations with the results from an ensemble of feed-forward neural network modelmodels  
385 (CMEMS-LSCE-FFNN or FFNN for simplicity here, Chau et al., 2022). The FFNN model allows mapping at  
386 global scale monthly surface  $f\text{CO}_2$  givenfrom the SOCAT gridded datasets and ancillary variables. The  
387 reconstructed  $f\text{CO}_2$  is then used to derive monthly surface  $C_T$  and pH fields as well as air-sea  $\text{CO}_2$  fluxes. This  
388 data product enablesis used to investigate the trends for different seasons and to derive estimates of annual air-  
389 sea  $\text{CO}_2$  fluxes to interpret the change in  $\text{CO}_2$  uptake, if any. For a full description of the model, access to the  
390 data and a statistical evaluation of  $f\text{CO}_2$  reconstructions please refer to Chau et al. (2022). Within this study, we  
391 compared the FFNN  $f\text{CO}_2$  with observations from 35 cruises for the years between 1991 and 2020 (Table S3,  
392 Figure S2a). Excepted for a few periods (January 1993 and January 2002), model-data differences are generally  
393 within  $\pm 10 \mu\text{atm}$  with a mean difference of 2.1 ( $\pm 7$ )  $\mu\text{atm}$  for the 35 co-located periods. Note that, as opposed  
394 to sea surface  $f\text{CO}_2$ , no temporal trend was identified for the differences between the observed and reconstructed  
395  $f\text{CO}_2$  (Figure S2b), i.e. the trends of sea surface  $f\text{CO}_2$  derived from the observations and from the FFNN model  
396 should be the same. Aside from the  $f\text{CO}_2$  reconstructions, surface ocean alkalinity ( $A_T$ ) fields are also provided  
397 by using the multivariate linear regression model LIAR (Carter et al., 2016; 2018) based on sea surface  
398 temperature, salinity, and nutrientnutrients concentration.

Mis en forme : Police :Non Italique

399

#### 400 2.2.5 Calculations of carbonate properties

401

Based on the data available for each cruise ( $f\text{CO}_2$ , or  $A_T$  and  $C_T$ ) or from the FFNN model ( $f\text{CO}_2$  and  
403  $A_T$ ), other carbonate system properties (pH,  $[\text{H}^+]$ ,  $[\text{CO}_3^{2-}]$  and  $\Omega$ ) were calculated using the CO2sys program  
404 (version CO2sys\_v2.5, Orr et al., 2018) developed by Lewis and Wallace (1998) and adapted by Pierrot et al.  
405 (2006) with K1 and K2 dissociation constants from Lueker et al. (2000) as recommended (Dickson et al., 2007;  
406 Orr et al., 2015; Wanninkhof et al., 2015). The total boron concentration was calculated according to Uppström  
407 (1974) and  $\text{KSO}_4$  from Dickson (1990). To calculate the properties with the underway surface  $f\text{CO}_2$  dataset, we

408 | used the  $A_T/S$  relationship based on  $A_T$ - and  $C_T$  data from [the OISO cruises](#) [inover the period](#) 1998-2019 in the  
409 | South Indian sector as described by Leseurre et al. (2022):

410 |

$$411 | A_T = 64.341 \times S + 106.764 \text{ (rmse} = 7.4855 \text{ } \mu\text{mol.kg}^{-1}, n = 4775) \quad (\text{Eq. 1})$$

412 |

413 | The use of other  $A_T/S$  relationships (e.g. Millero et al., 1998; Jabaud-Jan et al., 2004; Lee et al., 2006;  
414 | Carter et al., 2018) would change slightly the  $A_T$  concentrations but neither the  $A_T$  trend nor the interpretation of  
415 | the  $C_T$ , pH or  $\Omega$  trends. However, as salinity is an important predictor in the calculation of  $A_T$ ,  $C_T$  or pH from  
416 |  $f\text{CO}_2$  data, we have assessed the original underway salinity data and found biases for [a few cruises](#) in 1992, 1993  
417 | and 1995 (Table S1b). For these cruises or when salinity was not measured we used the salinity from the World  
418 | Ocean Atlas, WOA (Antonov et al., 2006) in the SOCAT data-sets (Pfeil et al., 2013, identified “WOA” in Table  
419 | S1b). Monthly  $f\text{CO}_2$  and  $A_T$  data extracted from the CMEMS-LSCE-FFNN datasets at the station location  
420 | ( $50.5^\circ\text{S}$ - $68.5^\circ\text{E}$ ) over 1985-2020 were used to calculate the carbonate properties in the same way as from  
421 | observations.

422 |

#### 423 | 2.2.6 Comparisons of different datasets and the FFNN model

424 |

425 | To validate the properties calculated using the  $f\text{CO}_2$  data for 1991-2021 or from the FFNN model over  
426 | 1985-2020 we compared the calculated values ( $A_T$ ,  $C_T$ , pH,  $[\text{H}^+]$ ,  $[\text{CO}_3^{2-}]$ ,  $\Omega$ ) with those [calculated from  \$A\_T\$ - and](#)  
427 |  $C_T$  data measured in the mixed-layer at [stations](#) [the KERFIX/OISO station](#) occupied in 1985 and [inbetween](#) 1993-  
428 | [and 2021](#). For this comparison, we averaged the continuous underway  $f\text{CO}_2$  data selected in a box around the  
429 | station location ( $50^\circ\text{S}$ - $51.5^\circ\text{S}$ / $67.5^\circ\text{E}$ - $69^\circ\text{E}$ , yellow box in Figure 1). Results of the comparisons between various  
430 | datasets are detailed in the Supplementary Material (Tables S3 and S4). During the period 1993-2021, there are  
431 | [22 stationsstation occupations](#) with co-located [underway](#)  $f\text{CO}_2$  data for different seasons (but mainly in summer).  
432 | Since we found a close agreement between measured  $f\text{CO}_2$  and the FFNN model (Table S3, Figure S2),  
433 | mismatches in all calculated carbonate system properties between the underway  $f\text{CO}_2$  dataset and the FFNN  
434 | model are small, falling within the range of the errors associated with the calculations (Orr et al., 2018). For  
435 | example, for 35 co-located periods, the mean differences in calculated  $C_T$  of  $1.5 (\pm \pm 5) \mu\text{mol.kg}^{-1}$  or pH of -  
436 |  $0.002 (\pm \pm 0.008)$  are in the range of the theoretical error of about  $5 \mu\text{mol.kg}^{-1}$  and 0.007 respectively when taking  
437 | into account measurements errors on salinity, temperature, nutrients,  $f\text{CO}_2$  and  $A_T$  (Orr et al., 2018). On the other  
438 | hand, compared to the station data in the mixed-layer (Table S4), [bias forthe](#) calculated  $A_T$  using Equation 1 is  
439 | slightly higher by about  $5 \mu\text{mol.kg}^{-1}$ . This explains the relatively high differences for  $C_T$  (mean difference around  
440 |  $8 \mu\text{mol.kg}^{-1}$ ) and for pH (mean difference around 0.008) calculated with  $f\text{CO}_2$  and the  $A_T/S$  relationship. The  
441 | differences of calculated values with observations [in 1991-2021](#) are, on average, in the range of uncertainties of  
442 | the carbonate system calculations using  $A_T$ - $C_T$  pairs (error for  $f\text{CO}_2$  around  $13 \mu\text{atm}$  and for pH around 0.0144).  
443 | Importantly, there is no temporal trend for the differences between calculated and observed properties (Figure  
444 | S3b). We are thus confident using the selected  $f\text{CO}_2$  data for the trend analysis presented in this study. The  
445 | independent comparison with  $A_T$ - and  $C_T$  [data at stationsmeasurements in the mixed-layer](#) also indicates that the  
446 | FFNN model results for  $A_T$ - and  $C_T$ , are close to the observations (Table S4, Table S5, Figure S4) as well as for  
447 | calculated pH,  $[\text{H}^+]$ ,  $[\text{CO}_3^{2-}]$ ,  $\Omega_{\text{ca}}$  and  $\Omega_{\text{Ar}}$ . This somehow validates the use of the FFNN data for the trend  
448 | analysis over the period 1985-2020 and for different seasons, although the FFNN model was not constrained by

449 in-situ  $f\text{CO}_2$  before 1991 or, few data in austral winter since 1991, and no Chl-a satellite data available before  
450 1998. Interestingly, in 1985 Nevertheless, the atmospheric  $f\text{CO}_2$  was around 335-339  $\mu\text{atm}$  (Dlugokenky and  
451 Tans, 2022) and the oceanic  $f\text{CO}_2$  from the FFNN model was higher than shows a good agreement with  
452 observations collected in the atmosphere from March to October (1985 (Table S5, Figure S4) resulting in an  
453 annual  $\text{CO}_2$  source of  $+0.8 \text{ mol.m}^{-2}.\text{yr}^{-1}$  in 1985.)  
454

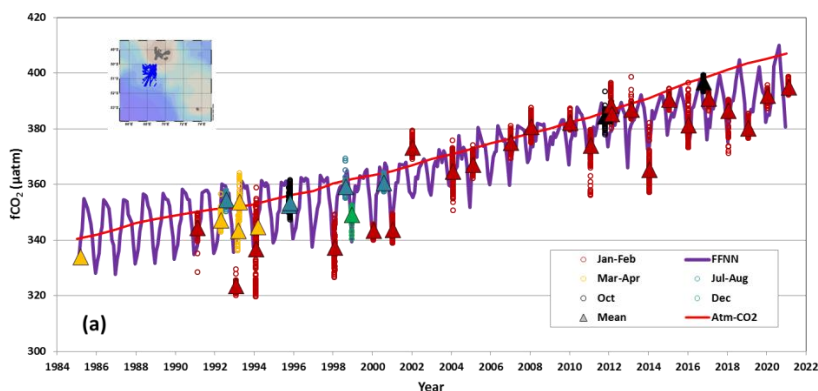
Mis en forme : Police :Times New Roman, 10 pt

455 **3 Results and discussion**

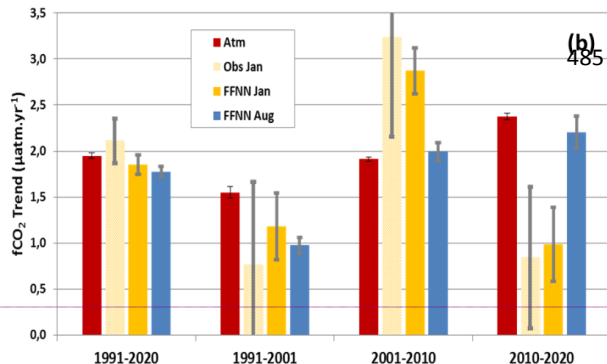
456  
457 **3.1 Variability and trend of sea surface fCO<sub>2</sub> and air-sea CO<sub>2</sub> fluxes: 1985-2021**  
458

459 The fCO<sub>2</sub> observations around 50°S-68°E and their mean values for each cruise are shown in Figure 2a.  
460 The fCO<sub>2</sub> data in 1991-2021 were measurements are available for different seasons but the sampling locations  
461 were mainly re-occupied since 1991, though most of them stem from austral summer (January-February).  
462 During austral summer, the ocean fCO<sub>2</sub> was generally lower than in the atmosphere (i.e. the ocean was a CO<sub>2</sub>  
463 sink) whereas in March from July to October it was near equilibrium. The same distribution seasonal change is  
464 obtained from the FFNN model for the period 1991-2020 (Figure 2a). The model also indicates that between  
465 1985-1998 and the mid-1990s the fCO<sub>2</sub> during austral winter (May-September) was always higher than the  
466 atmospheric fCO<sub>2</sub> leading to an annual CO<sub>2</sub> source during this period (Figure 3). In 1985 the oceanic fCO<sub>2</sub> from  
467 the FFNN model was higher than in the atmosphere from March to October (Figure S4) resulting in an annual  
468 CO<sub>2</sub> source of +0.8 molC.m<sup>-2</sup>.yr<sup>-1</sup>. The model estimates a decrease of the annual CO<sub>2</sub> source in 1985-2001 until  
469 the end of the 1990's followed by an increase of the source in 2001-2010 and an increase of the sink in 2010-  
470 2020.

Mis en forme : Police :Non Gras,  
Couleur de police : Rouge foncé  
Mis en forme : Espace Après : 10 pt,  
Interligne : Multiple 1,15 li



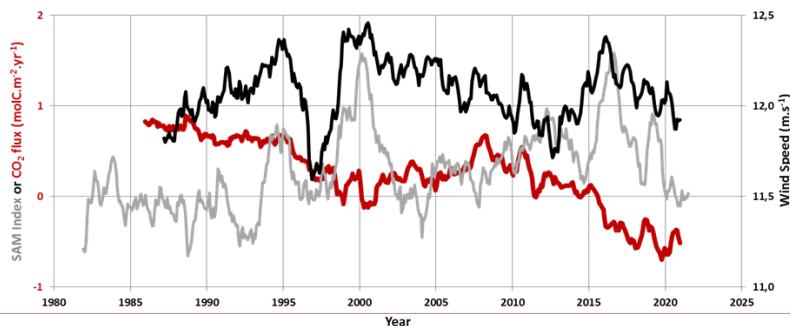
473  
474  
475  
476  
477  
478  
479  
480  
481  
482  
483  
484  
485 over the decade ( following



Mis en forme : Couleur de police :  
Automatique  
Mis en forme : Retrait : Première ligne  
: 1,25 cm  
Mis en forme : Police :Times New  
Roman, 9 pt, Couleur de police :  
Automatique  
Mis en forme : Interligne : simple

495  
496 **Figure 2:** (a): Time series of sea surface fCO<sub>2</sub> observations (µatm) South West of Kerguelen Island in 1985-2021 (insert map  
497 shows the location of observations selected around station at 50°40'S 68°25'E). The color dots correspond to 5 seasons

498 (January-February, March-April, July-August, October and December) and triangles the average for each period. The  
 499 monthly sea surface  $f\text{CO}_2$  from the FFNN model is presented for the period 1985-2020 (purple line) and the atmospheric  
 500  $f\text{CO}_2$  represented by red line. In March 1985 there were no underway  $f\text{CO}_2$  observations and the triangle corresponds to  $f\text{CO}_2$   
 501 calculated with  $A_T$ - $C_T$  data in the mixed layer. (b): Trends of atmospheric and oceanic  $f\text{CO}_2$  ( $\mu\text{atm}\cdot\text{yr}^{-1}$ ) for different season  
 502 and periods based on observations (January) and the FFNN model (January or August).



Mis en forme : Interligne : Multiple 1,15 li

Mis en forme : Police : +Corps (Calibri), 11 pt

Mis en forme : Couleur de police : Rouge foncé

Mis en forme : Police : 10 pt

Mis en forme : Police : 10 pt

Mis en forme : Police : 10 pt

Mis en forme : Police : 10 pt

519 **Figure 3:** Time series of the SAM index (in grey) in the Southern Ocean, wind speed (in black,  $\text{m}\cdot\text{s}^{-1}$ ) and air-sea  $\text{CO}_2$  flux (in red) from the FFNN model (in red) at location  $50.5^\circ\text{S}$ -  
 520  $68.5^\circ\text{E}$ . Positive (negative) flux represents  $\text{CO}_2$  source (sink). Wind speed and SAM are presented for respectively 12-months  
 521 and 24-months running mean based on monthly values. Note the positive SAM in 1998-2003 and 2010-2020. SAM data from  
 522 Marshall (2003), <http://www.nere-bas.ac.uk/ied/gjma/sam.html>, and then decreased over the last access 14/8/2021. Wind  
 523 speed data from ERA5 (Hersbach et al., 2020).  
 524  
 525

526 For the last cruise in February 2021, the average  $f\text{CO}_2$  was  $394.9 (\pm 1.5) \mu\text{atm}$  (Figure 2a), about 10  
 527  $\mu\text{atm}$  lower than in the atmosphere (a small decade to change into an annual  $\text{CO}_2$  sink). This is  $+50.5 \mu\text{atm}$  higher  
 528 than  $f\text{CO}_2$  observed during the first cruise in February 1991 ( $f\text{CO}_2 = 344.4 \pm 5.2 \mu\text{atm}$ ). During the same period,  
 529 the atmospheric  $\text{CO}_2$  that increased from 354 ppm in 1991 to 411 ppm reach  $-0.5 \text{ molC}\cdot\text{m}^{-2}\cdot\text{yr}^{-1}$  in 2021 in 2020.  
 530 For this region (recorded at Crozet Island, Dlugokeneky and Tans, 2022). This first comparison of two cruises 30  
 531 years apart indicates that the ocean  $f\text{CO}_2$  increased at a rate ( $+1.7 \mu\text{atm}\cdot\text{yr}^{-1}$ ) close to that of the atmosphere ( $+1.9$   
 532  $\mu\text{atm}\cdot\text{yr}^{-1}$ ). During the same period reason and given the data available since 1991, we observed some variations  
 533 in  $A_T$  (average  $A_T = 2276.5 \pm 4.5 \mu\text{mol}\cdot\text{kg}^{-1}$ ) and a clear increase in  $C_T$  (Figure 4a and S5).

534 The  $C_T$  concentration in the mixed layer in evaluated the summer 2021 was  $2134.0 (\pm 1.8) \mu\text{mol}\cdot\text{kg}^{-1}$ ,  
 535 much higher than in summer 1993 ( $C_T = 2115.8 \pm 2.6 \mu\text{mol}\cdot\text{kg}^{-1}$ ). The difference over 28 years of  $+22.1$   
 536  $\mu\text{mol}\cdot\text{kg}^{-1}$  corresponds to an annual  $C_T$  increase of  $+0.8 \mu\text{mol}\cdot\text{kg}^{-1}\cdot\text{yr}^{-1}$ . At constant temperature and  $A_T$  this  
 537 would translate in an increase of oceanic  $f\text{CO}_2$  of  $+1.9 \mu\text{atm}\cdot\text{yr}^{-1}$ , i.e. equal to the atmospheric rate. The same  
 538 comparison for October shows that  $f\text{CO}_2$  in 2016 was  $+43.8 \mu\text{atm}$  higher and winter trends in  $f\text{CO}_2$ ,  $C_T$  and  $\text{pH}$   
 539 from the FFNN model over 3 periods 1991-2001, 2001-2010, 2010-2020 and compared to 1995 (Figure 2a), i.e.  
 540 a rate of  $+2.1 \mu\text{atm}\cdot\text{yr}^{-1}$ . The  $C_T$  concentrations in October 2016 were also much higher than in 1993 (Figure 4a  
 541 and S5). Over 23 years the observed  $C_T$  increase in October ( $+22.6 \mu\text{mol}\cdot\text{kg}^{-1}$ ) corresponds to a rate of  $+0.98$   
 542  $\mu\text{mol}\cdot\text{kg}^{-1}\cdot\text{yr}^{-1}$  that is faster than the rate of  $+0.8 \mu\text{mol}\cdot\text{kg}^{-1}\cdot\text{yr}^{-1}$  derived from summer data in 2021 and 1993. At  
 543 constant  $A_T$  this would translate in an increase of oceanic  $f\text{CO}_2$  of  $+2.5 \mu\text{atm}\cdot\text{yr}^{-1}$  in October, higher than the  
 544 trend of  $+2.1 \mu\text{atm}\cdot\text{yr}^{-1}$  computed from  $f\text{CO}_2$  data. Part of the difference may be explained by  $A_T$  that was  
 545 slightly higher ( $+6 \mu\text{mol}\cdot\text{kg}^{-1}$ ) in October 2016 compared to 1993 (Figure S5).

546 Given the temporal variability of observed  $C_T$  in summer and the evolution of the annual air-sea  $CO_2$   
547 flux (Figure 3), decadal  $fCO_2$  and pH trends as well as the summer trends with those deduced from observations  
548 (Table 2). The analysis of trends and their associated drivers need to be analyzed for different seasons and  
549 periods. This approach allows exploring will allow to explore links with the variability of primary production  
550 and/or the Southern Annual Mode (SAM). Shifts from a negative to a positive to a negative SAM index (Figure  
551 3) will strengthen may have strengthened the upwelling of deep waters and could therefore impact ocean  
552 properties throughout the water column including  $C_T$ , nutrients, primary production or pH (e.g. Lovenduski and  
553 Gruber, 2005; Lenton et al., 2009; Hauck et al., 2013; Hoppema et al., 2015; Pardo et al., 2017).

554 From the first underway measurements obtained at the OISO-KERFIX site in February 2021 to the last  
555 measurements used in this study in February 1991, the average oceanic  $fCO_2$  increased by +50.5  $\mu atm$  (from  
556  $344.4 \pm 1.5 \mu atm$  to  $394.9 \pm 1.5 \mu atm$ , Figure 2a). During the same period, the atmospheric  $CO_2$  increased by 57  
557  $\mu atm$  in this region (recorded at Crozet Island, Dlugokencky and Tans, 2022). This first comparison of two  
558 cruises 30 years apart indicates that the oceanic  $fCO_2$  increase was close to that of the atmosphere. During the  
559 same period, we observed small variations in  $A_T$  (average  $A_T = 2276.5 \pm 4.5 \mu mol.kg^{-1}$ ) and a clear increase in  $C_T$   
560 (Figure 4a and S5). This suggests that most of the change observed in oceanic  $fCO_2$  and  $C_T$  over the last 30 years  
561 is due to the uptake of anthropogenic  $CO_2$ . However, the evolution of air-sea  $CO_2$  fluxes (Figure 3) suggests that  
562 other mechanisms were at play over shorter periods, and changes in the air-sea  $fCO_2$  disequilibrium (Figure 2a)  
563 suggests that different drivers may be involved in summer and in winter.  
564

Mis en forme : Couleur de police :  
Automatique



565  
566  
567  
568  
569  
570  
571  
572  
573  
574  
575  
576  
577  
578  
579  
580  
581  
582  
583  
584  
585  
586  
587  
588  
589  
590  
591  
592  
593  
594  
595  
596  
597  
598  
599  
600  
601  
602  
603  
604  
605  
606  
607  
608  
609  
610  
611  
612

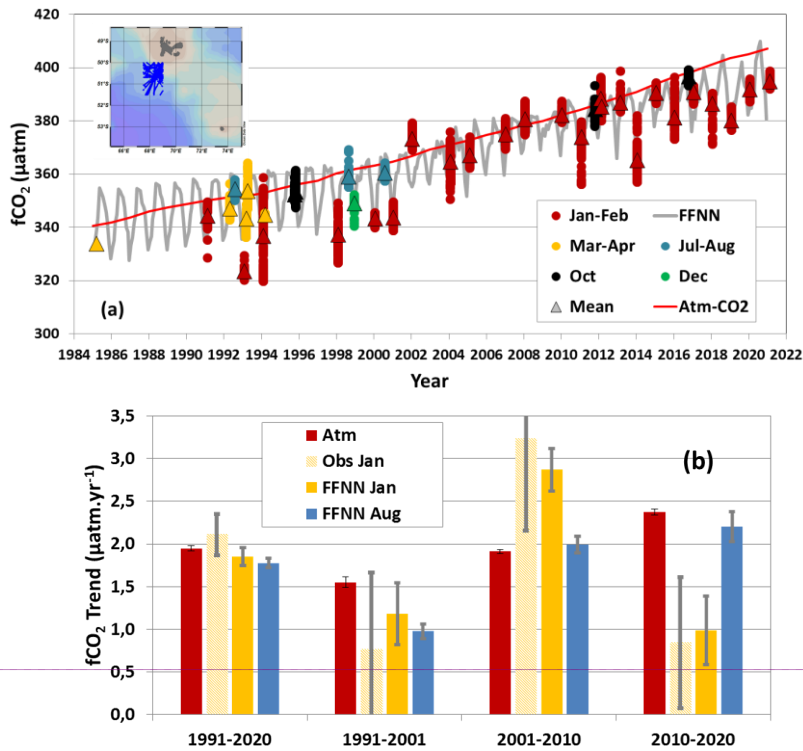
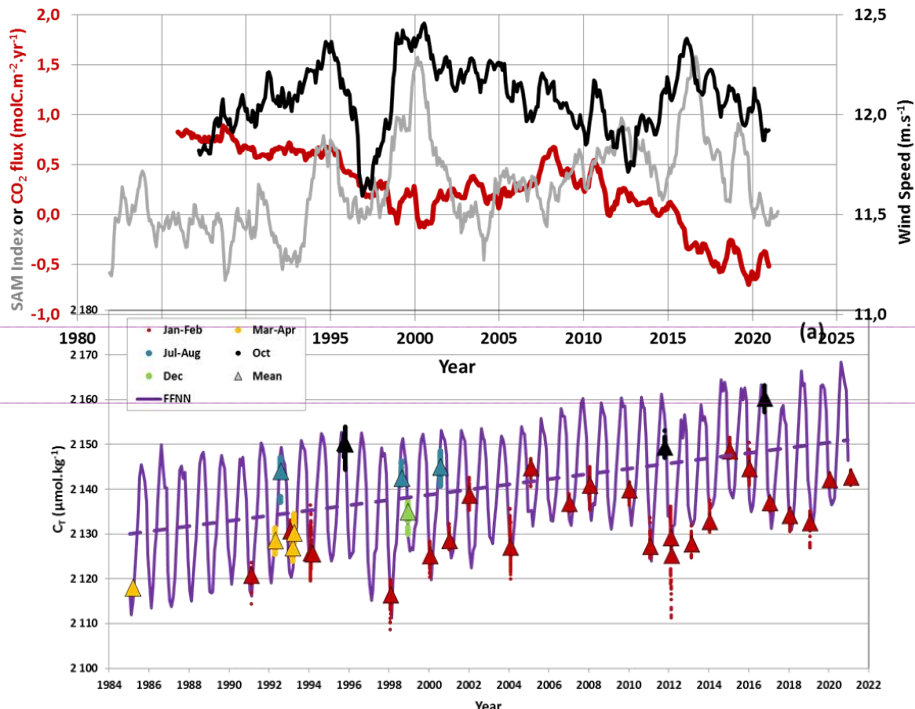


Figure 2: (a): Time-series of sea surface  $f\text{CO}_2$  observations ( $\mu\text{atm}$ ) south-west of Kerguelen Islands in 1985-2021 (insert map shows the location of observations selected around station OISO-KERFIX at  $50^{\circ}40'S-68^{\circ}25'E$ ). The color dots correspond to 5 periods of the year (January-February, March-April, July-August, October and December) and triangles show the average for each month. The monthly sea surface  $f\text{CO}_2$  from the FFNN model is presented for the period 1985-2020 (grey line) and the atmospheric  $f\text{CO}_2$  is represented by the red line. In March 1985 there was no underway  $f\text{CO}_2$  observation and the triangle corresponds to  $f\text{CO}_2$  calculated with  $A_T$  and  $C_T$  measured in the mixed-layer. (b): Trends of atmospheric and oceanic  $f\text{CO}_2$  ( $\mu\text{atm.yr}^{-1}$ ) in summer and winter over four different periods based on observations (January) and the FFNN model (January and August).

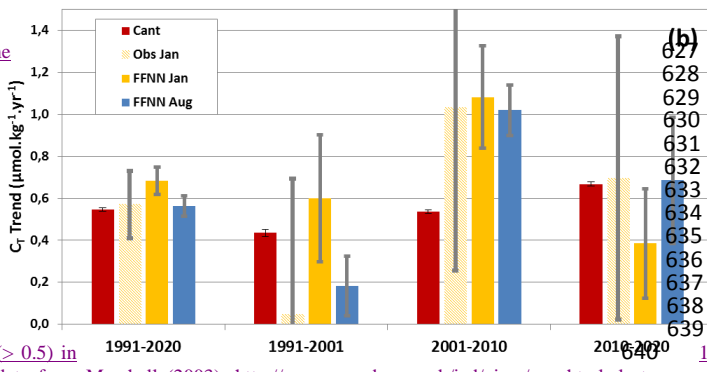
- Mis en forme : Couleur de police : Automatique
- Mis en forme : Retrait : Première ligne : 1,25 cm
- Mis en forme : Police : Times New Roman, 9 pt, Couleur de police : Automatique
- Mis en forme : Interligne : simple



- Mis en forme : Interligne : Multiple 1,15 li
- Mis en forme : Police : +Corps (Calibri), 11 pt
- Mis en forme : Couleur de police : Rouge foncé

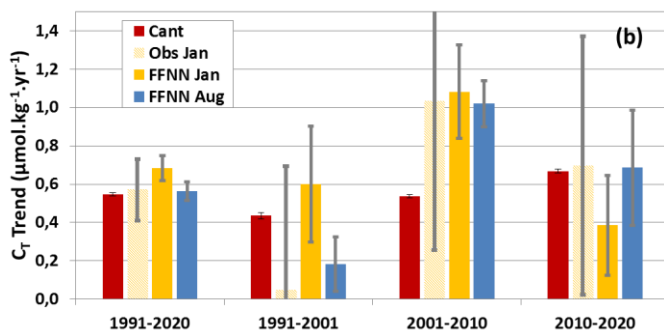
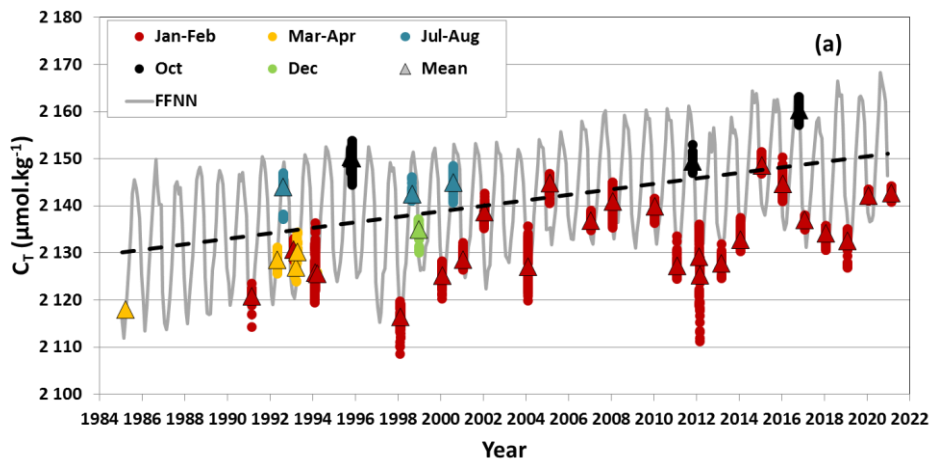
613  
614  
615  
616  
617  
618  
619  
620  
621  
622  
623  
624  
625  
626  
627  
628  
629  
630  
631  
632  
633  
634  
635  
636  
637  
638  
639  
640  
641  
642  
643

Figure 3: Time series of the SAM index in the Southern Ocean (in grey), CO<sub>2</sub> flux (in black, m.s<sup>-1</sup>) from the location A (in red) at 50.5°S-68.5°E. A positive flux (negative flux) represents a CO<sub>2</sub> source (sink). Wind-speed and SAM for 24-months based on monthly the positive SAM (> 0.5) in 1991-2020, 1991-2001, 2001-2010, 2010-2019, SAM data from Marshall (2003), <http://www.nerc-bas.ac.uk/icd/gjma/sam.html>, last access 14/8/2021. Wind speed data from ERA5 (Hersbach et al., 2020).



series of the the Southern wind-speed and air-sea (molC.m<sup>-2</sup>.yr<sup>-1</sup>) FFNN model location A positive represents a (sink). Wind-are presented running mean values. Note 1998-2002 and

644  
645  
646  
647  
648  
649  
650  
651  
652  
653  
654  
655  
656  
657  
658  
659  
660  
661  
662  
663  
664



665  
666  
667  
668  
669  
670  
671  
672  
673  
674  
675  
676  
677  
678  
679  
680  
681  
682  
683  
684  
685  
686  
687  
688  
689  
690  
691  
692  
693  
694  
695  
696  
697  
698  
699  
700  
701  
702  
703  
704  
705  
706  
707  
708  
709  
710  
711  
712  
713  
714  
715

Figure 4: (a): Time-series of surface  $C_T$  ( $\mu\text{mol.kg}^{-1}$ ) around station OISO/KERFIX at  $50^\circ40'S-68^\circ25'E$  calculated from  $f\text{CO}_2$  data (Figure 2) using the A<sub>T</sub>/S relation (see textSect 2.2.5). The color dots correspond to 5 seasons periods of the year (January-February, March-April, July-August, October and December) and triangles show the average for each cruise month. The monthly sea surface  $C_T$  from the FFNN model is presented for the period 1985-2020 (purplegrey line). The annual  $C_T$  trend of  $+0.58 \pm 0.05 \mu\text{mol.kg}^{-1}.\text{yr}^{-1}$  (dashed line) is derived from the FFNN monthly data. In March 1985 the triangle corresponds to the observed  $C_T$  in the mixed-layer. (b): Trends of sea surface  $C_T$  ( $\mu\text{mol.kg}^{-1}.\text{yr}^{-1}$ ) for in summer and winter over four different season-and-periods based on observations (for January) and the FFNN model (for January and August). The trend for  $C_{\text{ant}}$  ( $\mu\text{mol.kg}^{-1}.\text{yr}^{-1}$ ) is also shown (red bars) based on estimates in the winter-water Winter Water.

Mis en forme : Couleur de police : Automatique

Mis en forme : retrait : Première ligne : 0 cm

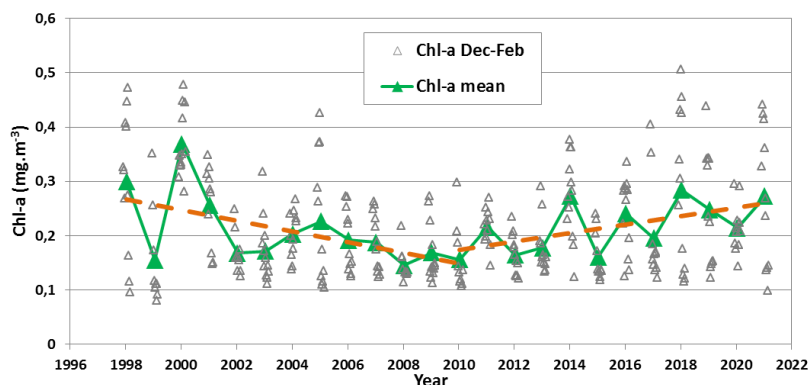
Summer data are characterized by a strong inter-annual variability between 1991-2021 in both  $f\text{CO}_2$  and  $C_T$  (Figures 2a and 4a) with the ocean being a  $\text{CO}_2$  source in January 2002, but a strong sink in January 1993, 1998, 2014, 2016 and 2019. In January 1998, when the surface ocean experienced a warm anomaly (Jabaud-Jan et al., 2004), the low  $f\text{CO}_2$  of  $337 \mu\text{atm}$  and the low  $C_T$  of  $2110 \mu\text{mol.kg}^{-1}$  (Figure 4a and S5) co-occurred with intense primary production (Figure 5), probably supported by diatoms as suggested by very low DSI concentrations ( $< 2 \mu\text{mol.kg}^{-1}$  down to 100m, Figure S6). In January 2014 and 2016, mixed-layer DSI concentrations were also remarkably small ( $< 5 \mu\text{mol.kg}^{-1}$  down to 75m, Figure S6). In 2014 low DSI coincided with Chl-a levels that started to increase in mid-November 2013 and stayed at high level until February 2014 (Surface Chl-a  $> 0.3 \text{ mg.m}^{-3}$ , Figures 5 and S7). The intense primary production contributed to the low  $f\text{CO}_2$  of  $365 \mu\text{atm}$  reached by mid-January 2014, a value as low as in 2004 10 years earlier (Figure 2a). To the contrary, in 2002 relatively low Chl-a (mean Chl-a  $< 0.2 \text{ mg.m}^{-3}$ , Figure 5) was associated with higher levels of  $f\text{CO}_2$  ( $373 \mu\text{atm}$ ),  $C_T$  ( $2128 \mu\text{mol.kg}^{-1}$ , Figure 4a, Figure S5a) and DSI (Figure S6). This was also associated with higher salinity indicative of entrainment that might be related to storm events that would have occurred few days before the measurements leading to brief positive  $f\text{CO}_2$  anomaly as recently observed from Glider data in the subpolar South Atlantic (Nicholson et al., 2022). As opposed to the other periods the ocean was a source of  $\text{CO}_2$  in summer 2002 (this particular year was not well reconstructed by the FFNN model, Figure 2a and Figure S2b). The important inter-annual variability observed in summer indicates that in this region historically referred to as HNLC (Minas and Minas, 1992), primary production could significantly impact  $f\text{CO}_2$  level in summer (Jabaud-Jan et al., 2004; Pasquer et al., 2015; Gregor et al., 2018), a result that needs to be taken into account when evaluating drivers of inter-annual variability (Rustogi et al., 2023) and the decadal trends of  $f\text{CO}_2$  or pH.

Table 2: Trends of oceanic  $f\text{CO}_2$  ( $\mu\text{atm.yr}^{-1}$ ), pH (TS.decade<sup>-1</sup>) and  $C_T$  ( $\mu\text{mol.kg}^{-1}.\text{yr}^{-1}$ ) at the OISO-KERFIX location ( $50^\circ40'S-68^\circ25'E$ ) in the Southern Indian Ocean for different periods based on observations (Obs.) and the FFNN model (FFNN). Standard-deviations are given in brackets.

Period	Season	Trend $f\text{CO}_2$ $\mu\text{atm.yr}^{-1}$	Trend pH TS.decade <sup>-1</sup>	Trend $C_T$ $\mu\text{mol.kg}^{-1}.\text{yr}^{-1}$	
1962-2016	November	1.31 (0.32)	-0.014 (0.002)	0.47 (0.01)	Obs.
1991-2021	Summer	2.10 (0.22)	-0.022 (0.002)	0.57 (0.16)	Obs.
1991-2001	Summer	0.76 (0.90)	-0.009 (0.010)	0.05 (0.64)	Obs.
2001-2010	Summer	3.23 (1.07)	-0.035 (0.011)	1.03 (0.77)	Obs.
2010-2020	Summer	0.84 (0.77)	-0.008 (0.008)	0.70 (0.68)	Obs.
1985-2020	Summer	1.71 (0.08)	-0.018 (0.001)	0.68 (0.05)	FFNN

716	1991-2020	Summer	1.85 (0.11)	-0.020 (0.001)	0.68 (0.07)	FFNN
717	1991-2001	Summer	1.18 (0.26)	-0.013 (0.004)	0.60 (0.30)	FFNN
718	2001-2010	Summer	2.87 (0.25)	-0.030 (0.003)	1.08 (0.24)	FFNN
719	2010-2020	Summer	0.98 (0.40)	-0.010 (0.004)	0.38 (0.26)	FFNN
720						
721	1985-2020	Winter	1.64 (0.05)	-0.017 (0.001)	0.55 (0.04)	FFNN
722	1991-2020	Winter	1.78 (0.15)	-0.018 (0.001)	0.56 (0.05)	FFNN
723	1991-2001	Winter	0.98 (0.09)	-0.010 (0.001)	0.18 (0.14)	FFNN
724	2001-2010	Winter	1.99 (0.10)	-0.021 (0.001)	1.02 (0.12)	FFNN
725	2010-2020	Winter	2.21 (0.17)	-0.022 (0.002)	0.69 (0.30)	FFNN
726						
727	1985-2020	Annual	1.57 (0.03)	-0.0165(0.0004)	0.58 (0.05)	FFNN

730 The Chl-a time-series derived from MODIS suggests higher concentrations in recent years compared to  
731 2002-2013, with Chl-a peaks identified in 2014, 2016, 2018, 2019 and 2021 (Figure 5 and S7) when the oceanic  
732 fCO<sub>2</sub> in summer was well below the atmospheric level (Figure 2a).



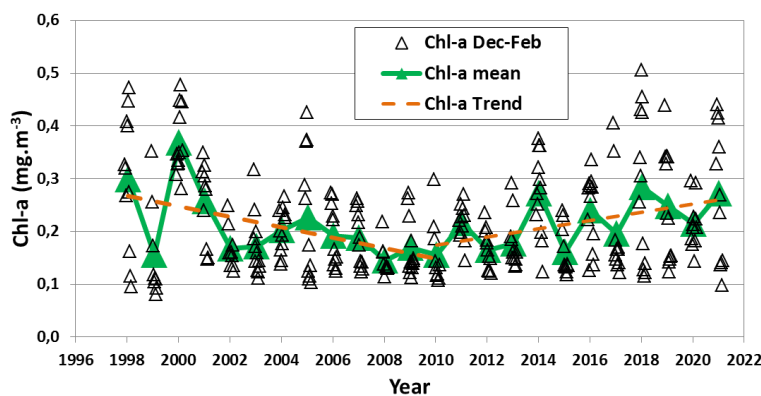
744 Figure 5: Time-series (1998-2021) of sea surface Chl-a (mg.m<sup>-3</sup>) in summer (December-February) from weekly satellite data  
745 (SeaWiFS and MODIS, triangles) and associated mean (green triangles). The trends in 1998-2010 and 2010-2021 of  
746 respectively -0.0099 (± 0.0041) and +0.0078 (± 0.0032) mg.m<sup>-3</sup>.yr<sup>-1</sup> (dashed orange) indicate a decrease or increase of the  
747 primary production that drives part of the fCO<sub>2</sub> and C<sub>T</sub> stability observed in the recent period (Figure 2, Figure 4). The full  
748 Chl-a record is shown in Supp. Mat. Figure S7.

Mis en forme : Retrait : Première ligne : 0 cm, Interligne : simple

750 The primary production lowers C<sub>T</sub> concentrations and fCO<sub>2</sub>, i.e. opposite to the C<sub>T</sub> increase from  
751 anthropogenic CO<sub>2</sub> uptake. These counteracting processes might explain the relatively stable fCO<sub>2</sub> previously  
752 observed in the Indian POOZ in summer 2007-2019 with an annual fCO<sub>2</sub> rate of increase of only +0.3 (± ±0.2)  
753 μatm.yr<sup>-1</sup> (Leseurre et al., 2022). This low rate is confirmed here with the new recent data obtained in 2020-2021  
754 (Figure 2b and Figure S8). For the period 2010-2021, the oceanic fCO<sub>2</sub> trend in summer derived from  
755 observations and the FFNN model is lower than +1 μatm.yr<sup>-1</sup> (Table 42), i.e. much lower than the atmospheric  
756 fCO<sub>2</sub> rate of +2.4 μatm.yr<sup>-1</sup> and the oceanic fCO<sub>2</sub> trend of +2.21 (± ±0.17) μatm.yr<sup>-1</sup> estimated in winter (by the  
757 FFNN model (Table 2, Figure 2b). This rate is also lower compared to the change observed in October (+2.9  
758 μatm.yr<sup>-1</sup>) albeit being only based on 2 cruises in October 2011 and 2016 (Figure 2a). As the low fCO<sub>2</sub> trend in  
759 recent years is detected for summer only this is likely linked to an increase in primary production, as suggested  
760 by Chl-a records (Figure 5). InFrom 1998- to 2010 the summer Chl-a concentrations decreased at a rate of -0.099  
761 (± ±0.041) mg.m<sup>-3</sup>.decade<sup>-1</sup> whereas in 2010- from 2020 to 2021 Chl-a increased by +0.078 (± ±0.032) mg.m<sup>-3</sup>  
762 .decade<sup>-1</sup> (Figure 5). These trends are coherent with previous studies, e.g. the reduced net primary productivity  
763 reported in the Indian Antarctic zone in over 1997-2007 (e.g. Arrigo et al., 2008; Takao et al., 2012) and the shift

Mis en forme : Couleur de police : Automatique

764 of the Chl-a trend in 2010 also reported at large scale in the HNLC region of the Southern Ocean in 2010  
 765 (Basterretxea et al., 2023). As a consequence, after 2010 the difference between oceanic and atmospheric  $f\text{CO}_2$   
 766  $\Delta f\text{CO}_2$  (where  $\Delta f\text{CO}_2 = f\text{CO}_2^{\text{occ}} - f\text{CO}_2^{\text{atm}}$ ) decreased in summer ( $-1.4 \mu\text{atm.yr}^{-1}$ ) and as it remains relatively  
 767 steady during winter, the annual  $\text{CO}_2$  flux progressively varied from a source of  $+0.45 \text{ molC.m}^{-2}.\text{yr}^{-1}$  in 2010 to a  
 768 sink of  $-0.63 \text{ molC.m}^{-2}.\text{yr}^{-1}$  in 2020 (Figure 3). In addition, because the wind speed was stable during this  
 769 period ( $12.0 \pm 0.9 \text{ m.s}^{-1}$  on average in 2010-2020, Figure 3), the variation of the air-sea  $\text{CO}_2$  flux was mainly  
 770 controlled by  $\Delta f\text{CO}_2$  (e.g. Gu et al., 2023) and the decadal variation of primary production imprinted a  
 771 significant change on the  $f\text{CO}_2$  trend and air-sea  $\text{CO}_2$  flux in this HNLC region. In the region investigated here,  
 772 increasing Chl-a levels co-occurred with shifts of the SAM index to a positive state (Figure 3), a link previously  
 773 suggested south of the Polar Front in the SO but for a short period over 1997-2004 (Lovenduski and Gruber,  
 774 2005). Modeling studies also suggest that summertime biological activity could play an important role for the  
 775 variability of the  $\text{CO}_2$  sink in the SO in response to the SAM (Hauck et al, 2013).



777  
 778  
 779  
 780  
 781  
 782  
 783  
 784  
 785  
 786  
 787 Figure 5: Time-series (1998-2021) of sea surface Chl-a ( $\text{mg.m}^{-3}$ ) in summer (December-February) from weekly satellite data  
 788 (SeaWiFS and MODIS, triangles) and associated mean (green triangles). The trends in 1998-2010 and 2010-2021 of  
 789 respectively  $-0.0099 \pm 0.0041$  and  $+0.0078 \pm 0.0032 \text{ mg.m}^{-3}.\text{yr}^{-1}$  (dashed orange) indicate a decrease or increase of the  
 790 primary production. The full Chl-a record is shown in Supp. Mat. Figure S7.

Mis en forme : Retrait : Première ligne : 0 cm, Interligne : simple

Mis en forme : Retrait : Première ligne : 0 cm

793 Another process to take into account for interpreting  $f\text{CO}_2$  trends is the change in temperature in surface  
 794 waters. Previous analysis suggested a progressive warming in the region investigated here (Auger et al., 2021 for  
 795 summer 1993-2017). For 1998-2019 Leseurre et al. (2022) estimated a warming of Indian POOZ surface  
 796 waters of  $+0.03 (\pm \pm 0.02) \text{ }^\circ\text{C.yr}^{-1}$ . Extending the time-series for the period 1991-2021 (Figure S9a) we note that  
 797 the surface temperature presents sub-decadal variability and that the ocean cooled after 2018 with a trend of  $-$   
 798  $0.474 (\pm \pm 47 \pm 0.164)16 \text{ }^\circ\text{C.yr}^{-1}$  in 2018-2021 based on the monthly sea surface temperature (SST, Figure  
 799 S9b). The trend derived from our in-situ observations in summer 2018-2021 over this period was  $-0.253 (\pm \pm 25$   
 800  $\pm 0.092)09 \text{ }^\circ\text{C.yr}^{-1}$ .

801 In 2019, the lower temperature and relatively high Chl-a leaded to low  $f\text{CO}_2$  ( $380 \mu\text{atm}$ , Figure 2a) and  
 802 low  $C_T$  ( $2128 \mu\text{mol.kg}^{-1}$ ) compared to 2018 ( $f\text{CO}_2 = 386 \mu\text{atm}$ ;  $C_T = 2137 \mu\text{mol.kg}^{-1}$ , Figure 4a). The decrease in  
 803 observed  $f\text{CO}_2$  from summer 2018 to 2019, also reconstructed by the FFNN model (Figure 2a), is contrary to the  
 804 expected  $f\text{CO}_2$  and  $C_T$  increase due to anthropogenic uptake. In 2020, although the temperature was also lower  
 805 than in 2019, the oceanic  $f\text{CO}_2$  was higher ( $392 \mu\text{atm}$ ) probably due to lower primary production as suggested by  
 806 higher DSi (Figure S6), as well as from  $C_T$  ( $2135 \mu\text{mol.kg}^{-1}$ , Figure 4a) and Chl-a records (Figure 5). In January

807 2021 the temperature was close to that in January 2020, and both  $f\text{CO}_2$  and  $C_T$  were slightly higher ( $395 \mu\text{atm}$ ,  
 808  $2139 \mu\text{mol.kg}^{-1}$ ).  $A_T$  concentrations were stable between 2018 and 2021 ( $2278.9 \pm 1.8 \mu\text{mol.kg}^{-1}$ , Figure S5)  
 809 indicating no effect of  $A_T$  on the observed  $f\text{CO}_2$  change in this region as opposed to the areas north of the Polar  
 810 Front in the Indian Ocean where  $A_T$  variations are often linked to coccolithophores blooms (Balch et al., 2016;  
 811 Smith et al., 2017).

812 The inter-annual and pluri-annual variability observed ~~in~~over 1991-2021 highlights the competitive  
 813 processes that drive  $C_T$ ,  $f\text{CO}_2$  or pH temporal variations. ~~In summer 2018-2019, cooling and increased primary~~  
 814 ~~production both lead to low  $f\text{CO}_2$ , counteracting the effect of anthropogenic  $\text{CO}_2$  uptake. Given the changes of~~  
 815 ~~Chl-a, SST and air-sea  $\text{CO}_2$  flux, trends will be evaluated for three periods, 1991-2001, 2001-2010 and 2010-~~  
 816 ~~2020.~~ In order to separate natural and anthropogenic contributions, the anthropogenic  $\text{CO}_2$  signal is estimated in  
 817 the following section.

818

### 819 3.2 Anthropogenic $\text{CO}_2$

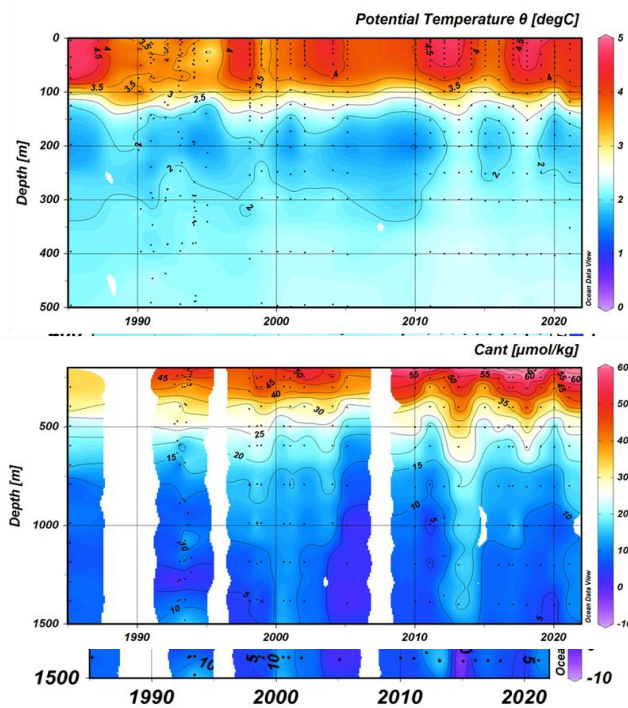
820

#### 821 3.2.1 Anthropogenic $\text{CO}_2$ in the water column

822

823 To calculate anthropogenic  $\text{CO}_2$  concentrations ( $C_{\text{ant}}$ ), we used the TrOCA method developed by  
 824 Touratier et al. (2007) and previously applied in the southern Indian Ocean (Mahieu et al., 2020; Leseurre et al.,  
 825 2022). Such an indirect method is not suitable for evaluating  $C_{\text{ant}}$  concentrations in surface waters due to  
 826 biological activity and gas exchange and we restrict the  $C_{\text{ant}}$  calculations below the productive layer around  
 827 150m. In the region south of the Polar Front, a well-defined subsurface temperature minimum is observed each  
 828 year characterizing the ~~winter water (WW)~~Winter Water (WW) at depth range 150-250m (Figure 6a).

829



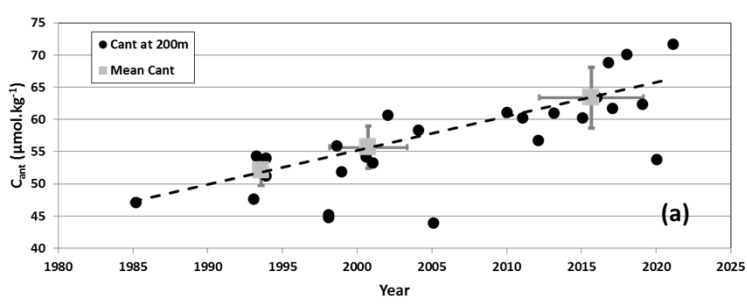
846

848 Figure 6: Hovmoller section (Depth-Time) of (a) potential temperature ( $^{\circ}\text{C}$ ) and (b) anthropogenic  $\text{CO}_2$  ( $C_{\text{ant}}$ ,  $\mu\text{mol.kg}^{-1}$ )  
 849 ~~in~~over 1985-2021 at station OISO-KERFIX ( $50^{\circ}40'S-68^{\circ}25'E$ ). The section for temperature is presented in the layer 0-500m  
 850 and for summer to highlight the temperature minimum around 200m (winter water, WW). The section for  $C_{\text{ant}}$  is limited  
 851 below 200m. Section produced with ODV (Schlitzer, 2018).  
 852

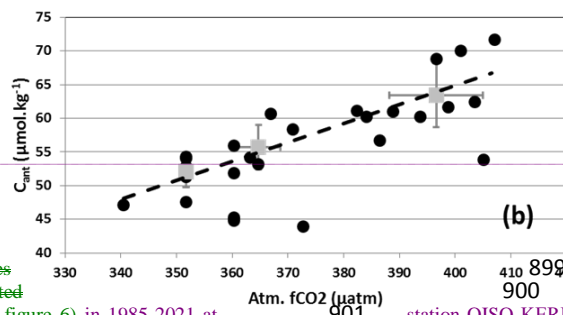
853 The  $C_T$  and  $C_{\text{ant}}$  concentrations increased over time in the water column, a signal that is most  
 854 pronounced in the top layers (~~at~~200-400m, Figure 6b). In the deep layer, the presence of the Indo-Pacific Deep  
 855 Water (IPDW) around 600-800m is identified by a maximum of  $C_T$  ( $C_T > 2250 \mu\text{mol.kg}^{-1}$ ) and a minimum of  $\text{O}_2$   
 856 ( $\text{O}_2$  close to or  $< 180 \mu\text{mol.kg}^{-1}$ , Figure S10) (Talley, 2013; Chen et al., 2022). In the IPDW layer restricted to  
 857 the neutral density (ND) range  $27.75-27.85 \text{ kg.m}^{-3}$  there is no significant change in  $C_T$  over time (Figure S10). In  
 858 that layer the  $C_{\text{ant}}$  concentrations in 1985 ( $17.3 \mu\text{mol.kg}^{-1}$ ) were almost identical to those evaluated in 2021 ( $21.2$   
 859  $\mu\text{mol.kg}^{-1}$ ), considering the uncertainty in the  $C_{\text{ant}}$  calculations ( $\pm 6.5 \mu\text{mol.kg}^{-1}$ , Touratier et al., 2007). ~~As~~  
 860 ~~discussed above (section 2.2.3) the  $C_T$  and  $A_T$  concentrations in the bottom layer ( $>1450\text{m}$ ) were stable in 1985-~~  
 861 ~~2021 (Table S2, Figure S1).~~ Below 800m, the  $C_{\text{ant}}$  concentrations were small but not null (Figure 6b). The  
 862 average  $C_{\text{ant}}$  concentration below 800m for all years and seasons ~~is  $7.97 (\pm \text{was } 8.0 \pm 5.31)3 \mu\text{mol.kg}^{-1}$  ( $n=123$ )~~  
 863 ~~with a very small change detected over time ( $C_{\text{ant}} = 7.73 \pm 7 \pm 1.273 \mu\text{mol.kg}^{-1}$  in 1985 and  $C_{\text{ant}} = 10.45 \pm 4$~~   
 864  ~~$\pm 0.626 \mu\text{mol.kg}^{-1}$  in 2021).~~ ~~As discussed above (section 2.2.3) the  $C_T$  and  $A_T$  concentrations in the bottom layer~~  
 865 ~~( $>1450\text{m}$ ) were stable over 1985-2021 (Table S2, Figure S1).~~  
 866

867 **3.2.2 Anthropogenic  $\text{CO}_2$  trend in the subsurface Winter Water**  
 868

869 To separate the natural and anthropogenic signals in surface waters for the driver analysis we assume  
 870 that  $C_{\text{ant}}$  in the WW is representative of  $C_{\text{ant}}$  in the mixed-layer (ML). This is confirmed with few stations  
 871 occupied during winter showing that  $C_{\text{ant}}$  concentrations in the WW in summer are almost equal to  $C_{\text{ant}}$  in the  
 872 ML during the preceding winter (Figure S11). The ~~variation~~evolution of  $C_{\text{ant}}$  in the WW ~~for~~from 1985- to 2021  
 873 is presented in Figure 7a for all seasons. In 1985 the  $C_{\text{ant}}$  concentration in the WW was  $47.1 \mu\text{mol.kg}^{-1}$  and  $C_{\text{ant}}$   
 874 reached a maximum of  $71.7 \mu\text{mol.kg}^{-1}$  in 2021. The data selected at 200m present some inter-annual variability  
 875 ~~likesuch as~~ the relatively low  $C_{\text{ant}}$  in 1998, 2005 ~~or~~and 2020 probably related to natural variability. In 1998 and  
 876 in 2020 the  $\text{O}_2$  concentrations were slightly lower in the WW ( $< 300 \mu\text{mol.kg}^{-1}$ ) explaining the lower  $C_{\text{ant}}$   
 877 concentration ( $44.8 \mu\text{mol.kg}^{-1}$  in 1998 and  $53.8 \mu\text{mol.kg}^{-1}$  in 2020). ~~In 2005 anomalies of  $C_T$ ,  $\text{O}_2$  and~~  
 878 ~~temperature) but no anomaly was observed for  $C_T$ . This suggests that the biological contribution may have been~~  
 879 ~~overestimated (lower  $\text{O}_2$  is interpreted by the TrOCA method as more organic matter remineralization which~~  
 880 ~~should be associated with higher  $C_T$ ). This could be instead related to a change in mixing or circulation. In 2005~~  
 881 ~~anomalies of  $C_T$ ,  $A_T$  and  $\text{O}_2$  concur to explain the lower  $C_{\text{ant}}$  ( $43.9 \mu\text{mol.kg}^{-1}$ ).~~  
 882



890  
891  
892  
893  
894  
895  
896  
897  
898  
899  
900  
901  
902  
903  
904  
905



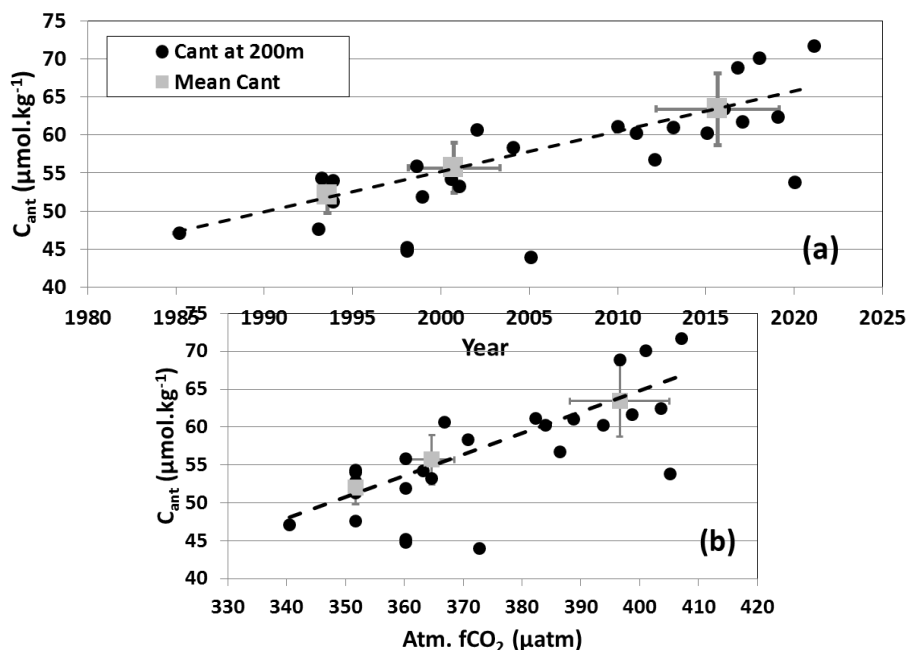
Mis en forme : Police :9 pt, Couleur de police : Rouge foncé  
Mis en forme : Retrait : Première ligne : 0 cm, Interligne : simple, Taquets de tabulation : 12,75 cm,Gauche

Figure 7: (a): Time series of anthropogenic CO<sub>2</sub> (C<sub>ant</sub> μmol.kg<sup>-1</sup>) estimated in the winter water layer (WW around 200m, see figure 6) in 1985-2021 at station OISO KERFIX (50°40'S 68°25'E). Black dots are the individual data in the WW and the grey squares the average for the 1990s, 2000s and 2010s (anomalies in 1998, 2005 and 2020 filtered). The C<sub>ant</sub> trend of +0.53 (± 0.01) μmol.kg<sup>-1</sup>.yr<sup>-1</sup> is represented (dashed line). (b): same data for C<sub>ant</sub> versus atmospheric fCO<sub>2</sub> (the slope is +0.263 ± 0.042 μmol.kg<sup>-1</sup>.μatm<sup>-1</sup>).

906  
907  
908  
909  
910  
911  
912  
913  
914  
915  
916  
917  
918  
919  
920

From 1985 to 2021, we estimate a C<sub>ant</sub> trend in WW of +0.49 (±0.09) μmol.kg<sup>-1</sup>.yr<sup>-1</sup>. When the C<sub>ant</sub> anomalies in 1998, 2005 and 2020 were discarded, this C<sub>ant</sub> trend was +0.53 (±0.01) μmol.kg<sup>-1</sup>.yr<sup>-1</sup> (Figure 7a). As expected, the C<sub>ant</sub> concentrations in the ocean are positively related to atmospheric CO<sub>2</sub> (slope +0.263 ± 0.042 μmol.kg<sup>-1</sup>.μatm<sup>-1</sup>, Figure 7b). Interestingly the slope observed south of the PF in the Indian Ocean is close to that observed in the Antarctic Intermediate waters (AAIW) in the South Atlantic (+0.23 ± 0.05 μmol.kg<sup>-1</sup>.μatm<sup>-1</sup>, Fontela et al., 2021). At large scale, Gruber et al. (2019 a, b) evaluated C<sub>ant</sub> changes between 1994 and 2007 in the global ocean. In the South Indian sector, they estimated a mean C<sub>ant</sub> accumulation in at the surface of +6.0 (±1.1) μmol kg<sup>-1</sup> in the band 50-55°S south of the PF. At our station location (50-52°S/68°E) in the layer 0-250m, the C<sub>ant</sub> accumulated from 1994 to 2007 was +5.67 (±1.47) μmol kg<sup>-1</sup>. In 13 years, this corresponds to a trend of +0.44 (±0.11) μmol.kg<sup>-1</sup>.yr<sup>-1</sup>. Gruber et al. (2019 a, b) did not use the data presented here allowing for an independent comparison to the present study. Estimates of C<sub>ant</sub> accumulation by Gruber et al. (2019 a, b) are in agreement with ours for 1991-2008 the period 1994-2007 (+0.46 μmol ± 0.01 μmol.kg<sup>-1</sup>.yr<sup>-1</sup>) but lower than reported here between 2008 and 2021 in recent years (+0.61 ± 0.01 μmol.kg<sup>-1</sup>.yr<sup>-1</sup> over 2008-2021). Indeed our estimates over 3 decades indicate an increase in the uptake of anthropogenic CO<sub>2</sub> with time (Figure 4b).

921  
922  
923  
924  
925  
926  
927  
928  
929  
930  
931  
932  
933  
934





935  
936  
937  
938  
939  
940  
941  
942  
943  
944  
945  
946  
947  
948  
949

Figure 7: (a): Time-series of anthropogenic CO<sub>2</sub> (C<sub>ant</sub>, μmol.kg<sup>-1</sup>) estimated in the winter water layer (WW around 200m, see figure 6) from 1985 to 2021 at station OISO-KERFIX (50°40'S-68°25'E). Black dots are the individual data in the WW and the grey squares the average for the 1990s, 2000s and 2010s (anomalies in 1998, 2005 and 2020 discarded). The C<sub>ant</sub> trend of +0.53 ± 0.01 μmol.kg<sup>-1</sup>.yr<sup>-1</sup> is represented (dashed line). (b): same data for C<sub>ant</sub> versus atmospheric fCO<sub>2</sub> (the slope is +0.263 ± 0.042 μmol.kg<sup>-1</sup>.μatm<sup>-1</sup>).

Mis en forme : Police : 9 pt, Couleur de police : Rouge foncé  
Mis en forme : Retrait : Première ligne : 0 cm, Interligne : simple, Taquets de tabulation : 12,75 cm, Gauche

### 950 3.2.3 Anthropogenic and surface C<sub>T</sub> seasonal trends

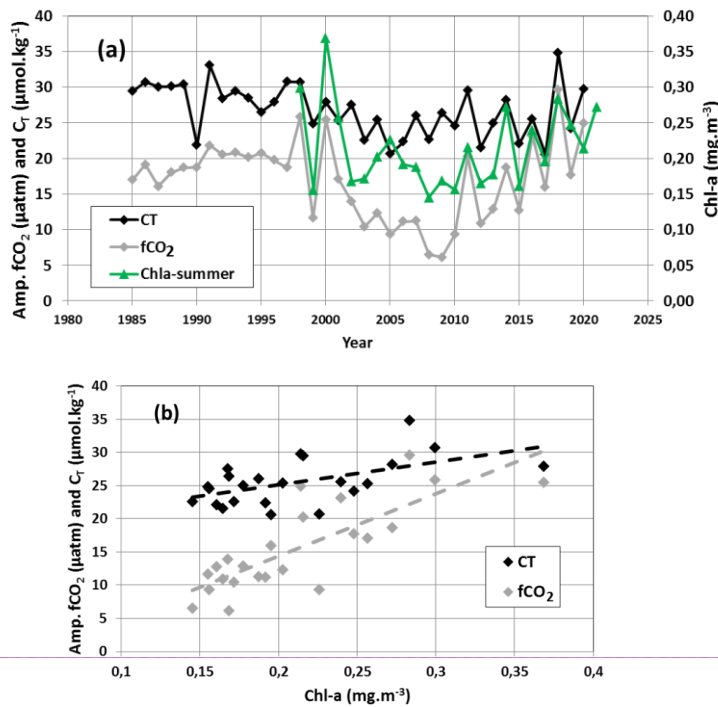
951

952 The C<sub>ant</sub> trend in the WW over 1985-2021 (+0.53 ± 0.01 μmol.kg<sup>-1</sup>.yr<sup>-1</sup>) is slightly lower than the annual  
953 surface C<sub>T</sub> trend in surface derived from the FFNN model for 1985-2020 (C<sub>T</sub> trend = +0.58 ± 0.05 μmol.kg<sup>-1</sup>.yr<sup>-1</sup> Figure 4a, Table 2) suggesting that anthropogenic CO<sub>2</sub> uptake explains 86% of the C<sub>T</sub> increase in surface-  
954 in waters. Over 1991-2020 the surface C<sub>T</sub> trend appears slightly higher in January (+0.68 ± 0.07 μmol.kg<sup>-1</sup>.yr<sup>-1</sup>)  
955 than in August (+0.56 ± 0.04 μmol.kg<sup>-1</sup>.yr<sup>-1</sup>), (Figure 4b, Table 2). This suggests that in addition to the increase of  
956 C<sub>T</sub> due to anthropogenic CO<sub>2</sub> other processes ~~count~~ such as the variability of the biological activity, vertical  
957 mixing or upwelling contributed to the observed trend. Indeed, as for fCO<sub>2</sub> (Figures 2b), the C<sub>T</sub> growth rate also  
958 depends on seasons and decades (Figure 4b). In Over 1991-2001 the C<sub>T</sub> trend from the observations (+0.05 ±  
959 0.64 μmol.kg<sup>-1</sup>.yr<sup>-1</sup>, Table 2) is highly uncertain due to few data and the large variability (Figures 4a, b). The  
960 FFNN model showed that the C<sub>T</sub> trend in summer was faster than the trend in C<sub>ant</sub> (Figure 4b), suggesting that  
961 natural processes would have increased C<sub>T</sub>. This could be explained by an increase in vertical mixing due to the  
962 increase in wind speed (Figure 3). On the contrary, the winter and the winter C<sub>T</sub> trend was lower than the C<sub>ant</sub>  
963 trend estimated in subsurface (Figure 4b). This is because during that decade, the higher primary production in  
964 1998 created a negative C<sub>T</sub> anomaly (Figure 4a) not compensated by the accumulation of C<sub>ant</sub> waters (Figure 4b).

965 In Over 2001-2010 the C<sub>T</sub> trends were much faster than in 1991-2001 over the previous decade and they  
966 were the same for both seasons (around 1 μmol.kg<sup>-1</sup>.yr<sup>-1</sup>, Figure 4b, Table 2). For this decade the summer C<sub>T</sub>  
967 trends from the observations and the FFNN model are coherent. They were also twice the C<sub>ant</sub> rate in the WW  
968 that, which could be explained by enhanced upwelling of C<sub>T</sub>-rich deep waters during this period after the SAM  
969 reached a high positive index (Figure 3; Lenton and Matear, 2007; Le Quéré et al., 2007; Hauck et al., 2013).  
970 However, in 2001-2010 over this period we did not detect any clear change at depth for ocean properties (except  
971 for C<sub>T</sub> and C<sub>ant</sub>) that would support this assumption (enhanced upwelling). The rapid C<sub>T</sub> (and fCO<sub>2</sub>) trend for this  
972 decade is probably due to processes occurring at the surface (e.g. biological activity, as discussed later) rather  
973 than changes in the water column (vertical mixing or upwelling). In 2010-2020 over the last decade C<sub>T</sub> trends  
974 are were lower than in 2001-2010 over the previous one (Figure 4b). For summer, this is identified from both  
975 observations and the FFNN model. In winter the C<sub>T</sub> trend (from FFNN) is close to C<sub>ant</sub> indicative of the  
976 anthropogenic CO<sub>2</sub> accumulation. The low C<sub>T</sub> trend at the surface in summer, about half the C<sub>ant</sub> trend for the  
977 FFNN model, is likely due to the increase of primary production after 2010 as described above (Figure 5).

Mis en forme : Couleur de police : Automatique

979 ~~It~~Thus, it appears ~~thus~~ that the impact of biological activity and its variability in summer could counteract that of  
 980 anthropogenic CO<sub>2</sub> and explain the low temporal change of the carbonate system ~~in~~at the surface in recent years.



1000 Figure 8: (a): Time-series of the seasonal amplitude (August minus January) for surface C<sub>T</sub> (black, μmol.kg<sup>-1</sup>) and fCO<sub>2</sub> (grey, μatm) from the FFNN model at station OISO-KERFIX (50°40'S-68°25'E). Also shown are the mean surface Chl-a (green, mg.m<sup>-3</sup>) in summer from 1998 to 2021. (b): Seasonal amplitude of fCO<sub>2</sub> and C<sub>T</sub> versus summer Chl-a over 1998-2020. The dashed lines indicate that the seasonal amplitude (August-January) increases when Chl-a is higher.

1008 Given the differences of the fCO<sub>2</sub> and C<sub>T</sub> trends in summer and winter (Figures 2b and 4b, Table 2) we  
 1009 explored the temporal variations of the seasonality. For each year we estimated the differences between August  
 1010 and January (Figure 8a). The seasonal amplitude for C<sub>T</sub> was on average 26.1 ~~For each year we estimated the~~  
 1011 ~~differences between August and January (Figure 8a). The seasonal amplitude for C<sub>T</sub> was on average 26.1 (±~~  
 1012 ~~±3.4) μmol.kg<sup>-1</sup> and for fCO<sub>2</sub> 15.1 (±±5.6) μatm. Some large inter-annual variations appear related to the~~  
 1013 variability of Chl-a in summer (Figure 8a). Interestingly, the fCO<sub>2</sub> seasonal amplitude reached a minimum  
 1014 around 2008-2010 ~~and, then~~ increased over 2010-2020. This signal also appears correlated with the evolution of  
 1015 surface Chl-a in summer (Figure 8b)-8). This supports the conclusion that low phytoplanktonic biomass between  
 1016 2008 and 2010 reduced the seasonal amplitude of fCO<sub>2</sub>.

1017 The inter-annual variability of the seasonality is clearly identified when comparing C<sub>T</sub> with C<sub>T</sub>  
 1018 calculated due only to C<sub>ant</sub> accumulation ~~after 2010~~ (Figure S12eS12). This supports the conclusion that in  
 1019 addition to the C<sub>ant</sub> accumulation, the variations of phytoplanktonic biomass imprinted inter-annual variability on  
 1020 C<sub>T</sub> and fCO<sub>2</sub> in summer. This holds for the seasonal amplitude as the results for winter follows the C<sub>ant</sub> trend  
 1021 (Figure 4b, Figure S12a). The same is true for pH for which reduced seasonal amplitude was found when the  
 1022 production was low (not shown). However, over 36 years (1985-2020) we did not identify a long-term trend of

Mis en forme : Interligne : Multiple 1,15 li

Mis en forme : Justifié

Mis en forme : Police : Times New Roman, 9 pt, Non souligné

Mis en forme : Justifié, Interligne : simple

Mis en forme : Police : Times New Roman, 9 pt, Couleur de police : Automatique

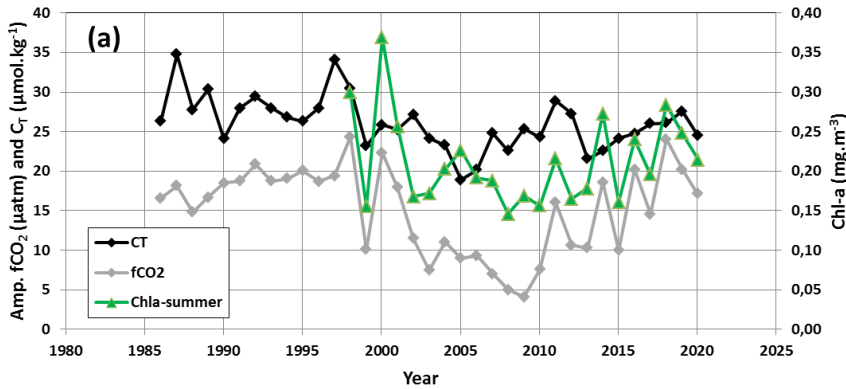
Mis en forme : Interligne : simple

Mis en forme : Police : 9 pt, Non Gras

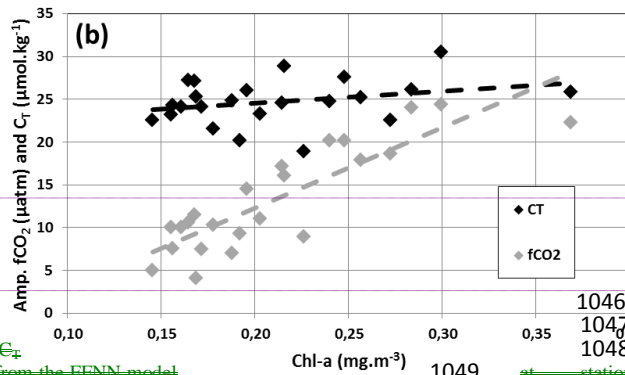
Mis en forme : Justifié, Interligne : simple

Mis en forme : Espace Après : 0 pt

1023 the seasonal amplitude for  $C_T$  or for  $fCO_2$  as suggested by other studies (Landschützer et al., 2018; Rodgers et  
 1024 al., 2023; Shadwick et al 2023). Our results highlight a variability over 5-10 years (Figure 8a) and suggest a  
 1025 potential change in seasonality and annual  $CO_2$  sink if primary production changes in the future (e.g. Bopp et al.,  
 1026 2013; Leung et al., 2015; Fu et al., 2016; Kwiatkowski et al., 2020; Krumhardt et al., 2022; Seifert et al., 2023).



Mis en forme : Police :Times New Roman, Gras, Couleur de police : Automatique



Mis en forme : Interligne : Multiple 1,15 li

Mis en forme : Justifié

Mis en forme : Police :Times New Roman, 9 pt, Non souligné

Mis en forme : Justifié, Interligne : simple

Mis en forme : Police :Times New Roman, 9 pt, Couleur de police : Automatique

Mis en forme : Interligne : simple

1046 Figure 8: (a): Time series of the seasonal amplitude (August minus January) for surface  $C_T$  (black,  $\mu\text{mol.kg}^{-1}$ ) and  $fCO_2$  (grey,  $\mu\text{atm}$ ) from the FFNN model at station OISO KERFIX (50°40'S 68°25'E). Also shown are the mean surface Chl-a (green,  $\text{mg.m}^{-3}$ ) in summer in 1998-2021. (b): Seasonal amplitude of  $fCO_2$  and  $C_T$  versus summer Chl-a for 1998-2020. The dashed lines indicate that the seasonal amplitude (August-January) increases when Chl-a is higher.

### 1055 3.3 Anthropogenic $CO_2$ drives acidification in surface waters and in the water column

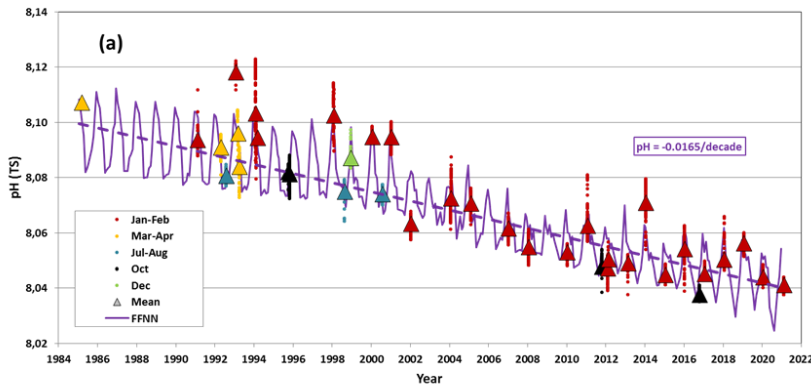
#### 1057 3.3.1 Surface pH trend

1059 To explore the temporal change of pH in surface waters we used the  $fCO_2$  observations and the  
 1060 monthly results from the FFNN model. For both data-sets pH was calculated from  $fCO_2$  and  $A_T$  reconstructed as  
 1061 described in section 2.2.5. Figure 9a presents the time-series of pH at the surface (the same time-series for  $[H^+]$   
 1062 concentrations is shown in Figure S13). For the full period, 1985-2020, the annual pH trend derived from the  
 1063 FFNN model is  $-0.0165 \pm 0.0004.\text{decade}^{-1}$  ( $\pm 0.0004$  Table 2) exactly the same as derived at large scale in the  
 1064 Southern Ocean (south of 44°S) for the period 1993-2018 (Iida et al., 2021, Table 1) but when restricted to this  
 1065 period, 1993-2018, the trend from the FFNN model appears slightly faster of  $-0.0182 \pm 0.0006.\text{decade}^{-1}$  ( $\pm$   
 1066  $0.0006$ ). This is less than the pH trend of  $-0.020 (\pm 0.002).\text{decade}^{-1}$  derived from  $pCO_2$  data in the SO SubPolar

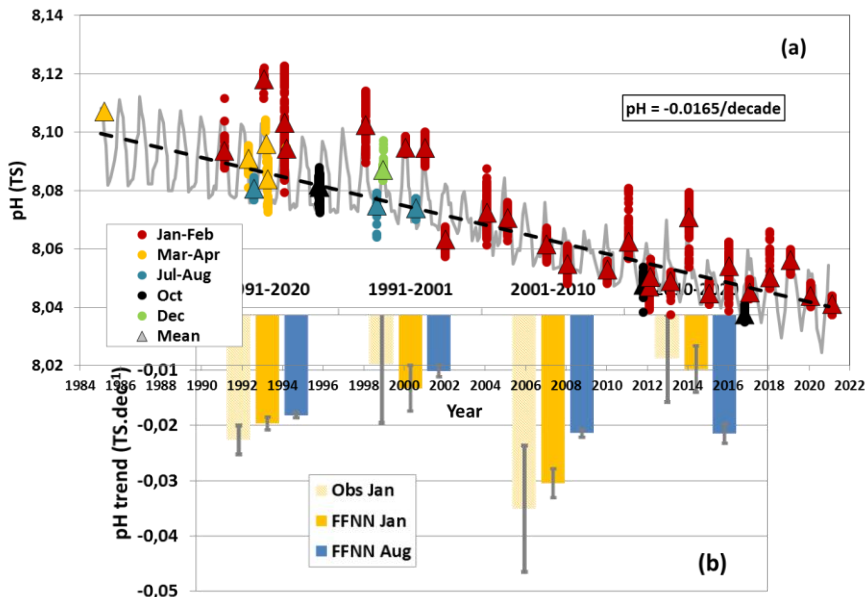
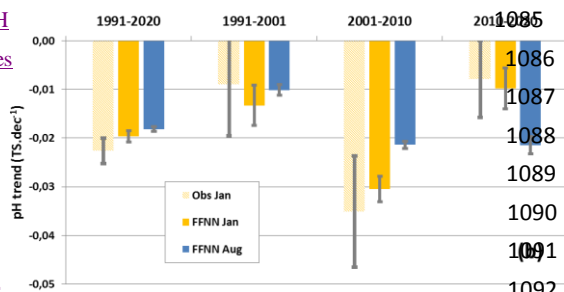
Mis en forme : Police :9 pt, Non Gras

Mis en forme : Justifié, Interligne : simple

1067 Seasonally Stratified biome around 40-50°S (SO-SPSS) for 1981-2011 ( $-0.020 \pm 0.002 \text{ decade}^{-1}$ , Table 1,  
 1068 Lauvset et al., 2015) and close to the pH trend of  $-0.0189 (\pm 0.0010) \text{ decade}^{-1}$  based on OceanSODA-ETH  
 1069 reconstructed fields in the SO-SPSS for the period 1982-2021 ( $-0.0189 \pm 0.0010 \text{ decade}^{-1}$ , Ma et al., 2023).  
 1070 However, as for  $f\text{CO}_2$  and  $C_T$ , we estimated different pH trends were estimated in summer and winter, as well as  
 1071 depending on the periods (Figure 9b, Table 2).



1085 The winter pH decrease estimated  
 1086 over the last two decades was twice as fast as  
 1087 estimated during the previous one.  
 1088 mirroring the winter fCO<sub>2</sub> trends (Table  
 1089 2). In summer, the pH trend presents a  
 1090 large variability at decadal scale as it  
 1091 was three times faster over 2001-2010  
 1092 than during the previous and following  
 1093 decades (Figure 9b, Table 2). Although the trends based on the observations are less robust because the cruises  
 1094 were not conducted each year, the reduced pH trend in summer after 2010 is confirmed from in-situ data (Figure  
 1095 9b, Table 2).



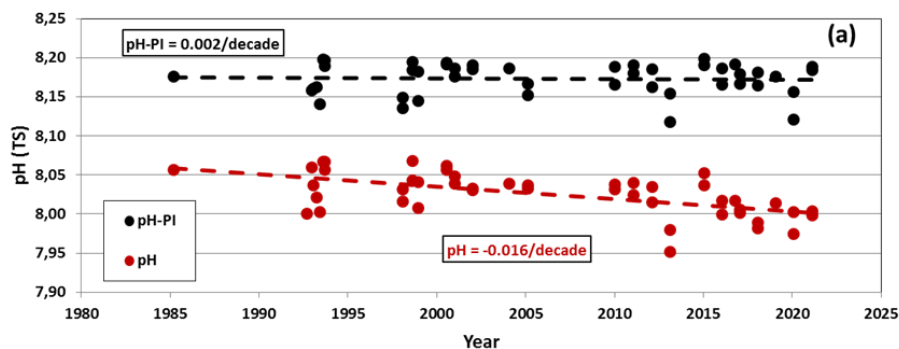
1114  
1115  
1116  
1117  
1118  
1119  
1120  
1121  
1122  
1123  
1124  
1125  
1126  
1127  
1128  
1129  
1130  
1131  
1132  
1133  
1134  
1135  
1136  
1137

Mis en forme : Police :Times New Roman, 9 pt, Couleur de police : Rouge foncé

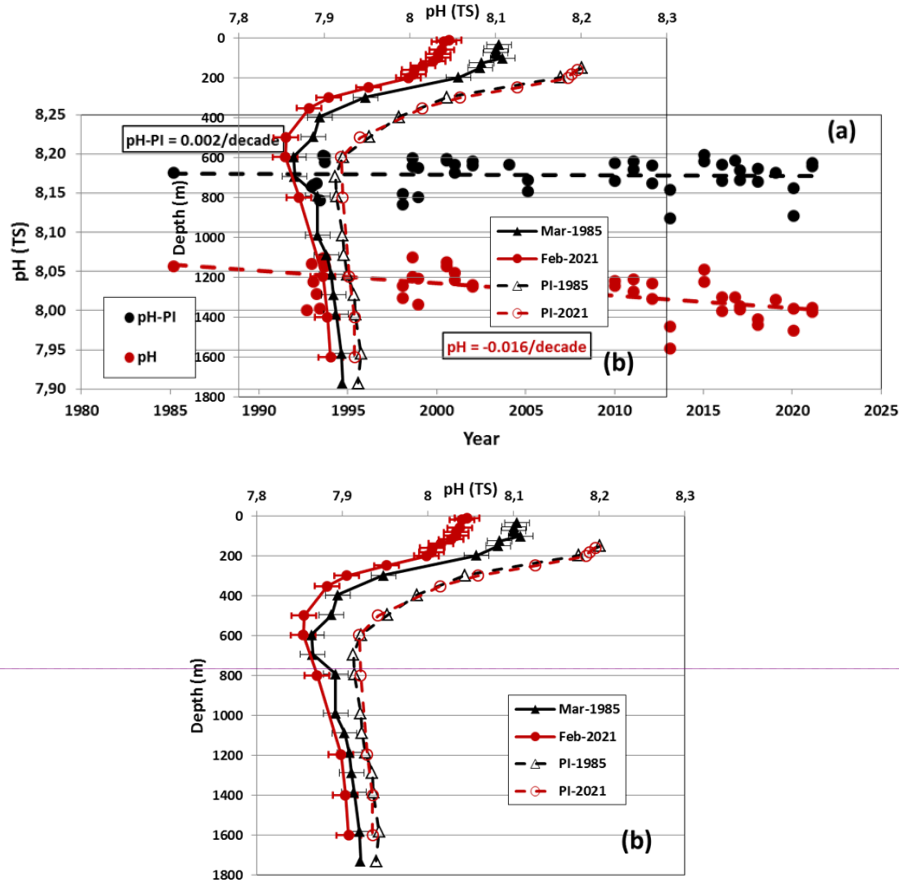
Figure 9: (a): Time-series of surface pH (Total Scale, TS) around station OISO-KERFIX (50°40'S-68°25'E) calculated from  $f\text{CO}_2$  data (Figure 2) using the  $A_T/S$  relation (see textSect.2.2.5). The color dots correspond to 5 seasons/periods of the year (January-February, March-April, July-August, October and December) and triangles show the average for each cruise/month. The monthly sea surface pH from the FFNN model is presented for the period 1985-2020 (purplegrey line). The annual pH trend in 1985-2020 of  $-0.0165 \pm 0.0004 \text{ decade}^{-1}$  ( $\pm 0.0004$ ) (dashed line-purple) is derived from the FFNN monthly data (the same figure for  $[\text{H}^+]$  concentrations is presented in Supp. Mat. Figure S13). (b): Trends of pH (TS.decade<sup>-1</sup>) for in summer and winter four over different seasons and periods based on observations (January) and the FFNN model (January or and August).

1138 The winter pH decreased was faster in recent years, mirroring the winter  $f\text{CO}_2$  trend (Figure 2b). On the  
1139 opposite, in summer, the pH trend presents a large variability at decadal scale and was lower in 2010-2020. In  
1140 summer 2001-2010, the pH trend from the FFNN model was  $-0.0304 \text{ decade}^{-1}$  ( $\pm 0.0026$ ) whereas in 2010-2020,  
1141 it was  $-0.0098 \text{ decade}^{-1}$  ( $\pm 0.0042$ ) (Figure 9b, Table 1). Although the trends based on the observations are less  
1142 robust because the cruises were not conducted each year the reduced pH trend in summer after 2010 is confirmed  
1143 from in-situ data ( $-0.0351 \pm 0.0114 \text{ decade}^{-1}$  in 2001-2010 against  $-0.0078 \pm 0.0079 \text{ decade}^{-1}$  in 2010-2020,  
1144 Figure 9b, Table 1). These Our results show that the pH trend varied significantly from decade to decade and that  
1145 part of the variations could be explained by the evolution of phytoplanktonic biomass, but overall the decrease of  
1146 pH since 1985 was mainly driven by the accumulation of anthropogenic  $\text{CO}_2$ . This is revealed in the winter  
1147 water/Winter Water when comparing pH and pre-industrial pH (Figure 10a). Here, the pre-industrial pH (pH-PI)  
1148 was calculated after subtracting  $C_{\text{ant}}$  values from the observed  $C_T$  concentrations for each sample in the WW  
1149 layer. Interestingly the pH trend in the WW of  $-0.0161$  ( $\pm \pm 0.0033$ )  $\text{decade}^{-1}$  (here deduced from the station  $A_T$   
1150 and  $C_T$  data in over 1985-2021) is very close to the long-term annual trend in at the surface deduced from the  
1151 FFNN model in over 1985-2020 ( $-0.0165 \pm 0.0004 \text{ decade}^{-1}$   $\pm 0.0004$ ). This trend is slightly faster than the pH  
1152 trends of  $-0.0134$  ( $\pm \pm 0.001$ )  $\text{decade}^{-1}$  recently estimated in subsurface waters (100-210m) of the Southern  
1153 Ocean south of the PF and derived for years 1994-2017 from historical data and BGC-Argo floats (Mazloff et  
1154 al., 2023). For the same period, 1994-2017, at the OISO-KERFIX station we estimate/estimated a pH trend in the  
1155 WW of  $-0.0168$  ( $\pm \pm 0.0043$ )  $\text{decade}^{-1}$  and of  $-0.0186$  ( $\pm \pm 0.0006$ )  $\text{decade}^{-1}$  in surface waters from the FFNN  
1156 model.

1157  
1158  
1159  
1160  
1161  
1162  
1163



1164  
1165  
1166  
1167  
1168  
1169  
1170  
1171  
1172  
1173  
1174  
1175  
1176  
1177  
1178  
1179  
1180  
1181  
1182  
1183  
1184  
1185  
1186  
1187  
1188  
1189  
1190  
1191  
1192  
1193  
1194  
1195  
1196  
1197  
1198  
1199  
1200  
1201  
1202  
1203  
1204  
1205  
1206  
  
1207  
1208  
1209  
1210  
1211  
1212



Mis en forme : Police :Times New Roman, 9 pt, Non souligné  
Mis en forme : Justifié, Interligne : simple

Mis en forme : Couleur de police : Automatique

Figure 10: (a): Time-series of pH (red dots) and pre-industrial pH (pH-PI, black dots) estimated in the winter water layer (WW around 200m, see figure 6) in 1985-2021 at station OISO-KERFIX (50°40'S-68°25'E). pH-PI for each sample was calculated after subtracting  $C_{\text{ant}}$  to  $C_T$ . The pH trend from the present days is  $-0.0161 (\pm \pm 0.0033) \text{ decade}^{-1}$  (red dashed line). No trend is observed for pH-PI (black dashed). The mean pH-PI in the WW is  $8.173 (\pm \pm 0.020, n = 45)$ . (b): Profiles of pH and pH-PI evaluated from March 1985 (black symbols) and February 2021 data (red symbols). The profiles for pH-PI are shown below 150m only as  $C_{\text{ant}}$  estimates are not available in the surface layer. Note that the pH-PI profiles are the same either using either the 1985 or 2021 data.

As for other properties ( $A_T$ ,  $O_2$ , temperature, salinity and nutrients), the pre-industrial pH (pH-PI) does not change over time in the WW (mean pH-PI =  $8.173 \pm 0.020$ ,  $n=45$ , Figure 10a). The pH-PI in the WW is in the range of the pre-industrial surface pH value in the Southern Ocean (8.2 for year 1750 and 8.18 for year 1850) derived from Earth system Models (Jiang et al., 2023, their Table S9). In the WW at our location the modern pH (1985-2021) was on average  $-0.147 (\pm \pm 0.021)$  lower than pre-industrial pH. In 1985 pH in the WW was  $-0.119$  lower than pH-PI and in 2021 it was  $-0.184$  lower than pH-PI (Figure 10a). The progressive decrease

1213 of pH was clearly linked to  $C_{\text{ant}}$  concentrations in the WW layer and the pH decrease identified below that layer  
1214 in the water column (Figure 10b).

1215 |

1216  
 1217  
 1218  
 1219  
 1220  
 1221  
 1222  
 1223  
 1224  
 1225  
 1226  
 1227  
 1228  
 1229  
 1230  
 1231  
 1232  
 1233  
 1234  
 1235  
 1236  
 1237  
 1238  
 1239  
 1240  
 1241  
 1242  
 1243  
 1244  
 1245  
 1246  
 1247  
 1248  
 1249  
 1250  
 1251  
 1252  
 1253  
 1254  
 1255  
 1256  
 1257  
 1258

### 3.3.2 Temporal change in the water column

From 1985 to 2021, signals of decreasing pH and increasing  $C_T$  in surface waters are propagated in the water column down to about 500m. As mentioned above the data in 1985 (first occupation of the station) reveal significant  $C_{ant}$  levels across the water column (Figure 6b). Therefore the pH down to 1400m the bottom was already lower in 1985 than at pre-industrial times (Figure 10b). However, the largest  $C_{ant}$  increases were found in the top layers and changes in pH from 1985 to 2021 were small below 500m (Figure 10b, Figure S14). While observations for all years fall on a common linear relationship between  $C_{ant}$  and  $pH_{ant}$  for depths greater than 500 m, the change in pH for a given level of  $C_{ant}$  increases with time for layers shallower than 500 m (Figure 11).

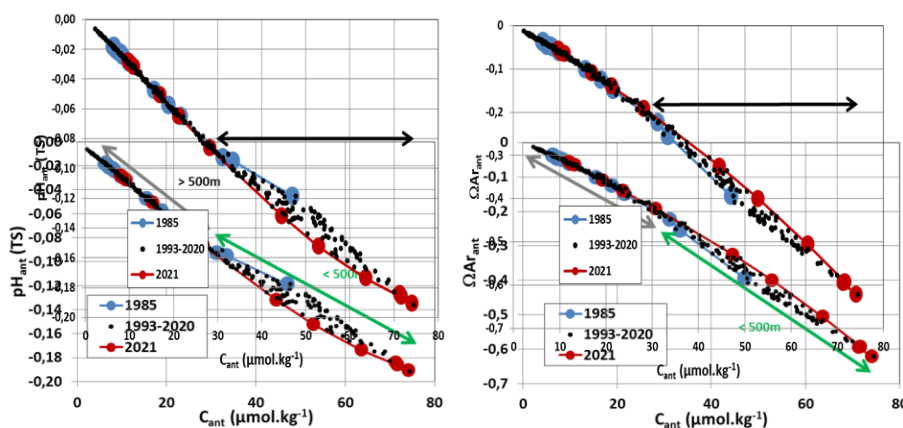


Figure 11: Anthropogenic pH ( $pH_{ant}$ ) and anthropogenic  $\Omega_{ar}$  ( $\Omega_{ar_{ant}}$ ) versus anthropogenic  $CO_2$  concentrations ( $C_{ant}$ ,  $\mu mol.kg^{-1}$ ) at station OISO-KERFIX ( $50^{\circ}40'S-68^{\circ}25'E$ ). The data are selected in the layer 150-1600m for the periods 1985 (blue), 1993-2020 (black) and 2021 (red). The green arrow identifies the data in the layer 150-500m (for  $C_{ant} > 30 \mu mol.kg^{-1}$ ). Below 500m (brown arrow) no change of  $C_{ant}$  was observed from 1985 to 2021 and thus for  $pH_{ant}$  and  $\Omega_{ar_{ant}}$ .

Mis en forme : Retrait : Première ligne : 1,25 cm

The increase in  $C_{ant}$  concentrations over time (Figure 6b) also leads to a decrease of carbonate ion concentrations [ $CO_3^{2-}$ ] and of  $\Omega_{ar}$  and  $\Omega_{ca}$  (Figure S14, S15). These decreases are well identified since the pre-industrial era in the whole water column but in the last 36 years, observations do not show any appreciable changes below 500m (Figure 11). The aragonite saturation state horizon ( $\Omega_{ar}=1$ ) was found around 600m in 1985 and around 400m in recent years (2015-2021, Figures S14, S15). Moreover, during the period covered by observations (1985-2021), we did not detect abrupt change of the aragonite saturation horizon from one year to the next (including from season to season nor between winter and summer, Figure S16). This contrasts with previous regional studies in the SO and most notably with results from the layers close to the deep minimum of carbonate ion concentrations (Hauri et al., 2015; Negrete-Garcia et al., 2019). At our station the [ $CO_3^{2-}$ ] minimum lies around 500-600m (Figure S14, S15) and, along with the superimposed  $C_{ant}$  accumulation, explains the upward shift of the aragonite and calcite saturation horizon between the pre-industrial and modern periods (Figure S15). At pre-industrial time under-saturation with regard to aragonite ( $\Omega_{ar}<1$ ) was found at the bottom only (1600m) whereas inbetween 1985- and 2021 it was found in the water column below 600 m or 400 m



1259 (Figure S15). The subsurface pre-industrial  $\Omega_{ar}$  value was around 1.9-2 (Figure S15) and in the range of  $\Omega_{ar}$   
1260 value in the Southern Ocean at pre-industrial time from ESM models (Jiang et al., 2023, their Figure 4).

1261 The aragonite under-saturation already occurred in 1985 at ~~500-600m~~ 600-700m, a layer corresponding  
1262 to the  $[\text{CO}_3^{2-}]$  minimum (Figure S15) and a small increase of  $C_T$  just above this layer (via  $C_{ant}$  accumulation)  
1263 close to the  $[\text{CO}_3^{2-}]$  minimum would rapidly shift the aragonite saturation horizon in layers above ~~500m~~ 600m.  
1264 This might have already occurred and ~~explains~~ could explain that  $\Omega_{ar}$  value was 1.02 at 350m in 2021 (Figure  
1265 S15). These results suggest that for pelagic calcifiers living in subsurface waters (150m or deeper) such as  
1266 pteropods and/or foraminifera (e.g. Hunt et al., 2008; Meilland et al., 2018) the impact of acidification might  
1267 occur sooner than ~~in at the~~ in at the surface.

1268 For the interpretation of the trend analysis based on observations, only data below 150m could be used  
1269 as  $C_{ant}$  was not evaluated in the surface layer. At 200m, based on  $A_T$  and  $C_T$  data, we estimated a decrease in pH  
1270 and  $\Omega_{ar}$  decreased from 1985 to 2021 by -0.059 ~~for pH~~ (Figure 10b)), corresponding to an increase by +1.1  
1271  $\text{nmol.kg}^{-1}$  in  $[\text{H}^+]$  (Figure S13), and a decrease by -0.16 ~~for in~~  $\Omega_{ar}$  (Figure S15). ~~In~~ Over 36 years, this represents  
1272 about 30% of the total change since the pre-industrial era for pH (-0.184 ~~for pH~~),  $[\text{H}^+]$  (+3.5  $\text{nmol.kg}^{-1}$ ) and  $-\Omega_{ar}$   
1273 (-0.6 ~~for~~  $\Omega_{ar}$  at 200m). This is mainly linked to the  $C_{ant}$  change that also represents also 30% increase in over 36  
1274 years 30% of the total accumulation (+24.6  $\mu\text{mol.kg}^{-1}$  from 1985 to 2021 for a total concentration of +71.7  
1275  $\mu\text{mol.kg}^{-1}$   ~~$\text{CO}_2$  accumulated~~ at 200m in 2021, Figure 7). We conclude that the accumulation of anthropogenic  
1276  $\text{CO}_2$  drives the change of the carbonate system in subsurface waters and probably also in surface waters.

Mis en forme : Anglais (États Unis)

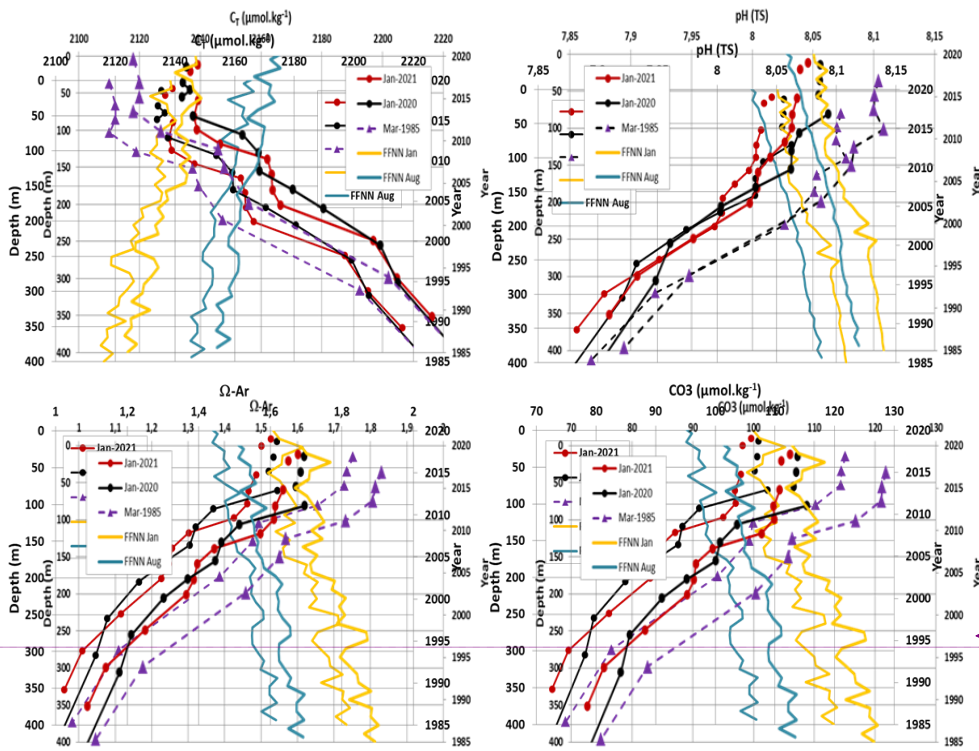
1277 In order to quantify the propagation of surface trends to depth, the temporal variations of carbonate  
1278 system properties in at the surface for both summer and winter derived from the FFNN model are compared to  
1279 the changes observed across the water column (Figure 12). The comparison shows that the seasonal amplitude of  
1280 surface waters properties was of a similar magnitude to the observed changes in the mixed layer between 1985  
1281 and 2021. For example, the  $C_T$  and  $\Omega_{ar}$  seasonality seasonal amplitude, respectively around 20  $\mu\text{mol.kg}^{-1}$  and 0.2,  
1282 corresponds to the  $C_T$  increase and  $\Omega_{ar}$  decrease from 1985 to 2021. The comparisons also highlight that in  
1283 summer the FFNN results were close to observations in the mixed-layer (e.g.  $C_T$  was 2120  $\mu\text{mol.kg}^{-1}$  in 1985 and  
1284 2140  $\mu\text{mol.kg}^{-1}$  in 2021). In winter, at the surface properties are different ( $C_T$  was higher, and pH,  $[\text{CO}_3^{2-}]$ ,  $\Omega_{ar}$   
1285 were lower) and intercept the (from the FFNN model, blue line in Figure 12). The winter surface values in 1985  
1286 and 2020/2021 are in good agreement with observations at depth close to in the winter water (150-200m). This is  
1287 true As an example, in 1985 and 2020/2021. Specifically, surface  $C_T$  from the FFNN model in winter 1985 (was  
1288 2145.5  $\mu\text{mol.kg}^{-1}$ ) equaled the  $C_T$ , which corresponds to the concentration measured at 150 m in March  
1289 1985 (2148  $\mu\text{mol.kg}^{-1}$  150m during summer (purple line in Figure 12)). In 2020, the winter  $C_T$  at the surface  
1290 (2168.3  $\mu\text{mol.kg}^{-1}$ ) is equal to  $C_T$  concentrations observed at 150-180 m in January 2020 or in 2021. For  $\Omega_{ar}$ , the  
1291 surface value derived from the FFNN model in winter 1985 (1.6) was equal to the  $\Omega_{ar}$  observed at 125 m in  
1292 March 1985. In 2020, the surface winter estimate of  $\Omega_{ar}$  (1.42) was equal to  $\Omega_{ar}$  observed at 100-150 m in  
1293 January 2020 or 2021. The same correspondences between winter surface and WW data were identified for pH  
1294 and  $[\text{CO}_3^{2-}]$  (Figure 12). This supports the use of winter and summer surface data from the FFNN model to  
1295 investigate the seasonal  $\Omega_{ar}$  trends and their projection in the future.

Mis en forme : Anglais (États Unis)

Mis en forme : Non Exposant/ Indice

1296 The surface water  $\Omega_{ar}$  ( $\Omega_{ca}$ ) trend from the FFNN model in summer of -0.0059. $\text{yr}^{-1}$  (-0.0094. $\text{yr}^{-1}$ ) was  
1297 stronger than in the winter of -0.0050. $\text{yr}^{-1}$  (-0.0079. $\text{yr}^{-1}$ ) and also higher than the trend derived from observations  
1298 in the WW (-0.0043. $\text{yr}^{-1}$  for  $\Omega_{ar}$  and -0.0069. $\text{yr}^{-1}$  for  $\Omega_{ca}$ ). The Our results indicate that the change of carbonate  
1299 properties in the years 1985-2021 were mainly driven by  $C_{ant}$  accumulation in surface waters and across the

1300 | water column. However, a potential **changesincrease** in primary productivity after 2010 mitigated the effects of  
 1301 | increasing  $C_{ant}$  accumulation in response to increasing atmospheric  $CO_2$  leading to relatively stable summer  $C_T$   
 1302 | and  $fCO_2$  and to a stronger  $CO_2$  sink (Figure 3). Consequently, when restricted to the period 2010-2020, the  
 1303 | trend of  $\Omega_{ar}$  in surface waters in summer was much smaller,  $-0.024 \pm 0.027 \text{ decade}^{-1}$  ( $\pm 0.027$ ) than during the  
 1304 | preceding period. This was much smaller than derived from **all** the **all**-data **inover** 1985-2021 ( $-0.048 \text{ decade}^{-1}$ ) or  
 1305 | estimated from reconstructed fields in the SO-SPSS **inover** 1982-2021 ( $-0.0616 \text{ decade}^{-1}$ , Ma et al., 2023). It  
 1306 | underscores the uncertainty in extrapolating **long-term** time-series **to the future** depending on the selection of  
 1307 | data and periods.



1308  
1309  
1310  
1311  
1312  
1313  
1314  
1315  
1316  
1317  
1318  
1319  
1320  
1321  
1322  
1323  
1324  
1325  
1326  
1327  
1328  
1329  
1330  
1331  
1332  
1333  
1334

1335 | Figure 12: Profiles (0-400m left axis) of observed and calculated properties ( $C_T$ , pH,  $\Omega_{-ar}$ ,  $[CO_3^{2-}]$ ) at station OISO-KERFIX  
 1336 | ( $50^{\circ}40'S-68^{\circ}25'E$ ) in March 1985, January 2020 and January 2021 along with surface time-series in 1985-2020 (right axis) of  
 1337 | the same properties in January (yellow line) and August (blue line) from the FFNN model. The FFNN values in January 2020  
 1338 | are coherent with January 2021 **or January 2021** observations in the mixed-layer and in January 1985 are close to the  
 1339 | observations in March 1985. Note that the differences of properties between 2020-21 and 1985 have a similar magnitude as  
 1340 | the seasonal amplitude (illustrated by the FFNN values for January and August).

Mis en forme : Police :Times New Roman, 9 pt

Mis en forme : Justifié, Interligne : simple

Mis en forme : Indice

Mis en forme : Couleur de police : Automatique

1342 | **3.4 Long-term change in surface water, from the sixties to the future.**

1343

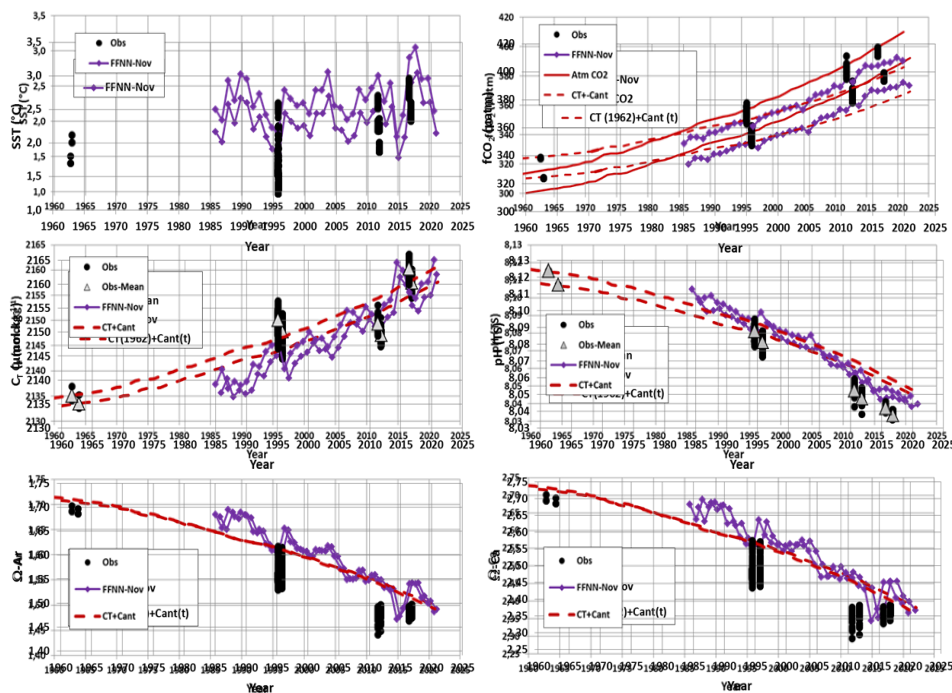
1344 | The data described above allowed evaluating the temporal variations of the properties of the carbonate  
 1345 | system and  $C_{ant}$  over 1985-2021 along with a comparison to the pre-industrial state in the water column  
 1346 | **excluding the surface layer.** The results over 36 years informed on the recent changes, inter-annual variations

1347 and trends, but the time-series appears somehow short to extrapolate the trends over time. What was the change  
 1348 of the carbonate system in surface waterwaters before 1985 and what will be its future evolution ?

1349  
 1350 **3.4.1 Back to the sixties: observed trends since 1962.**

1351  
 1352 To explore the long-term change, we start by comparing our recent data with ~~the~~ observations from the  
 1353 LUSIAD cruise conducted in 1962-1963 (Keeling and Waterman, 1968). Some data from this cruise were  
 1354 obtained in mid-November 1962 south of the Polar Front, in the region south-west off Kerguelen Islands.  
 1355 Because of the seasonality, we compared the November 1962 data with our observations obtained in October-  
 1356 November in 1995, 2011 and 2016, and with the FFNN model results for November (Figure 13). The  $C_T$   
 1357 concentration, pH,  $\Omega_{ar}$  and  $\Omega_{ca}$  for 1962 were calculated using  $fCO_2$  data and  $A_T$  (from the  $A_T/S$  relationship Eq.  
 1358 41) with salinity from the World Ocean Atlas (Antonov et al, 2006).

Mis en forme : Police :Gras, Couleur de police : Automatique  
 Mis en forme : Gauche, Retrait : Première ligne : 0 cm



1382 Figure 13: Observed (black dots) sea surface temperature ( $^{\circ}\text{C}$ ),  $fCO_2$  ( $\mu\text{atm}$ ),  $C_T$  ( $\mu\text{mol.kg}^{-1}$ ), pH (TS),  $\Omega_{ar}$  and  $\Omega_{ca}$  around  
 1383 station OISO-KERFIX at  $50^{\circ}40'S-68^{\circ}25'E$  for October-November. Also shown are the results for the FFNN model for  
 1384 November in 1985-2020 (Purple). The  $C_T$  concentrations, pH,  $\Omega_{ar}$  and  $\Omega_{ca}$  were calculated from  $fCO_2$  data using the  $A_T/S$   
 1385 relation (Eq. 1). The red line is the atmospheric  $fCO_2$  and red dashed-lines in each plot are the evolution of properties since  
 1386 1960 corrected for  $C_{ant}$  where  $fCO_2$ , pH,  $\Omega_{ar}$  and  $\Omega_{ca}$  were recalculated using  $C_T+C_{ant}$ ,  $A_T$  constant at  $2290 \mu\text{mol.kg}^{-1}$  and  
 1387 SST at  $2^{\circ}\text{C}$ . Grey triangles identify the mean values for  $C_T$  and pH.

Mis en forme : Couleur de police : Automatique  
 Mis en forme : Couleur de police : Automatique

1389 First, we note that the measured SST in November 1962 ( $1.7^{\circ}\text{C}$ ) was slightly lower (~~on average about~~  
 1390  $0.6^{\circ}\text{C}$ ) compared to recent years, (on average by about  $-0.6^{\circ}\text{C}$ ), but SST as low as  $1.8^{\circ}\text{C}$  for this season were  
 1391 also recorded in other periods (e.g. November 1995, 2014). The change in SST is unlikely to explain  
 1392 the long-term increase in  $fCO_2$  or decrease in pH since 1962 (Figure 13). In 1962, the ocean  $fCO_2$  was

1393 324  $\mu\text{atm}$ , which is slightly higher than in the atmosphere ( $\Delta f\text{CO}_2 = +8 \mu\text{atm}$ , a small source), whereas in  
 1394 November 1985-2020 the ocean was a small  $\text{CO}_2$  sink on average ( $\Delta f\text{CO}_2 = -3.3 \pm 4.5 \mu\text{atm}$ ). The  $C_T$   
 1395 concentration in 1962 ( $2135 \mu\text{mol.kg}^{-1}$ ) was much lower than observed in the 90s since 1995 and the pH (8.115)  
 1396 was much higher than in recent years the last three decades (Figure 13). Compared to 1962, pH in 2016 was -  
 1397 0.078 lower, i.e. representing 70% of the pH decrease of -0.11 in the global ocean since the beginning of the  
 1398 industrial era (Jiang et al, 2019). In November 1962, surface  $C_T$  was lower by  $-15.1 \mu\text{mol.kg}^{-1}$  compared to the  
 1399 data in October 1995, i.e. a trend of  $+0.46 \mu\text{mol.kg}^{-1}.\text{yr}^{-1}$  in over 33 years close to the  $C_{\text{ant}}$  trend observed in the  
 1400 WW in over 1985-2021 as described above ( $+0.53 \pm 0.01 \mu\text{mol.kg}^{-1}.\text{yr}^{-1}$ ). Having the  $C_T$  value in 1962, we can  
 1401 project the  $C_T$  in time by adding the  $C_{\text{ant}}$  concentration based on the relationship observed between  $C_{\text{ant}}$  and  
 1402 atmospheric  $\text{CO}_2$  (Figure 7b) assuming that the anthropogenic  $\text{CO}_2$  uptake since the sixties is representative of  
 1403 the  $C_T$  change (i.e. the change of  $C_T$  due to natural variability is was small). This projection is shown for all  
 1404 properties (red dashed-lines in Figure 13) and confirms that the progressive  $C_{\text{ant}}$  accumulation explained most of  
 1405 the  $C_T$  and  $f\text{CO}_2$  increase in surface waters since 1962. We note that the  $C_T$  derived from the FFNN model  
 1406 suggests slightly lower  $C_T$  compared to the  $C_{\text{ant}}$  projection especially before 2004-2006. The difference of  
 1407 projected  $C_T$  and the FFNN model (on average  $-2.2 \pm 2.7 \mu\text{mol.kg}^{-1}$ ) is within the uncertainty of  $C_T$  calculations  
 1408 (error is  $\pm 5 \mu\text{mol.kg}^{-1}$  when using the  $A_T/f\text{CO}_2$  pairs) and the trend of the difference over 1985-2020 ( $-0.15$   
 1409  $\mu\text{mol.kg}^{-1}.\text{yr}^{-1}$ ) is too small to be related with confidence to changes associated with natural processes. On the  
 1410 other hand, the oceanic  $f\text{CO}_2$  recalculated with the projected  $C_{\text{ant}}$  trend suggested that for this season  
 1411 (November) the ocean moved from a  $\text{CO}_2$  source in 1962-1985 ( $\Delta f\text{CO}_2 > 0$ ) to a sink in 1986-2021 ( $\Delta f\text{CO}_2 < 0$ )  
 1412 in line with results from the FFNN model. The recalculated  $f\text{CO}_2$  with  $C_{\text{ant}}$  (dashed red line in Figure 13) was  
 1413 close to that observed in 1995 or from the FFNN model in 1985-2014 (mean difference over 1985-2014 is  $-1.2 \pm$   
 1414  $5.2 \mu\text{atm}$ ). After 2016, the recalculated  $f\text{CO}_2$  suggest a stronger sink and the difference with observations in 2011  
 1415 and 2016 or the FFNN model is slightly higher (mean difference over 2016-2020 is  $-8.8 \pm 1.5 \mu\text{atm}$ ). Although  
 1416 the differences are in the range of the error in  $f\text{CO}_2$  calculation using  $A_T-C_T$  pairs ( $\pm 13 \mu\text{atm}$ ), this might  
 1417 indicate that after 2016 a process could contribute to increase  $f\text{CO}_2$  faster than the effect of  $C_{\text{ant}}$  only. This  
 1418 difference could be due to the warming that occurred after 2016 when SST was higher than  $2^\circ\text{C}$  and up to  $3^\circ\text{C}$  in  
 1419 November 2017 (Figure 13 and Figure-S9). The same could be applied for pH that was slightly lower  
 1420 than the pH recalculated from  $C_{\text{ant}}$  trend after 2015 (the mean difference between recalculated pH and FFNN-pH  
 1421 over 1985-2020 is only  $0.002 \pm 0.006$ ). Therefore, we conclude that for November the pH decrease since 1962  
 1422 was mainly driven by the accumulation of anthropogenic  $\text{CO}_2$ . Aragonite and calcite saturation states also show  
 1423 a clear decrease since 1962 (Figure 13), a diminution of 11% in over 59 years for both  $\Omega_{\text{ar}}$  and  $\Omega_{\text{ca}}$ . Based on  
 1424 these results over almost 60 years that confirm the conclusions from the observations in 1985-2021, we now  
 1425 evaluate the long-term change of the carbonate system in surface waters in the future.

### 1427 3.4.2 Projecting the observed trends in the future

1428  
 1429 The trends of the properties based on observations in 1962-2021 and the FFNN model in 1985-2020  
 1430 indicate relatively linear trends linked to  $C_{\text{ant}}$  uptake albeit with some decadal variability in summer (Figure 4). A  
 1431 simple linear extrapolation of the trends in the future suggests that aragonite under-saturation in surface  
 1432 waters would be reached in year 2110 for the winter season and 2120 for summer (Figure S17) whereas the  
 1433 trend in subsurface trend suggests under-saturation in 2090. In year 2100, surface pH and  $[\text{H}^+]$  would be around

1434 7.9 and 12 nmol.kg<sup>-1</sup> (Figure S17). However, ESM CMIP6 models suggest that under a high emission scenario  
1435 (SSP5-8.5), pH in 2100 in the Southern Ocean near 50°S would be around 7.65 and [H<sup>+</sup>] around 22 nmol.kg<sup>-1</sup>  
1436 (Jiang et al., 2023, their figure 4). This ~~suggests~~shows that the simple linear extrapolation based on recent  
1437 observed trends (Figure S17) underestimated the future change of the carbonate system for a high emission  
1438 scenario as previously shown in the South-Eastern Indian Ocean based on summer trends derived from  
1439 observations in 1969-2003 (Midorikawa et al., 2012, their figure 4).

1440 To better investigate the changes ~~infor~~for the next decades, we assumed that the C<sub>ant</sub> trend for the modern  
1441 period (Figure 7) that experienced a “business as usual” scenario after the sixties is representative of the future  
1442 changes in the surface ocean carbonate system. For this analysis, we ~~useused~~used two emissions scenarios (Shared  
1443 Socioeconomic Pathways, SSP, Meinshausen et al., 2020) with atmospheric xCO<sub>2</sub> reaching 1135 ppm in 2100 (a  
1444 “high” emission scenario SSP5-8.5) or xCO<sub>2</sub> reaching 603 ppm in 2100 after a stabilization around 2080  
1445 (scenario SSP2-4.5). This enables to simulate future C<sub>T</sub> concentrations for summer or winter (Figure 14) and to  
1446 calculate other carbonate properties using C<sub>T</sub> and A<sub>T</sub> (Figure 15, Table 23) in response to approximated future  
1447 changes in physical and geochemical properties excluding impacts of changes in atmospheric and oceanic  
1448 circulation. As the calculated properties are sensitive to A<sub>T</sub> values, we used a fixed A<sub>T</sub> of 2280 μmol.kg<sup>-1</sup> or  
1449 applied a correction based on the long-term change of sea surface salinity observed in the last 6 decades (1960-  
1450 2017), i.e. a freshening in the Southern Ocean of around -0.01 to -0.02.decade<sup>-1</sup> (Durack and Wijffels, 2010;  
1451 Cheng et al., 2020b). The decrease in salinity in the South Indian Ocean (-0.02- ~~±0.01~~ decade<sup>-1</sup> ~~± 0.01~~) was  
1452 recently analyzed by Akhoudas et al. (2023) who showed that in the years 1993-2021 the freshening was mainly  
1453 due to an increase in ~~the precipitation~~precipitations linked to the acceleration of the atmospheric hydrological  
1454 cycle. From our data in the mixed-layer over 1985-2021, we estimated a trend in salinity of -0.0207-0.021 ±0.004  
1455 decade<sup>-1</sup> (~~± 0.0041~~). For the A<sub>T</sub> sensitivity test we thus ~~selectselected~~selected a salinity trend of -0.01.decade<sup>-1</sup> in 1962-  
1456 1985 and -0.02.decade<sup>-1</sup> after 1985 and ~~applyapplied~~applied these trends to simulate A<sub>T</sub> over 1960-2100 using the  
1457 A<sub>T</sub>/Salinity relationship (Equation 1). This leads to a salinity of 33.650 and A<sub>T</sub> of 2272 μmol.kg<sup>-1</sup> in ~~the~~ year  
1458 2100, about 8 μmol.kg<sup>-1</sup> lower than observed in 2021 (2280 μmol.kg<sup>-1</sup>). Compared to the C<sub>T</sub> change from 2021 to  
1459 2100 (+50 and +193 μmol.kg<sup>-1</sup> for the “low” and “high” emissions scenario, Figure 14), the impact of ~~the~~ A<sub>T</sub>  
1460 decrease has a minor effect on the future change for pH, [CO<sub>3</sub><sup>2-</sup>] ~~orand~~ Ω (Table 23). For example, in winter for  
1461 the SSP5-8.5 scenario, when the A<sub>T</sub> decrease is taken into account, pH in 2100 is 7.316 and Ω<sub>A<sub>T</sub></sub> is 0.33 against  
1462 7.372 and 0.34 when A<sub>T</sub> is constant (Table 23). In both cases, the ~~surface~~ aragonite ~~under~~-saturation (Ω<sub>A<sub>T</sub>=1</sub>) in  
1463 winter occurred in 2055, whereas in summer it is identified in 2070. The effect of lower A<sub>T</sub> in the future  
1464 appeared also small compared to the seasonal differences of pH and Ω in 2100.

1465 As noted above, the Southern Ocean experienced a warming in recent decades (e.g. Auger et al., 2021)  
1466 and it is projected that warming will continue in the future (IPCC, 2022). Therefore, to test the sensitivity of  
1467 calculated properties to warming we applied a ~~correctionwarming~~warming of +0.0125°C.yr<sup>-1</sup> in 1985-2020 and  
1468 +0.025°C.yr<sup>-1</sup> after 2020 (Azarian et al, 2023). As for A<sub>T</sub>, these results are compared for winter using constant  
1469 SST (Table 3 2). The effect of the long-term warming does mainly impact the projection of [H<sup>+</sup>] and pH (Table  
1470 23).

1471 These sensitivity tests for temperature and A<sub>T</sub> showed that as for the observed period 1962-2021 (Figure  
1472 13), the projection in the future depends mainly on the anthropogenic CO<sub>2</sub> accumulation. Here, the C<sub>T</sub>  
1473 concentrations were calculated using the C<sub>ant</sub> versus atmospheric CO<sub>2</sub> relationship (Figure 7b). We thus tested  
1474 the results for winter based on the error associated with this relationship (Figure S18). This leads to either higher

Mis en forme : Barré

1475 | or lower  $C_T$  compared to [the](#) original calculation (Figure 14). For the SSP5-8.5 scenario, the winter  $C_T$   
1476 | concentrations in 2100 range between 2328 and 2378  $\mu\text{mol.kg}^{-1}$ , higher than simulated in the ESM CMIP6  
1477 | models around 50°S (2300  $\mu\text{mol.kg}^{-1}$ , Jiang et al., 2023). As in the ESM models ~~for the SSP2-4.5 scenario~~, the  
1478 | projected  $C_T$  concentration in 2100 at our location [for the SSP2-4.5 scenario](#) is much lower 2217  $\mu\text{mol.kg}^{-1}$   
1479 | (Figure 14). The future change of the carbonate system is not significantly different using low or high  $C_{\text{ant}}$   
1480 | accumulation (Figure S18) but this test gives a range of years to reach aragonite and calcite under-saturation. In  
1481 | winter (SSP5-8.5 scenario), aragonite ([calcite](#)) would reach under-saturation between year 2050 and 2060 ~~and~~  
1482 | ~~(between year 2070 and 2080 for calcite.)~~. Note that for summer we derived under-saturation for  $\Omega_{\text{Ar}}$  in year  
1483 | 2065 and for  $\Omega_{\text{Ca}}$  in year 2085. For the SSP2-4.5 scenario, where  $C_T$  is 143  $\mu\text{mol.kg}^{-1}$  lower in 2100 compared to  
1484 | SSP5-8.5, aragonite under-saturation would not be reached before 2070 (Figure 15).  
1485 |

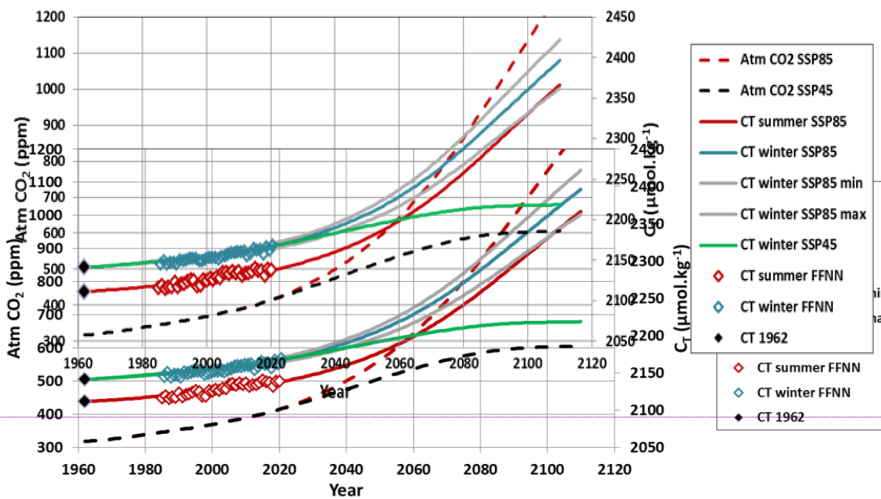
1486

1487 Table 23: Results of the simulated properties for year 2020, 2050 and 2100 for two emission scenarios (SSP5-8.5  
 1488 or SSP2-4.5). For 2020 the results based on observations in January (Obs) and the FFNN model in January and August  
 1489 also listed. Sensitivity tests: "SSP85 W-T" is for winter with constant temperature and "SSP85 W-A-T" is for winter with  
 1490 constant  $A_T$  and temperature.

Method	Year	Atm-CO <sub>2</sub> ppm	fCO <sub>2</sub> µatm	C <sub>T</sub> µmol.kg <sup>-1</sup>	A <sub>T</sub>	pH TS	[H <sup>+</sup> ] nmol.kg <sup>-1</sup>	[CO <sub>3</sub> <sup>2-</sup> ] µmol.kg <sup>-1</sup>	Ωca	Ωar
Obs Jan	2020	410.6	391.9	2142.2	2281.8	8.044	9.04	105.2	2.53	1.59
Std obs.			(2.0)	(0.7)	(0.3)	(0.002)	(0.04)	(0.5)	(0.01)	(0.01)
FFNN Jan	2020	410.6	385.1	2138.5	2280.1	8.051	8.90	106.3	2.55	1.61
SSP Summer	2020	414.9	375.4	2137.5	2282.1	8.061	8.70	108.0	2.60	1.63
FFNN Aug	2020	410.6	410.0	2168.3	2289.8	8.024	9.45	94.2	2.27	1.42
SSP Winter	2020	414.9	434.5	2167.3	2282.1	8.001	9.98	90.4	2.18	1.37
SSP85SSP585 Summer	2050	562.8	526.5	2177.2	2278.3	7.928	11.79	84.2	2.02	1.28
SSP85SSP585 Winter	2050	562.8	624.7	2207.0	2278.3	7.857	13.91	68.5	1.65	1.04
SSP85SSP585 W-A-T	2050	562.8	585.7	2207.0	2280.0	7.880	13.17	69.0	1.66	1.04
SSP85SSP585 W-T	2050	562.8	592.7	2207.0	2278.3	7.875	13.32	68.1	1.64	1.03
SSP45 SSP245 Winter	2050	506.9	554.8	2192.0	2278.3	7.905	12.46	75.8	1.92	1.15
SSP85SSP585 Summer	2100	1135.2	1986.9	2330.6	2271.8	7.394	41.31	26.9	0.65	0.41
SSP85SSP585 Winter	2100	1135.2	2306.3	2360.4	2271.8	7.316	48.26	21.8	0.52	0.33
SSP85SSP585 W-A-T	2100	1135.2	1993.1	2360.4	2280.0	7.372	42.44	22.6	0.54	0.34
SSP85SSP585 W-T	2100	1135.2	2097.0	2360.4	2271.8	7.349	44.74	21.3	0.51	0.32
SSP45 SSP245 Winter	2100	602.8	753.9	2217.7	2271.8	7.782	16.51	60.9	1.47	0.92

Mis en forme : Gauche, Espace Après : 10 pt, Interligne : Multiple 1,15 li  
 Mis en forme : Police : Times New Roman, 10 pt  
 Mis en forme : Police : 9 pt  
 Mis en forme : Police : 9 pt  
 Mis en forme : Police : 9 pt  
 Mis en forme : Police : 9 pt

1519

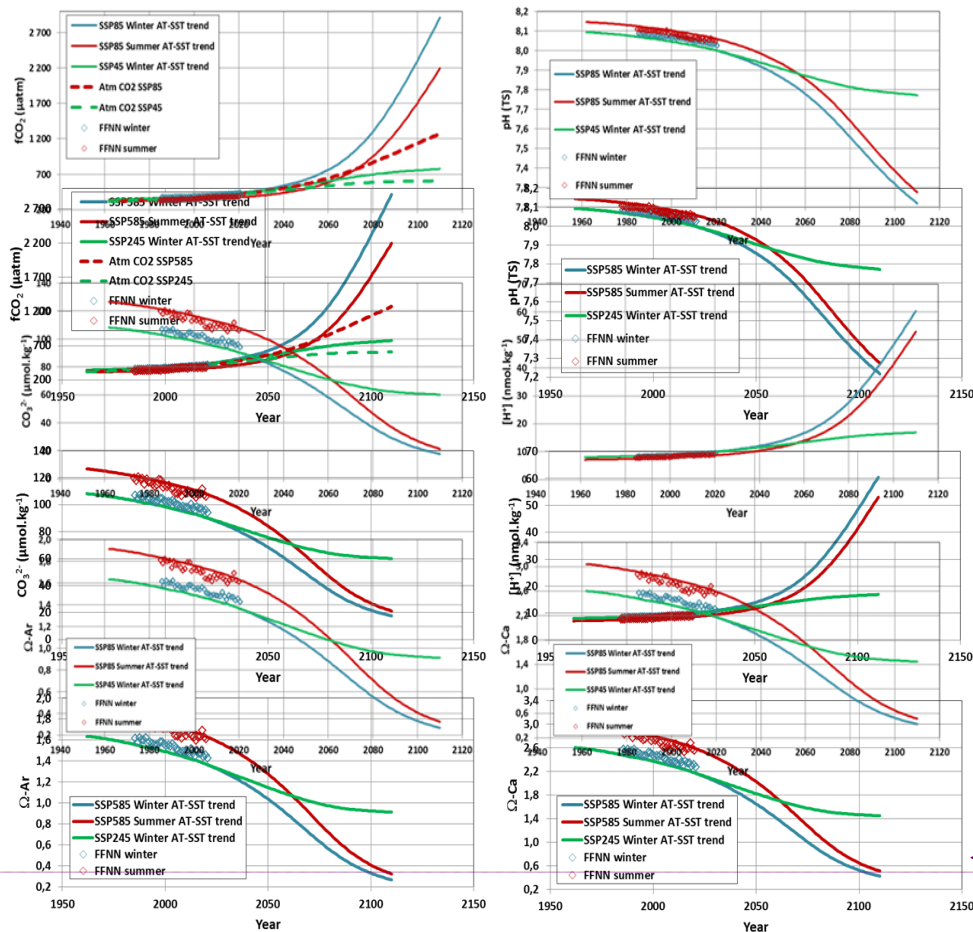


Mis en forme : Police : 10 pt, Soulignement  
 Mis en forme : Interligne : Multiple 1,15 li  
 Mis en forme : Couleur de police : Rouge foncé

1538 Figure 14: Evolution of atmospheric CO<sub>2</sub> (ppm) and sea surface C<sub>T</sub> (µmol.kg<sup>-1</sup>) between 1960 and 2110 evaluated for 2  
 1539 scenarios (SSP2-4.5 black dashed and SSP5-8.5 red dashed), for summer (red line for SSP5-8.5) and winter (blue line for  
 1540 SSP5-8.5 and green line for SSP2-4.5). Grey lines are the high and low C<sub>T</sub> for winter SSP85 based on the error in the  
 1541 C<sub>ant</sub>/fCO<sub>2</sub> relationship (figure 7b). Also shown are the results for the FFNN model in 1985-2020 for summer (red diamonds)  
 1542 and winter (blue diamonds) and C<sub>T</sub> in 1962 (black diamonds). The C<sub>T</sub> values for different seasons and scenarios were used to  
 1543 calculate the carbonate properties in the future (Figure 15).

1544

1545  
 1546  
 1547  
 1548  
 1549  
 1550  
 1551  
 1552  
 1553  
 1554  
 1555  
 1556  
 1557  
 1558  
 1559  
 1560  
 1561  
 1562  
 1563  
 1564  
 1565  
 1566  
 1567  
 1568  
 1569  
 1570  
 1571  
 1572  
 1573



Mis en forme : Police : +Corps (Calibri), 11 pt, Couleur de police : Violet  
 Mis en forme : Gauche, Interligne : Multiple 1,15 li

1574  
 1575  
 1576  
 1577  
 1578  
 1579  
 1580  
 1581  
 1582  
 1583  
 1584  
 1585  
 1586  
 1587  
 1588  
 1589  
 1590  
 1591  
 1592

Figure 15: Evolution of sea surface  $f\text{CO}_2$  ( $\mu\text{atm}$ ), pH (TS),  $[\text{CO}_3^{2-}]$  ( $\mu\text{mol.kg}^{-1}$ ),  $[\text{H}^+]$  ( $\text{nmol.kg}^{-1}$ ),  $\Omega\text{-Ar}$  and  $\Omega\text{-Ca}$  *inbetween* 1960- *and* 2110 evaluated for the SSP5-8.5 scenario for winter (blue line) and summer (red line) taking into account both  $A_T$  and SST future trends. For winter *the* results are also presented using the SSP2-4.5 scenario (green line). Also shown are the results for the FFNN model in 1985-2020 for summer (red diamonds) and winter (blue diamonds). Atmospheric  $f\text{CO}_2$  is also shown for SSP5-8.5 (red dashed) and SSP2-4.5 (green dashed). Values in 2020, 2050 and 2100 for different sensitivity tests are listed in Table 23.

#### 4 Summary and concluding remarks

The times-series of high quality observations *incollected between* 1985- *and* 2021 and the results from the FFNN model at one location, south of the Polar Front in the Southern Indian Ocean ( $50^\circ\text{S}$ - $68^\circ\text{E}$ ) presented in this analysis offered new results on the inter-annual variability, decadal to long-term trends of the carbonate system in surface waters, air-sea  $\text{CO}_2$  fluxes and associated drivers. The evaluation of anthropogenic  $\text{CO}_2$  concentrations in the water column *indicatesindicated* that the trends of the carbonate species are mainly driven by the *anthropogenic*  $\text{CO}_2$  uptake leading to a progressive acidification in surface waters and at depth.

In 1985, the  $C_{\text{ant}}$  concentrations were approaching  $50 \mu\text{mol.kg}^{-1}$  at 200 m and  $C_{\text{ant}}$  was detected in the water column down to the bottom (1600m). This explains why aragonite under-saturation was observed at *around 600m600-700m* in 1985, where  $[\text{CO}_3^{2-}]$  concentration was at *its* minimum, whereas *atfor the* pre-



1593 industrial era the whole water column was super-saturated (this study Figure S15; Lauvset et al., 2020, their  
1594 Figure S15). 36 years later, because of the anthropogenic CO<sub>2</sub> accumulation, we observed an upward migration  
1595 of the aragonite saturation horizon that was found around 400 m in 2021 (a shoaling rate of around -6 m.yr<sup>-1</sup>).

1596 At subsurface, in the ~~winter-water~~ Winter Water layer, the C<sub>ant</sub> trend is estimated at +0.53 (~~±±0.01~~)  
1597 μmol.kg<sup>-1</sup>.yr<sup>-1</sup> ~~inover~~ 1985-2021 with a detectable increase of the trend in recent years (~~up to 72 μmol.kg<sup>-1</sup> in~~  
1598 ~~2021 compared to 47 μmol.kg<sup>-1</sup> in 1985~~). The C<sub>ant</sub> concentrations in the ocean are closely related to the  
1599 atmospheric CO<sub>2</sub> concentrations and the slope we observed south of the PF in the Indian sector of +0.263 ±  
1600 0.042 μmol.kg<sup>-1</sup>.μatm<sup>-1</sup> is close to that observed in the AAIW in the South Atlantic (~~+0.23 ± 0.05 μmol.kg<sup>-1</sup>~~  
1601 ~~μatm<sup>-1</sup>~~, (Fontela et al., 2021). This suggests that local observations in the South Indian POOZ captured the link  
1602 between C<sub>ant</sub> and atmospheric CO<sub>2</sub> at larger scale.

1603 In surface waters, over 1991-2020 the oceanic fCO<sub>2</sub> increased at a rate close or slightly lower than in  
1604 the atmosphere (Figure 2b) and the C<sub>T</sub> trend followed the C<sub>ant</sub> accumulation (Figure 4b, S12a). However in the  
1605 last decade both observations and the FFNN model showed low fCO<sub>2</sub> trends in summer (less than 1 μatm.yr<sup>-1</sup>).  
1606 The change in summer trend appears related to primary production as revealed by a decrease of Chl-a in 1998-  
1607 2010 followed by an increase after 2010. Biological activity counteracts the C<sub>T</sub> increase due to C<sub>ant</sub>, resulting in  
1608 rather stable C<sub>T</sub> and fCO<sub>2</sub> in summer ~~2010-2020 (+0.38±0.26 μmol.kg<sup>-1</sup>.yr<sup>-1</sup> and +0.98 ± 0.40 μatm.yr<sup>-1</sup>)~~, during  
1609 the last decade. As a result, the region moved from an annual source of +0.8 molC.m<sup>-2</sup>.yr<sup>-1</sup> in 1985 to a sink of -  
1610 0.5 molC.m<sup>-2</sup>.yr<sup>-1</sup> in 2020. ~~The~~ Adding historical data from November 1962 that indicate an annual source of 2.2  
1611 molC.m<sup>-2</sup>.yr<sup>-1</sup>, and extrapolating to the entire South Indian POOZ (50-58°S/20-120°E, 6.5 Mkm<sup>2</sup>), suggest that  
1612 this region changed from a CO<sub>2</sub> source of 0.17 PgC.yr<sup>-1</sup> in 1962, reduced to 0.06 PgC.yr<sup>-1</sup> in 1985 and a CO<sub>2</sub> sink  
1613 of -0.04 PgC.yr<sup>-1</sup> in 2020. This can be compared with reconstructed fluxes from a data-based model that  
1614 produced a CO<sub>2</sub> source around 0.10 PgC.yr<sup>-1</sup> in 1960-1990 and a sink around -0.05 PgC.yr<sup>-1</sup> in 2020 in the south  
1615 Indian sector (Rödenbeck et al., 2022, their Figure 6). Based on the FFNN reconstructions, the increase of the  
1616 ocean CO<sub>2</sub> sink was particularly pronounced after 2011 (Figure 3) when phytoplankton biomass was  
1617 stronger increasing in this HNLC region and occurred when the SAM index was in a positive state. Although  
1618 observations in the water column do not suggest enhanced upwelling, we cannot eliminate the possibility that the  
1619 SAM influenced changes in primary production.

1620 In 1959-1963, the SAM was also positive on average and moved to a negative phase in 1964 (Marshall,  
1621 2003; King et al., 2023). Historical data from 1962 suggest that in For October/November the region was a small  
1622 CO<sub>2</sub> source (ΔfCO<sub>2</sub>=+8 μatm). Assuming the seasonality was the same as in the 80s, we estimate that in 1962 the  
1623 annual flux would be around 2.2 molC.m<sup>-2</sup>.yr<sup>-1</sup>. Extrapolating to the entire South Indian POOZ (50-58°S/20-  
1624 120°E, 6.5 Mkm<sup>2</sup>), this region was a CO<sub>2</sub> source of 0.17 PgC.yr<sup>-1</sup> in 1962, reduced to 0.06 PgC.yr<sup>-1</sup> in 1985 and a  
1625 CO<sub>2</sub> sink of -0.04 PgC.yr<sup>-1</sup> in 2020. This could be compared with reconstructed fluxes from a data-based model  
1626 that produced a CO<sub>2</sub> source in 1960-1990 and a sink in 2020 in the south Indian sector (Rödenbeck et al., 2022,  
1627 their Figure 6).

1628 For ~~November 1962~~, the estimated increase in C<sub>T</sub> concentration in surface (~~2135 μmol.kg<sup>-1</sup>) is waters~~  
1629 over 54 years (+21 μmol.kg<sup>-1</sup> lower than observed mid-October 2016 in the mixed-layer (2156 μmol.kg<sup>-1</sup>). This  
1630 is) was almost equal to the increase of C<sub>ant</sub> in 54 years (+22.3 μmol.kg<sup>-1</sup>). As a result, surface ocean pH dropped  
1631 from 8.11 in 1962 to 8.044 in 2020. Over a multi-decadal time scale (30 years or more), acidification in the  
1632 South Indian POOZ has been was mainly controlled by the uptake of anthropogenic CO<sub>2</sub>. However, our data also  
1633 indicate a modulation of the summer pH trend by natural processes. After 2010, a very small pH trend was

1634 | estimated in summer ( $-0.0098.\text{decade}^{-1} \pm 0.0042$ ) when the region experienced ~~higher in increase in~~ primary  
1635 | productivity. On the opposite, in winter, the pH trends continuously increased with time, ~~-0.010.decade<sup>-1</sup> ( $\pm$~~   
1636 | ~~0.001) in 1991-2001 and -0.021.decade<sup>-1</sup> ( $\pm$  0.002) in 2010-2020. In, At the subsurface (~~winter water~~ Winter  
1637 | ~~Water~~ layer), the trend of pH based on ~~A<sub>T</sub> and C<sub>T</sub> data in over~~ 1985-2021 ~~of (-0.0161 ( $\pm$  0.0033).decade<sup>-1</sup>)~~ is  
1638 | also almost equal to the annual surface trend from the FFNN model. A simple extrapolation of the trends in the  
1639 | WW indicated that under-saturation ( $\Omega < 1$ ) would be reached at year 2090 for aragonite and year 2180 for  
1640 | calcite. However, as atmospheric CO<sub>2</sub> ~~will desperately continue is expected~~ to ~~rise increase~~ and ocean C<sub>T</sub> will  
1641 | increase in the future, ~~the~~ pH and  $\Omega$  will decrease at a faster rate than observed in ~~recent years the last decades~~. A  
1642 | projection of future C<sub>T</sub> concentrations based on ~~emissions scenariotwo emission scenarios~~, excluding changes in  
1643 | ocean circulation, indicated that the winter surface pH in 2100 would decrease to 7.32 for a high emission  
1644 | scenario (SSP5-8.5) or to 7.782 for a low emission scenario (SSP2-4.5). This is up to -0.86 lower than pre-  
1645 | industrial pH and -0.71 lower than pH observed in 2020. For the winter season the aragonite ~~under~~-saturation in  
1646 | surface would be reached around 2050 for a high emissions scenario and 2070 for a low emission scenario.~~

1647 | The time-series presented here for the Southern Ocean, along with other historical time-series of A<sub>T</sub>  
1648 | ~~and~~ C<sub>T</sub> in the water-column (BATS, HOT, ESTOC, KNOT, Iceland or Irminger seas; Bates et al., 2014; Lange et  
1649 | al., 2023) or the recent ~~BGBGC~~-Argo floats in the Southern Ocean (Mazloff et al., 2023) offer useful data for the  
1650 | evaluation of biogeochemical and Earth system models, especially ~~for the coupling of fCO<sub>2</sub>, C<sub>T</sub>, A<sub>T</sub> physical and~~  
1651 | ~~pH biological drivers of the carbonate system~~ not well represented in current models at seasonal to decadal  
1652 | ~~sealescales~~ in the Southern Ocean (e.g. Hauck et al., ~~20232023a~~; Rodgers et al., 2023; Joos et al., 2023).  
1653 | Observing the decadal changes of the carbonate system in the water column is also an important step to extend  
1654 | the evaluation of biogeochemical and ESM models below the surface (Jiang et al., 2023). It is important to  
1655 | maintain such time-series for monitoring the future evolution of the ocean CO<sub>2</sub> sink, of the acidification and its  
1656 | impact on phytoplankton species and higher trophic levels. This is especially the case in Marine Protected Area  
1657 | such as the French Sub-Antarctic islands including the Kerguelen Archipelago which was listed as a UNESCO  
1658 | World Heritage site in 2019.

#### 1659 | **Data availability:**

1660 | Data used in this study are available in SOCAT ([www.socat.info](http://www.socat.info)) for fCO<sub>2</sub> surface data, in GLODAP  
1661 | ([www.glodap.info](http://www.glodap.info)) for water-column data and at NCEI/OCADS ([www.ncei.noaa.gov/access/ocean-carbon-data-](http://www.ncei.noaa.gov/access/ocean-carbon-data-system/oceans/VOS_Program/OISO.html)  
1662 | [system/oceans/VOS\\_Program/OISO.html](http://www.ncei.noaa.gov/access/ocean-carbon-data-system/oceans/VOS_Program/OISO.html)). The CMEMS-LSCE-FFNN model data are available at E.U.  
1663 | Copernicus Marine Service Information (<https://resources.marine.copernicus.eu/products>).

#### 1666 | **Authors contributions:**

1667 | CLM and NM are co-I of the ongoing OISO project. CLM, NM, CL and CR participated to OISO cruises.  
1668 | Underway fCO<sub>2</sub> was measured by CLM, NM, CL, and qualified by CLM and NM. Nutrients data were measured  
1669 | and qualified by CLM and CL. Chl-a data were measured and qualified by CR. Water column data were  
1670 | qualified by CLM, NM, CL, CR and GR. MG, FC and TTTC developed the CMEMS-LSCE-FFNN model and  
1671 | provided the model results. NM started the analysis, wrote the draft of the manuscript and prepared the figures  
1672 | All authors contributed to revising the draft manuscript.

1673 | **Competing interest:** The authors declare that they have no conflict of interest.

Mis en forme : Police : +Corps  
(Calibri), 11 pt, Français (France)

1675  
1676 **Acknowledgments:** The OISO program was supported by the French institutes INSU (Institut National des  
1677 Sciences de l'Univers) and IPEV (Institut Polaire Paul-Emile Victor), OSU Ecce-Terra (at Sorbonne Université),  
1678 and the French [programprograms](#) SOERE/Great-Gases- and [ICOS-France](#). We thank the French [oceanographic](#)  
1679 [fleet](#) ("Flotte océanographique française") [Oceanographic Fleet](#) for financial and logistic support for the OISO  
1680 program (<https://campagnes.flotteoceanographique.fr/series/228/>). We thank the captains and crew of *R.R.V.*  
1681 *Marion Dufresne* and the staff at IFREMER, GENAVIR and IPEV. We also thank Jonathan Fin and Claude  
1682 Mignon for their help during the OISO cruises. The development of the neural network model benefited from  
1683 funding by the French INSU-GMMC project "PPR-Green-Grog (grant no 5-DS-PPR-GGREOG), the EU H2020  
1684 project AtlantOS (grant no 633211), as well as through the Copernicus Marine Environment Monitoring Service  
1685 (project 83-CMEMS-TAC-MOB). We thank all colleagues that contributed to the quality control of ocean data  
1686 made available through CARINA and GLODAP ([www.glodap.info](http://www.glodap.info)). The Surface Ocean CO<sub>2</sub> Atlas (SOCAT,  
1687 [www.socat.info](http://www.socat.info)) is an international effort, endorsed by the International Ocean Carbon Coordination Project  
1688 (IOCCP), the Surface Ocean Lower Atmosphere Study (SOLAS) and the Integrated Marine Biogeochemistry  
1689 and Ecosystem Research program (IMBER), to deliver a uniformly quality-controlled surface ocean CO<sub>2</sub>  
1690 database. [We thank the associate editor, Ismael Hernández-Carrasco, and two anonymous reviewers for their](#)  
1691 [detailed comments and supportive reviews.](#)

1692  
1693 **References**

- 1694  
1695 Akhondas, C. H., Sallée, J.-B., Reverdin, G., Haumann, F. A., Pauthenet, E., Chapman, C. C., Margirier, F., Lo  
1696 Monaco, C., Metzl, N., Meilland, J., and Stranne, C.: Isotopic evidence for an intensified hydrological cycle in  
1697 the Indian sector of the Southern Ocean. *Nat Commun* 14, 2763. <https://doi.org/10.1038/s41467-023-38425-5>,  
1698 2023  
1699  
1700 Aminot, A., and Kérouel, R.: *Hydrologie des écosystèmes marins: paramètres et analyses*. Ed. Ifremer, 336 p.,  
1701 2004  
1702  
1703 Antonov, J. I., Locarnini, R. A., Boyer, T. P., Mishonov, A. V., and Garcia, H. E.: World Ocean Atlas 2005, in:  
1704 Volume 2: Salinity, edited by: Levitus, S., NOAA Atlas NESDIS 62, US Government Printing Office,  
1705 Washington, DC, 182 pp., <https://repository.library.noaa.gov/view/noaa/1127>, 2006.  
1706  
1707 Arrigo, K. R., van Dijken, G. L., and Bushinsky, S.: Primary production in the Southern Ocean, 1997–2006, *J.*  
1708 *Geophys. Res.-Oceans*, 113, C08004, doi:doi:10.1029/2007jc004551, 2008.  
1709  
1710 Auger, M., Morrow, R., Kestenare, E., Sallée, J.-B., and Cowley, R.: Southern Ocean in-situ temperature trends  
1711 over 25 years emerge from interannual variability, *Nat. Commun.*, 12, 514,  
1712 <https://doi.org/10.1038/s41467-020-20781-1>, 2021  
1713  
1714 Azarian, C., Bopp, L., Pietri, A., Sallée, J.-B., and d'Ovidio, F.: Current and projected patterns of warming and  
1715 marine heatwaves in the Southern Indian Ocean, *Progress in Oceanography*,  
1716 doi:<https://doi.org/10.1016/j.pocean.2023.103036>, 2023  
1717  
1718 Bakker, D. C. E., Pfeil, B., Landa, C. S., Metzl, N., O'Brien, K. M., Olsen, A., Smith, K., Cosca, C., Harasawa,  
1719 S., Jones, S. D., Nakaoka, S.-I., Nojiri, Y., Schuster, U., Steinhoff, T., Sweeney, C., Takahashi, T., Tilbrook, B.,  
1720 Wada, C., Wanninkhof, R., Alin, S. R., Balestrini, C. F., Barbero, L., Bates, N. R., Bianchi, A. A., Bonou, F.,  
1721 Boutin, J., Bozec, Y., Burger, E. F., Cai, W.-J., Castle, R. D., Chen, L., Chierici, M., Currie, K., Evans, W.,  
1722 Featherstone, C., Feely, R. A., Fransson, A., Goyet, C., Greenwood, N., Gregor, L., Hankin, S., Hardman-

1723 Mountford, N. J., Harlay, J., Hauck, J., Hoppema, M., Humphreys, M. P., Hunt, C. W., Huss, B., Ibáñez, J. S.  
1724 P., Johannessen, T., Keeling, R., Kitidis, V., Körtzinger, A., Kozyr, A., Krasakopoulou, E., Kuwata, A.,  
1725 Landschützer, P., Lauvset, S. K., Lefèvre, N., Lo Monaco, C., Manke, A., Mathis, J. T., Merlivat, L., Millero, F.  
1726 J., Monteiro, P. M. S., Munro, D. R., Murata, A., Newberger, T., Omar, A. M., Ono, T., Paterson, K., Pearce, D.,  
1727 Pierrot, D., Robbins, L. L., Saito, S., Salisbury, J., Schlitzer, R., Schneider, B., Schweitzer, R., Sieger, R.,  
1728 Skjelvan, I., Sullivan, K. F., Sutherland, S. C., Sutton, A. J., Tadokoro, K., Telszewski, M., Tuma, M., Van  
1729 Heuven, S. M. A. C., Vandemark, D., Ward, B., Watson, A. J., and Xu, S. : A multi-decade record of high-  
1730 quality fCO<sub>2</sub> data in version 3 of the Surface Ocean CO<sub>2</sub> Atlas (SOCAT), *Earth Syst. Sci. Data*, 8, 383-413,  
1731 doi:10.5194/essd-8-383-2016, 2016.

1732

1733 Bakker, D. C. E. et al: Surface Ocean CO<sub>2</sub> Atlas Database Version 2022 (SOCATv2022) (NCEI Accession  
1734 0253659). NOAA National Centers for Environmental Information. Dataset. <https://doi.org/10.25921/1h9f-nb73>.  
1735 Last Accessed [21 June 2022], 2022

1736

1737 Balch, W.M., Bates, N.R., Lam, P.J., Twining, B.S., Rosengard, S. Z., Bowler, B.C., Drapeau, D.T., Garley, R.,  
1738 Lubelczyk, L.C., Mitchell, C., and Rauschenberg, S.: Factors regulating the Great Calcite Belt in the Southern  
1739 Ocean and its biogeochemical significance. *Global Biogeochem. Cycles*, 30, doi: 10.1002/2016GB005414, 2016

1740

1741 Basterretxea, G., Font-Muñoz, J. S., Hernández-Carrasco, I., and Sañudo-Wilhelmy, S. A.: Global variability of  
1742 high-nutrient low-chlorophyll regions using neural networks and wavelet coherence analysis, *Ocean Sci.*, 19,  
1743 973–990, <https://doi.org/10.5194/os-19-973-2023>, 2023.

1744

1745 Bates, N., Astor, Y., Church, M., Currie, K., Dore, J., González-Dávila, M., Lorenzoni, L., Muller-Karger, F.,  
1746 Olafsson, J., and Santa-Casiano, M.: A Time-Series View of Changing Ocean Chemistry Due to Ocean Uptake  
1747 of Anthropogenic CO<sub>2</sub> and Ocean Acidification, *Oceanography*, 27, 126–141,  
1748 <https://doi.org/10.5670/oceanog.2014.16>, 2014.

1749

1750 Beaufort, L., Probert, I., de Garidel-Thoron, T., Bendif, E.M., Ruiz-Pino, D., Metzl, N., Goyet, C., Buchet, N.,  
1751 Coupel, P., Grelaud, M., Rost, B., Rickaby, R.E.M., and de Vargas C.: Sensitivity of coccolithophores to  
1752 carbonate chemistry and ocean acidification. *Nature*, doi:10.1038/nature10295. 2011

1753

1754 Bennington, V., Gloege, L., and McKinley, G. A.: Variability in the global ocean carbon sink from 1959 to 2020  
1755 by correcting models with observations. *Geophysical Research Letters*, 49, e2022GL098632.  
1756 <https://doi.org/10.1029/2022GL098632>, 2022

1757

1758 Benoiston, A.-S., Ibarbalz, F. M., Bittner, L., Guidi, L., Jahn, O., Dutkiewicz, S., and Bowler, C.: The evolution  
1759 of diatoms and their biogeochemical functions. *Phil. Trans. R. Soc. B* 372: 20160397.  
1760 <http://dx.doi.org/10.1098/rstb.2016.0397>, 2017

1761

1762 Bopp, L., Resplandy, L., Orr, J. C., Doney, S. C., Dunne, J. P., Gehlen, M., Halloran, P., Heinze, C., Ilyina, T.,  
1763 Séférian, R., Tjiputra, J., and Vichi, M.: Multiple stressors of ocean ecosystems in the 21st century: projections  
1764 with CMIP5 models, *Biogeosciences*, 10, 6225–6245, <https://doi.org/10.5194/bg-10-6225-2013>, 2013.

1765

1766 Brady, R. X., Maltrud, M. E., Wolfram, P. J., Drake, H. F., and Lovenduski, N. S.: The influence of ocean  
1767 topography on the upwelling of carbon in the Southern Ocean. *Geophysical Research Letters*, 48,  
1768 e2021GL095088. <https://doi.org/10.1029/2021GL095088>, 2021

1769

1770 Brandon, M., Goyet, C., Touratier, F., Lefèvre, N., Kestenare, E., and Morrow, R.: Spatial and temporal  
1771 variability of the physical, carbonate and CO<sub>2</sub> properties in the Southern Ocean surface waters during austral  
1772 summer (2005-2019), *Deep-Sea Research Part I*, <https://doi.org/10.1016/j.dsr.2022.103836>, 2022

1773

1774 Burger, F. A., John, J. G., and Frölicher, T. L.: Increase in ocean acidity variability and extremes under  
1775 increasing atmospheric CO<sub>2</sub>, *Biogeosciences*, 17, 4633–4662, <https://doi.org/10.5194/bg-17-4633-2020>, 2020

1776  
1777 Bushinsky, S. M., Landschützer, P., Rödenbeck, C., Gray, A. R., Baker, D., Mazloff, M. R., Resplandy, L.,  
1778 Johnson, K. S., and Sarmiento, J. L.: Reassessing Southern Ocean air-sea CO<sub>2</sub> flux estimates with the addition of  
1779 biogeochemical float observations. *Global Biogeochemical Cycles*, 33. doi: 10.1029/2019GB006176, 2019  
1780  
1781 Caldeira, K., and Wickett, M.: Anthropogenic carbon and ocean pH. *Nature*, 425, 365. doi: 10.1038/425365a,  
1782 2003  
1783  
1784 Canadell, J. G., Monteiro, P. M. S., Costa, M. H., Cotrim da Cunha, L., Cox, P. M., Eliseev, A. V., Henson, S.,  
1785 Ishii, M., Jaccard, S., Koven, C., Lohila, A., Patra, P. K., Piao, S., Rogelj, J., Syampungani, S., Zaehle, S., and  
1786 Zickfeld, K.: Global Carbon and other Biogeochemical Cycles and Feedbacks, in: *Climate Change 2021: The*  
1787 *Physical Science Basis. Contribution of Working Group I to the Sixth Assessment Report of the*  
1788 *Intergovernmental Panel on Climate Change*, edited by: Masson-Delmotte, V., Zhai, P., Pirani, A., Connors, S.  
1789 L., Péan, C., Berger, S., Caud, N., Chen, Y., Goldfarb, L., Gomis, M. I., Huang, M., Leitzell, K., Lonnoy, E.,  
1790 Matthews, J. B. R., Maycock, T. K., Waterfield, T., Yelekçi, O., Yu, R., and Zhou, B., Cambridge University  
1791 Press, Cambridge, United Kingdom and New York, NY, USA, 673–816, doi:10.1017/9781009157896, 2021  
1792  
1793 Carpenter, J. H.: The Accuracy of the Winkler Method for Dissolved Oxygen Analysis, *Limnol. Oceanogr.*, 10,  
1794 135–140, <https://doi.org/10.4319/lo.1965.10.1.0135>, 1965.  
1795  
1796 Carter, B. R., Williams, N. L., Gray, A. R., and Feely, R. A.: Locally interpolated alkalinity regression for global  
1797 alkalinity estimation. *Limnol. Oceanogr.: Methods* 14: 268–277. doi:10.1002/lom3.10087, 2016  
1798  
1799 Carter, B. R., Feely, R. A., Williams, N. L., Dickson, A. G., Fong, M. B., and Takeshita, Y.: Updated methods  
1800 for global locally interpolated estimation of alkalinity, pH, and nitrate. *Limnology and Oceanography: Methods*,  
1801 16: 119-131. doi: 10.1002/lom3.10232, 2018  
1802  
1803 Carter, B. R., Feely, R. A., Wanninkhof, R., Kouketsu, S., Sonnerup, R. E., Pardo, P. C., et al: Pacific  
1804 anthropogenic carbon between 1991 and 2017. *Global Biogeochemical Cycles*, 33, 597–617.  
1805 <https://doi.org/10.1029/2018GB006154>, 2019  
1806  
1807 Chapman, C., Mcc Hogg, A., Kiss, A., and Rintoul, S.: The dynamics of Southern Ocean storm tracks. *Journal of*  
1808 *Physical Oceanography*, 45 (3), pp.884 - 903. 10.1175/JPO-D-14-0075.1, 2015  
1809  
1810 Chau, T. T. T., Gehlen, M., and Chevallier, F.: A seamless ensemble-based reconstruction of surface ocean pCO<sub>2</sub>  
1811 and air–sea CO<sub>2</sub> fluxes over the global coastal and open oceans, *Biogeosciences*, 19, 1087–1109,  
1812 <https://doi.org/10.5194/bg-19-1087-2022>, 2022.  
1813  
1814 Chen, H., Haumann, F. A., Talley, L. D., Johnson, K. S., and Sarmiento, J. L.: The deep ocean's carbon exhaust.  
1815 *Global Biogeochemical Cycles*. doi: <https://doi.org/10.1002/essoar.10507757.1>, 2022  
1816  
1817 Cheng, L. J., Abraham, J., Zhu, J., Trenberth, K. E., Fasullo, J., Boyer, T., Locarnini, R., Zhang, B., Yu, F. J.,  
1818 Wan, L. Y., Chen, X. R., Song, X. Z., Liu, Y. L., and Mann, M. E.: Record-setting ocean warmth continued in  
1819 2019, *Adv. Atmos. Sci.*, 37, 137-142. <https://doi.org/10.1007/s00376-020-9283-7>, 2020a  
1820  
1821 Cheng L., K. E. Trenberth, N. Gruber, J. P. Abraham, J. Fasullo, G. Li, M. E. Mann, X. Zhao, Jiang Zhu:  
1822 Improved estimates of changes in upper ocean salinity and the hydrological cycle. *Journal of Climate*. doi:  
1823 <https://doi.org/10.1175/JCLI-D-20-0366.1>, 2020b  
1824  
1825 Copin-Montégut, C.: A new formula for the effect of temperature on the partial pressure of CO<sub>2</sub> in seawater.  
1826 *Marine Chemistry*, 25, 29-37. [https://doi.org/10.1016/0304-4203\(88\)90012-6](https://doi.org/10.1016/0304-4203(88)90012-6), 1988.  
1827

1828 Copin-Montégut, C.: A new formula for the effect of temperature on the partial pressure of CO<sub>2</sub> in seawater.  
1829 Corrigendum. *Marine Chemistry*, 27, 143-144. [https://doi.org/10.1016/0304-4203\(89\)90034-0](https://doi.org/10.1016/0304-4203(89)90034-0), 1989.  
1830  
1831 Coverly, S. C., Aminot, A., and R. Kérouel: Nutrients in Seawater Using Segmented Flow Analysis, In: Practical  
1832 Guidelines for the Analysis of Seawater, Edited by: Oliver Wurl, CRC Press,  
1833 <https://doi.org/10.1201/9781420073072,2009>  
1834  
1835 Daniault, N., and Ménard, Y.: Eddy kinetic energy distribution in the Southern Ocean from altimetry and FGGE  
1836 drifting buoys, *J. Geophys. Res.*, 90 (C6), 11877–11889, doi:10.1029/JC090iC06p11877, 1985  
1837  
1838 Demuynek, P., Tyrrell, T., Naveira Garabato, A., Moore, M. C., and Martin, A. P.: Spatial variations in silicate-  
1839 to-nitrate ratios in Southern Ocean surface waters are controlled in the short term by physics rather than biology,  
1840 *Biogeosciences*, 17, 2289–2314, <https://doi.org/10.5194/bg-17-2289-2020>, 2020.  
1841  
1842 DeVries, T., Yamamoto, K., Wanninkhof, R., Gruber, N., Hauck, J., Müller, J. D., et al.: Magnitude, trends, and  
1843 variability of the global ocean carbon sink from 1985-2018. *Global Biogeochemical Cycles*, 37,  
1844 e2023GB007780, doi:10.1029/2023GB007780, 2023.  
1845  
1846 Dickson, A. G.: Standard potential of the reaction: AgCl(s) + ½H<sub>2</sub>(g) = Ag(s) + HCl(aq), and the standard  
1847 acidity constant of the ion HSO<sub>4</sub><sup>-</sup> in synthetic sea water from 273.15 to 318.15 K. *J. Chem. Thermodyn.* **22**:  
1848 113–127. doi:10.1016/0021-9614(90)90074-Z, 1990  
1849  
1850 Dickson, A. G., Sabine, C. L. and Christian, J. R. (Eds.): Guide to Best Practices for Ocean CO<sub>2</sub> Measurements.  
1851 *PICES Special Publication* 3, 191 pp., [https://www.ncei.noaa.gov/access/ocean-carbon-acidification-data-](https://www.ncei.noaa.gov/access/ocean-carbon-acidification-data-system/oceans/Handbook_2007.html)  
1852 [system/oceans/Handbook\\_2007.html](https://www.ncei.noaa.gov/access/ocean-carbon-acidification-data-system/oceans/Handbook_2007.html), 2007  
1853  
1854 Dlugokencky, E. and Tans, P.: Trends in atmospheric carbon dioxide, National Oceanic & Atmospheric  
1855 Administration, Earth System Research Laboratory (NOAA/ESRL), available at: [http://](http://www.esrl.noaa.gov/gmd/ccgg/trends/global.html)  
1856 [www.esrl.noaa.gov/gmd/ccgg/trends/global.html](http://www.esrl.noaa.gov/gmd/ccgg/trends/global.html), (last access: 8 January 2022), 2022  
1857  
1858 Doney, S. C., Fabry, V. J., Feely, R. A., and Kleypas, J. A.: Ocean Acidification: The Other CO<sub>2</sub> Problem,  
1859 *Annu. Rev. Mar. Sci.*, 1, 169–192, <https://doi.org/10.1146/annurev.marine.010908.163834>, 2009.  
1860  
1861 Doney, S. C., Ruckelshaus, M., Duffy, J. E., Barry, J. P., Chan, F., English, C. A., Galindo, H. M., Grebmeier, J.  
1862 M., Hollowed, A. B., Knowlton, N., Polovina, J., Rabalais, N. N., Sydeman, W. J., and Talley, L. D.: Climate  
1863 change impacts on marine ecosystems, *Annu. Rev. Mar. Sci.*, 4, 11–37. 10.1146/annurev-marine-041911-  
1864 111611, 2012.  
1865  
1866 Dove, L. A., Balwada D., Thompson, A. F., and Gray, A. R.: Enhanced ventilation in energetic regions of the  
1867 Antarctic Circumpolar Current. *Geophys. Res. Lett.* 49(13):e2021GL097574,  
1868 <https://doi.org/10.1029/2021GL097574>. 2022.  
1869  
1870 Duncan, R.J., Nielsen, D.A., Sheehan, C.E., Deppeler, S., Hancock, A.M., Schulz, K.G., Davidson, A.T. and  
1871 Petrou, K.: Ocean acidification alters the nutritional value of Antarctic diatoms. *New Phytol*, 233: 1813-1827.  
1872 <https://doi-org.insu.bib.cnrs.fr/10.1111/nph.17868>, 2022  
1873  
1874 Durack, P. J. and Wijffels, S. E.: Fifty-year trends in global ocean salinities and their relationship to broad-scale  
1875 warming. *J. Climate*, 23, 4342–4362, <https://doi.org/10.1175/2010JCLI3377.1>, 2010  
1876  
1877 Fabry, V. J., Seibel, B. A., Feely, R. A., and Orr, J. C.: Impacts of ocean acidification on marine fauna and  
1878 ecosystem processes. – *ICES Journal of Marine Science*, 65: 414–432, doi: 10.1093/icesjms/fsn048, 2008  
1879

1880 Fassbender, A. J., Schlunegger, S., Rodgers, K. B., and Dunne, J. P.: Quantifying the role of seasonality in the  
1881 marine carbon cycle feedback: An ESM2M case study. *Global Biogeochemical Cycles*, 36, e2021GB007018.  
1882 doi:10.1029/2021GB007018, 2022

1883

1884 Fay, A. R., Munro, D. R., McKinley, G. A., Pierrot, D., Sutherland, S. C., Sweeney, C., and Wanninkhof, R.:  
1885 Updated climatological mean delta fCO<sub>2</sub> and net sea–air CO<sub>2</sub> flux over the global open ocean regions, Earth  
1886 Syst. Sci. Data Discuss. [preprint], <https://doi.org/10.5194/essd-2023-429>, in review, 2023.

1887

1888 Fox-Kemper, B., Hewitt, H. T. , Xiao, C., Adalgeirsdottir, G., Drijfhout, S. S., Edwards, T. L., Golledge, N. R.,  
1889 Hemer, M., Kopp, R. E., Krinner, G., Mix, A., Notz, D., Nowicki, S., Nurhati, I. S., Ruiz, L., Sallée, J.-B.,  
1890 Slangen, A. B. A., and Yu, Y.: *Climate Change 2021: The Physical Science Basis. Contribution of Working  
1891 Group I to the Sixth Assessment Report of the Intergovernmental Panel on Climate Change*, chapter Ocean,  
1892 Cryosphere and Sea Level Change, pages 1211-1362. Cambridge University Press, United Kingdom and New  
1893 York, NY, USA, August 2021. doi:10.1017/9781009157896.

1894

1895 Fontela, M., Vélo, A., Gilcoto, M., and Pérez, F.: Anthropogenic CO<sub>2</sub> and Ocean Acidification in Argentine  
1896 Basin Water Masses over Almost Five Decades of Observations. *Science of The Total Environment*, 779.  
1897 <https://doi.org/10.1016/j.scitotenv.2021.146570>, 2021

1898

1899 Franco, A. C., Ianson, D., Ross, T., Hamme, R. C., Monahan, A. H., Christian, J. R., et al.: Anthropogenic and  
1900 climatic contributions to observed carbon system trends in the northeast Pacific. *Global Biogeochemical Cycles*,  
1901 35, e2020GB006829. Doi: 10.1029/2020GB006829, 2021

1902

1903 Friedlingstein, P., O'Sullivan, M., Jones, M. W., Andrew, R. M., Gregor, L., Hauck, J., Le Quéré, C., Luijkx, I.  
1904 T., Olsen, A., Peters, G. P., Peters, W., Pongratz, J., Schwingshackl, C., Sitch, S., Canadell, J. G., Ciais, P.,  
1905 Jackson, R. B., Alin, S. R., Alkama, R., Arneeth, A., Arora, V. K., Bates, N. R., Becker, M., Bellouin, N., Bittig,  
1906 H. C., Bopp, L., Chevallier, F., Chini, L. P., Cronin, M., Evans, W., Falk, S., Feely, R. A., Gasser, T., Gehlen,  
1907 M., Gkritzalis, T., Gloege, L., Grassi, G., Gruber, N., Gürses, Ö., Harris, I., Hefner, M., Houghton, R. A., Hurtt,  
1908 G. C., Iida, Y., Ilyina, T., Jain, A. K., Jersild, A., Kadono, K., Kato, E., Kennedy, D., Klein Goldewijk, K.,  
1909 Knauer, J., Korsbakken, J. I., Landschützer, P., Lefèvre, N., Lindsay, K., Liu, J., Liu, Z., Marland, G., Mayot, N.,  
1910 McGrath, M. J., Metzl, N., Monacci, N. M., Munro, D. R., Nakaoka, S.-I., Niwa, Y., O'Brien, K., Ono, T.,  
1911 Palmer, P. I., Pan, N., Pierrot, D., Pockock, K., Poulter, B., Resplandy, L., Robertson, E., Rödenbeck, C.,  
1912 Rodriguez, C., Rosan, T. M., Schwinger, J., Séférian, R., Shutler, J. D., Skjelvan, I., Steinhoff, T., Sun, Q.,  
1913 Sutton, A. J., Sweeney, C., Takao, S., Tanhua, T., Tans, P. P., Tian, X., Tian, H., Tilbrook, B., Tsujino, H.,  
1914 Tubiello, F., van der Werf, G. R., Walker, A. P., Wanninkhof, R., Whitehead, C., Willstrand Wranne, A.,  
1915 Wright, R., Yuan, W., Yue, C., Yue, X., Zaehle, S., Zeng, J., and Zheng, B.: Global Carbon Budget 2022, Earth  
1916 Syst. Sci. Data, 14, 4811–4900, <https://doi.org/10.5194/essd-14-4811-2022>, 2022.

1917

1918 [Friedlingstein, P., O'Sullivan, M., Jones, M. W., Andrew, R. M., Bakker, D. C. E., Hauck, J., Landschützer, P.,](#)  
1919 [Le Quéré, C., Luijkx, I. T., Peters, G. P., Peters, W., Pongratz, J., Schwingshackl, C., Sitch, S., Canadell, J. G.,](#)  
1920 [Ciais, P., Jackson, R. B., Alin, S. R., Anthoni, P., Barbero, L., Bates, N. R., Becker, M., Bellouin, N., Decharme,](#)  
1921 [B., Bopp, L., Brasika, I. B. M., Cadule, P., Chamberlain, M. A., Chandra, N., Chau, T.-T.-T., Chevallier, F.,](#)  
1922 [Chini, L. P., Cronin, M., Dou, X., Enyo, K., Evans, W., Falk, S., Feely, R. A., Feng, L., Ford, D. J., Gasser, T.,](#)  
1923 [Ghattas, J., Gkritzalis, T., Grassi, G., Gregor, L., Gruber, N., Gürses, Ö., Harris, I., Hefner, M., Heinke, J.,](#)  
1924 [Houghton, R. A., Hurtt, G. C., Iida, Y., Ilyina, T., Jacobson, A. R., Jain, A., Jarníková, T., Jersild, A., Jiang, F.,](#)  
1925 [Jin, Z., Joos, F., Kato, E., Keeling, R. F., Kennedy, D., Klein Goldewijk, K., Knauer, J., Korsbakken, J. I.,](#)  
1926 [Körtzinger, A., Lan, X., Lefèvre, N., Li, H., Liu, J., Liu, Z., Ma, L., Marland, G., Mayot, N., McGuire, P. C.,](#)  
1927 [McKinley, G. A., Meyer, G., Morgan, E. J., Munro, D. R., Nakaoka, S.-I., Niwa, Y., O'Brien, K. M., Olsen, A.,](#)  
1928 [Omar, A. M., Ono, T., Paulsen, M., Pierrot, D., Pockock, K., Poulter, B., Powis, C. M., Rehder, G., Resplandy, L.,](#)  
1929 [Robertson, E., Rödenbeck, C., Rosan, T. M., Schwinger, J., Séférian, R., Smallman, T. L., Smith, S. M.,](#)  
1930 [Sospedra-Alfonso, R., Sun, Q., Sutton, A. J., Sweeney, C., Takao, S., Tans, P. P., Tian, H., Tilbrook, B., Tsujino,](#)  
1931 [H., Tubiello, F., van der Werf, G. R., van Ooijen, E., Wanninkhof, R., Watanabe, M., Wimart-Rousseau, C.,](#)

1932 | [Yang, D., Yang, X., Yuan, W., Yue, X., Zaehle, S., Zeng, J., and Zheng, B.: Global Carbon Budget 2023, Earth](#)  
1933 [Syst. Sci. Data, 15, 5301–5369, <https://doi.org/10.5194/essd-15-5301-2023>, 2023.](#)  
1934

1935 Frölicher, T. L., Sarmiento, J. L., Paynter, D. J., Dunne, J. P., Krasting, J. P., and Winton, M.: Dominance of the  
1936 southern ocean in anthropogenic carbon and heat uptake in CMIP5 models. *Journal of Climate*, 28(2), 862–886.  
1937 <https://doi.org/10.1175/JCLI-D-14-00117.1>, 2015  
1938

1939 Fu, W., Randerson, J. T., and Moore, J. K.: Climate change impacts on net primary production (NPP) and export  
1940 production (EP) regulated by increasing stratification and phytoplankton community structure in the CMIP5  
1941 models, *Biogeosciences*, 13, 5151–5170, <https://doi.org/10.5194/bg-13-5151-2016>, 2016.  
1942

1943 Gallego, M. A., Timmermann, A., Friedrich, T., and Zeebe, R. E.: Drivers of future seasonal cycle changes in  
1944 oceanic  $p\text{CO}_2$ , *Biogeosciences*, 15, 5315–5327, <https://doi.org/10.5194/bg-15-5315-2018>, 2018.  
1945

1946 Gangstø, R., Gehlen, M., Schneider, B., Bopp, L., Aumont, O., and Joos, F.: Modeling the marine aragonite  
1947 cycle: changes under rising carbon dioxide and its role in shallow water  $\text{CaCO}_3$  dissolution, *Biogeosciences*, 5,  
1948 1057–1072, <https://doi.org/10.5194/bg-5-1057-2008>, 2008.  
1949

1950 Gardner J., Peck, V. L., Bakker, D. C. E., Tarling, G. A. and Manno, C.: Contrasting life cycles of Southern  
1951 Ocean pteropods alter their vulnerability to climate change. *Front. Mar. Sci.* 10:1118570.  
1952 doi: 10.3389/fmars.2023.1118570, 2023  
1953

1954 [Gloege, L., McKinley, G. A., Landschützer, P., Fay, A. R., Frölicher, T. L., Fyfe, J. C., et al: Quantifying errors](#)  
1955 [in observationally based estimates of ocean carbon sink variability. \*Global Biogeochemical Cycles\*, 35,](#)  
1956 [e2020GB006788. <https://doi.org/10.1029/2020GB006788>, 2021.](#)  
1957

1958 Gooya, P., Swart, N. C., and Hamme, R. C.: Time-varying changes and uncertainties in the CMIP6 ocean carbon  
1959 sink from global to local scale, *Earth Syst. Dynam.*, 14, 383–398, <https://doi.org/10.5194/esd-14-383-2023>,  
1960 2023.  
1961

1962 Gray, A., Johnson, K. S., Bushinsky, S. M., Riser, S. C., Russell, J. L., Talley, L. D., et al.: Autonomous  
1963 biogeochemical floats detect significant carbon dioxide outgassing in the high-latitude Southern Ocean.  
1964 *Geophysical Research Letters*, 45, 9049–9057. <https://doi.org/10.1029/2018GL078013>, 2018.  
1965

1966 Gray, A., R.: The Four-Dimensional Carbon Cycle of the Southern Ocean. *Annu. Rev. Mar. Sci.* 16:23.1–23.28.  
1967 <https://doi.org/10.1146/annurev-marine-041923-104057>, 2024.  
1968

1969 Gregor, L., Kok, S., and Monteiro, P. M. S.: Interannual drivers of the seasonal cycle of  $\text{CO}_2$  in the Southern  
1970 Ocean, *Biogeosciences*, 15, 2361–2378, <https://doi.org/10.5194/bg-15-2361-2018>, 2018.  
1971

1972 Gruber, N., Clement, D., Carter, B. R., Feely, R. A., van Heuven, S., Hoppema, M., Ishii, M., Key, R. M.,  
1973 Kozyr, A., Lauvset, S. K., Lo Monaco, C., Mathis, J. T., Murata, A., Olsen, A., Perez, F. F., Sabine, C. L.,  
1974 Tanhua, T., and Wanninkhof, R.: The oceanic sink for anthropogenic  $\text{CO}_2$  from 1994 to 2007, *Science* vol. 363  
1975 (issue 6432), pp. 1193–1199. DOI: 10.1126/science.aau5153, 2019a.  
1976

1977 Gruber, N., Clement, D., Carter, B. R., Feely, R. A., Heuven, S., van, Hoppema, M., Ishii, M., Key, R. M.,  
1978 Kozyr, A., Lauvset, S. K., Lo Monaco, C., Mathis, J. T., Murata, A., Olsen, A., Perez, F. F., Sabine, C. L.,  
1979 Tanhua, T., and Wanninkhof, R.: The oceanic sink for anthropogenic  $\text{CO}_2$  from 1994 to 2007 – the data (NCEI  
1980 Accession 0186034), NOAA National Centers for Environmental Information [data set],  
1981 <https://doi.org/10.25921/wdn2-pt10>, 2019b.  
1982

1983 Gruber, N., Landschützer, P., and Lovenduski, N. S.: The Variable Southern Ocean Carbon Sink, *Annu.*  
1984 *Rev. Mar. Sci.*, Vol. 11, doi:10.1146/annurev-marine-121916-063407, 2019c.



1985  
1986 Gu, Y., Katul, G. G., & Cassar, N. Multiscale temporal variability of the global air-sea CO<sub>2</sub> flux anomaly.  
1987 Journal of Geophysical Research: Biogeosciences, 128, e2022JG006934. <https://doi.org/10.1029/2022JG006934>,  
1988 2023  
1989  
1990 Hauri, C., Friedrich, T., and Timmermann, A.: Abrupt onset and prolongation of aragonite undersaturation  
1991 events in the Southern Ocean, Nature Climate Change, doi:10.1038/nclimate2844, 2015.  
1992  
1993 Hauck J., Hoppema, M., Bellerby, R. G. J., Völker, C., and Wolf-Gladrow, D.: Data-based estimation of  
1994 anthropogenic carbon and acidification in the Weddell Sea on a decadal timescale. *J. Geophys. Res.* 115,  
1995 C03004. doi:10.1029/2009jc005479, 2010  
1996  
1997 Hauck, J., Völker, C., Wang, T., Hoppema, M., Losch, M., and Wolf-Gladrow, D. A.: Seasonally different  
1998 carbon flux changes in the Southern Ocean in response to the southern annular mode. *Global Biogeochemical*  
1999 *Cycles*, 27(4), 1236–1245. <https://doi.org/10.1002/2013GB004600>, 2013  
2000  
2001 [Hauck, J. and Völker, C.: Rising atmospheric CO<sub>2</sub> leads to large impact of biology on Southern Ocean CO<sub>2</sub>](#)  
2002 [uptake via changes of the Revelle factor, \*Geophys. Res. Lett.\*, 42, 1459–1464, doi:10.1002/2015GL063070,](#)  
2003 [2015](#)  
2004  
2005 [Hauck, J., Volker, C., Wolf-Gladrow, D. A., Laufkotter, C., Vogt, M., Aumont, O., et al.: On the Southern](#)  
2006 [Ocean CO<sub>2</sub> uptake and the role of the biological carbon pump in the 21st century. \*Global Biogeochemical\*](#)  
2007 [Cycles, 29\(9\), 1451–1470. <https://doi.org/10.1002/2015GB005140>, 2015](#)  
2008  
2009 Hauck, J., Zeising, M., Le Quéré, C., Gruber, N., Bakker, D. C. E., Bopp, L., Chau, T. T., Gürses, Ö., Ilyina, T.,  
2010 Landschützer, P., Lenton, A., Resplandy, L., Rödenbeck, C., Schwinger, J., and Séférian, R.: Consistency and  
2011 challenges in the ocean carbon sink estimate for the Global Carbon Budget. *Front. Mar. Sci.* doi:  
2012 10.3389/fmars.2020.571720, 2020  
2013  
2014 Hauck, J., Nissen, C., Landschützer, P., Rödenbeck, C., Bushinsky, S., and Olsen, A.: Sparse observations  
2015 induce large biases in estimates of the global ocean CO<sub>2</sub> sink: an ocean model subsampling experiment. *Phil.*  
2016 *Trans. R. Soc. A* 381: 20220063. <https://doi.org/10.1098/rsta.2022.0063>, [20232023a](#)  
2017  
2018 [Hauck, J., Gregor, L., Nissen, C., Patara, L., Hague, M., Mongwe, P., et al.: The Southern Ocean carbon cycle](#)  
2019 [1985–2018: Mean, seasonal cycle, trends, and storage. \*Global Biogeochemical Cycles\*, 37, e2023GB007848.](#)  
2020 [https://doi.org/10.1029/2023GB007848, 2023b](#)  
2021  
2022 Hersbach, H., Bell, B., Berrisford, P., Hirahara, S., Horányi, A., Muñoz-Sabater, J., Nicolas, J., Peubey, C.,  
2023 Radu, R., Schepers, D., Simmons, A., Soci, C., Abdalla, S., Abellan, X., Balsamo, G., Bechtold, P., Biavati, G.,  
2024 Bidlot, J., Bonavita, M., De Chiara, G., Dahlgren, P., Dee, D., Diamantakis, M., Dragani, R., Flemming, J.,  
2025 Forbes, R., Fuentes, M., Geer, A., Haimberger, L., Healy, S., Hogan, R. J., Hólm, E., Janisková, M., Keeley, S.,  
2026 Laloyaux, P., Lopez, P., Lupu, C., Radnoti, G., de Rosnay, P., Rozum, I., Vamborg, F., Villaume, S., and  
2027 Thépaut, J.-N.: The ERA5 global reanalysis, *Q. J. Roy. Meteor. Soc.*, 146, 1999–2049,  
2028 <https://doi.org/10.1002/qj.3803>, 2020.  
2029  
2030 Hoppema, M., Bakker, K., van Heuven, S. M. A. C., van Ooijen, J. C., and de Baar, H. J. W.: Distributions,  
2031 trends and inter-annual variability of nutrients along a repeat section through the Weddell Sea (1996–2011).  
2032 *Marine Chemistry*, 177, 545–553. <https://doi.org/10.1016/j.marchem.2015.08.007>, 2015  
2033  
2034 Hunt, B. P. V., Pakhomov, E. A., Hosie, G. W., Siegel, V., Ward, P., and Bernard, K.: Pteropods in Southern  
2035 Ocean ecosystems, *Progress in Oceanography*, Volume 78, Issue 3, Pages 193–221,  
2036 <https://doi.org/10.1016/j.pocean.2008.06.001>, 2008  
2037

Mis en forme : Couleur de police :  
Automatique

2038 Iida, T., Odate, T., and Fukuchi, M.: Long-term trends of nutrients and apparent oxygen utilization south of the  
2039 polar front in Southern Ocean intermediate water from 1965 to 2008. *PLoS One*, 8, e171766.  
2040 <https://doi.org/10.1371/journal.pone.0071766>, 2013  
2041  
2042 Iida, Y., Takatani, Y., Kojima, A., and Ishii, M.: Global trends of ocean CO<sub>2</sub> sink and ocean acidification: an  
2043 observation based reconstruction of surface ocean inorganic carbon variables, *J. Oceanogr.*, 77, 323–358,  
2044 <https://doi.org/10.1007/s10872-020-00571-5>, 2021.  
2045  
2046 IPCC: Changing Ocean, Marine Ecosystems, and Dependent Communities. in *The Ocean and Cryosphere in a*  
2047 *Changing Climate* 447–588 (Cambridge University Press, 2022). doi:10.1017/9781009157964.007, 2022  
2048  
2049 Ito, T., Minobe, S., Long, M. C., Deutsch, C. Upper ocean O<sub>2</sub> trends: 1958–2015. *Geophysical Research Letters*  
2050 44, 4214–4223, <https://doi.org/10.1002/2017GL073613>, 2017.  
2051  
2052 Jabaud-Jan, A., Metzl, N., Brunet, C., Poisson, A., and Schauer, B.: Variability of the Carbon Dioxide System in  
2053 the Southern Indian Ocean (20°S-60°S): the impact of a warm anomaly in austral summer 1998. *Global*  
2054 *Biogeochemical Cycles*, Vol. 18, No. 1, GB1042,10.1029/2002GB002017, 2004  
2055  
2056 Jeandel, C., Ruiz-Pino, D., Gjata, E., Poisson, A., Brunet, C., Charriaud, E., Dehairs, F., Delille, D., Fiala, M.,  
2057 Fravallo, C., Miquel, J. C., Park, Y. H., Pondaven, P., Quéguiner, B., Razouls, S., Schauer, B., and Tréguer, P.:  
2058 KERFIX, a time-series station in the Southern Ocean: a presentation. *Journal of Marine Systems*, 17, 1-4, 555-  
2059 569., [https://doi.org/10.1016/S0924-7963\(98\)00064-5](https://doi.org/10.1016/S0924-7963(98)00064-5), 1998  
2060  
2061 Jiang, L.-Q., Feely, R. A., Carter, B. R., Greeley, D. J., Gledhill, D. K., and Arzayus K. M.: Climatological  
2062 distribution of aragonite saturation state in the global oceans, *Global Biogeochem. Cycles*, 29, 1656–1673,  
2063 doi:10.1002/2015GB005198, 2015.  
2064  
2065 Jiang, L.-Q., Carter, B. R., Feely, R. A., Lauvset, S. K., and Olsen, A.: Surface ocean pH and buffer capacity:  
2066 past, present and future. *Sci Rep* 9, 18624, doi:10.1038/s41598-019-55039-4, 2019  
2067  
2068 Jiang, L.-Q., Dunne, J., Carter, B. R., Tjiputra, J. F., Terhaar, J., Sharp, J. D., et al.: Global surface ocean  
2069 acidification indicators from 1750 to 2100. *Journal of Advances in Modeling Earth Systems*, 15,  
2070 e2022MS003563. <https://doi.org/10.1029/2022MS003563>, 2023  
2071  
2072 Joos, F., Hameau, A., Frölicher, T. L., and Stephenson, D. B.: Anthropogenic attribution of the increasing  
2073 seasonal amplitude in surface ocean pCO<sub>2</sub>. *Geophysical Research Letters*, 50, e2023GL102857.  
2074 <https://doi.org/10.1029/2023GL102857>, 2023  
2075  
2076 Jouandet, M.-P., Blain, S., Metzl, N., Brunet, C., Trull, T., and Obernosterer, I.: A seasonal carbon budget for a  
2077 naturally iron fertilized bloom (Kerguelen I. Southern Ocean). *Deep-Sea Res II*, 55, 856-867.  
2078 doi:10.1016/j.dsr2.2007.12.037, 2008  
2079  
2080 Jouandet M.P., Blain, S., Metzl, N., and Mongin, C.: Interannual variability of the net community production and  
2081 air-sea CO<sub>2</sub> flux in a natural iron fertilization region of the Southern Ocean. (Kerguelen plateau), *Antarctic*  
2082 *Science*, doi:10.1017/S0954102011000411, 2011  
2083  
2084 Kane, A., Moulin, C., Thiria, S., Bopp, L., Berrada, M., Tagliabue, A., Crépon, M., Aumont, O., and Badran, F.:  
2085 Improving the parameters of a global ocean biogeochemical model via variational assimilation of in situ data at  
2086 five time series stations, *J. Geophys. Res.*, 116, C06011, doi:10.1029/2009JC006005, 2011  
2087  
2088 Kawaguchi, S., Ishida, A., King, R. et al.: Risk maps for Antarctic krill under projected Southern Ocean  
2089 acidification. *Nature Clim. Change*, 3, 843–847, DOI: 10.1038/NCLIMATE1937, 2013  
2090

2091 Keeling, C. D., and Waterman, L. S.: Carbon dioxide in surface ocean waters: 3. Measurements on Lusiad  
2092 Expedition 1962–1963, *J. Geophys. Res.*, 73( 14), 4529– 4541, doi:10.1029/JB073i014p04529, 1968  
2093  
2094 Keppler, L. and Landschützer, P.: Regional Wind Variability Modulates the Southern Ocean Carbon Sink, *Sci.*  
2095 *Rep.-UK*, 9, 7384, <https://doi.org/10.1038/s41598-019-43826-y>, 2019.  
2096  
2097 Kessler, A. and Tjiputra, J.: The Southern Ocean as a constraint to reduce uncertainty in future ocean carbon  
2098 sinks, *Earth Syst. Dynam.*, 7, 295-312, doi:10.5194/esd-7-295-2016, 2016.  
2099  
2100 Key, R. M., Kozyr, A., Sabine, C. L., Lee, K., Wanninkhof, R., Bullister, J. L., Feely, R. A., Millero, F. J.,  
2101 Mordy, C., and Peng, T. H.: A global ocean carbon climatology: Results from Global Data Analysis Project  
2102 (GLODAP), *Global Biogeochemical Cycles*, 18, GB4031, <https://doi.org/10.1029/2004GB002247>, 2004.  
2103  
2104 Khatiwala, S., Tanhua, T., Mikaloff Fletcher, S., Gerber, M., Doney, S. C., Graven, H. D., Gruber, N.,  
2105 McKinley, G. A., Murata, A., Ríos, A. F., and Sabine, C. L.: Global ocean storage of anthropogenic carbon,  
2106 *Biogeosciences*, 10, 2169–2191, <https://doi.org/10.5194/bg-10-2169-2013>, 2013.  
2107  
2108 ~~King, J., Anchukaitis, K. J., Allen, K. et al.: Trends and variability in the Southern Annular Mode over the~~  
2109 ~~Common Era. *Nat Commun* 14, 2324, <https://doi.org/insu.bib.cnrs.fr/10.1038/s41467-023-37643-1>, 2023~~  
2110  
2111 Krumhardt, K. M., Long, M. C., Sylvester, Z. T. and Petrik, C. M.: Climate drivers of Southern Ocean  
2112 phytoplankton community composition and potential impacts on higher trophic levels. *Front. Mar. Sci.*  
2113 9:916140. doi: 10.3389/fmars.2022.916140, 2022  
2114  
2115 Kwiatkowski, L., and Orr, J. C.: Diverging seasonal extremes for ocean acidification during the twenty-first  
2116 century. *Nature Climate Change*, 8(2), 141–145. <https://doi.org/10.1038/s41558-017-0054-0>, 2018  
2117  
2118 Kwiatkowski, L., Torres, O., Bopp, L., Aumont, O., Chamberlain, M., Christian, J. R., Dunne, J. P., Gehlen, M.,  
2119 Ilyina, T., John, J. G., Lenton, A., Li, H., Lovenduski, N. S., Orr, J. C., Palmieri, J., Santana-Falcón, Y.,  
2120 Schwinger, J., Séférian, R., Stock, C. A., Tagliabue, A., Takano, Y., Tjiputra, J., Toyama, K., Tsujino, H.,  
2121 Watanabe, M., Yamamoto, A., Yool, A., and Ziehn, T.: Twenty-first century ocean warming, acidification,  
2122 deoxygenation, and upper-ocean nutrient and primary production decline from CMIP6 model projections,  
2123 *Biogeosciences*, 17, 3439–3470, <https://doi.org/10.5194/bg-17-3439-2020>, 2020.  
2124  
2125 Lange, N., Fiedler, B., Álvarez, M., Benoit-Cattin, A., Benway, H., Buttigieg, P. L., Coppola, L., Currie, K.,  
2126 Flecha, S., Honda, M., Huertas, I. E., Lauvset, S. K., Muller-Karger, F., Körtzinger, A., O'Brien, K. M.,  
2127 Ólafsdóttir, S. R., Pacheco, F. C., Rueda-Roa, D., Skjelvan, I., Wakita, M., White, A., and Tanhua, T.: Synthesis  
2128 Product for Ocean Time-Series (SPOTS) – A ship-based biogeochemical pilot, *Earth Syst. Sci. Data Discuss.*  
2129 [preprint], <https://doi.org/10.5194/essd-2023-238>, in review, 2023.  
2130  
2131 Landschützer, P., Gruber, N., Haumann, F. A., Rödenbeck, C., Bakker, D. C. E., Van Heuven, S., Hoppema, M.,  
2132 Metzl, N., Sweeney, C., Takahashi, T., Tilbrook, B., and Wanninkhof, R.: The reinvigoration of the Southern  
2133 Ocean carbon sink, *Science*, 349, 1221–1224, <https://doi.org/10.1126/science.aab2620>, 2015.  
2134  
2135 Landschützer, P., Gruber, N., Bakker, D. C. E., Stemmler, I., and Six, K. D.: Strengthening seasonal marine CO<sub>2</sub>  
2136 variations due to increasing atmospheric CO<sub>2</sub>. *Nature Climate Change*, 8(2), 146–150.  
2137 <https://doi.org/10.1038/s41558-017-0057-x>, 2018  
2138  
2139 Lauvset, S. K., Gruber, N., Landschützer, P., Olsen, A., and Tjiputra, J.: Trends and drivers in global surface  
2140 ocean pH over the past 3 decades. *Biogeosciences*, 12, 1285-1298, doi:10.5194/bg-12-1285-2015, 2015  
2141

Mis en forme : Police :Times New Roman, 10 pt, Français (France)

Mis en forme : Normal, Justifié, Interligne : simple, Ne pas ajuster l'espace entre le texte latin et asiatique, Ne pas ajuster l'espace entre le texte et les nombres asiatiques

2142 Lauvset, S. K., Carter, B. R., Perez, F. F., Jiang, L.-Q., Feely, R. A., Velo, A., and Olsen, A.: Processes Driving  
2143 Global Interior Ocean pH Distribution, *Global Biogeochem. Cycles*, 34, e2019GB006 229,  
2144 <https://doi.org/10.1029/2019GB006229>, 2020.  
2145  
2146 Lauvset, S. K., Lange, N., Tanhua, T., Bittig, H. C., Olsen, A., Kozyr, A., Álvarez, M., Becker, S., Brown, P. J.,  
2147 Carter, B. R., Cotrim da Cunha, L., Feely, R. A., van Heuven, S., Hoppema, M., Ishii, M., Jeansson, E.,  
2148 Jutterström, S., Jones, S. D., Karlsen, M. K., Lo Monaco, C., Michaelis, P., Murata, A., Pérez, F. F., Pfeil, B.,  
2149 Schirnack, C., Steinfeldt, R., Suzuki, T., Tilbrook, B., Velo, A., Wanninkhof, R., Woosley, R. J., and Key, R. M.:  
2150 An updated version of the global interior ocean biogeochemical data product, GLODAPv2.2021, *Earth Syst. Sci.*  
2151 *Data*, 13, 5565–5589, <https://doi.org/10.5194/essd-13-5565-2021>, 2021a.  
2152  
2153 Lauvset, Siv K.; Lange, Nico; Tanhua, Toste; Bittig, Henry C.; Olsen, Are; Kozyr, Alex; Álvarez, Marta;  
2154 Becker, Susan; Brown, Peter J.; Carter, Brendan R.; Cotrim da Cunha, Leticia; Feely, Richard A.; van Heuven,  
2155 Steven M. A. C.; Hoppema, Mario; Ishii, Masao; Jeansson, Emil; Jutterström, Sara; Jones, Steve D.; Karlsen,  
2156 Maren K.; Lo Monaco, Claire; Michaelis, Patrick; Murata, Akihiko; Pérez, Fiz F.; Pfeil, Benjamin; Schirnack,  
2157 Carsten; Steinfeldt, Reiner; Suzuki, Toru; Tilbrook, Bronte; Velo, Antón; Wanninkhof, Rik; Woosley, Ryan J.;  
2158 Key, Robert M.: Global Ocean Data Analysis Project version 2.2021 (GLODAPv2.2021) (NCEI Accession  
2159 0237935). [subset used GLODAPv2.2021\_Indian\_Ocean.cvs]. NOAA National Centers for Environmental  
2160 Information. Dataset. <https://doi.org/10.25921/ttqg-n825>, Accessed 2/8/2021. 2021b.  
2161  
2162 Lee, K., Tong, L. T., Millero, F. J., Sabine, C. L., Dickson, A. G., Goyet, C., Park, G. H., Wanninkhof, R., Feely,  
2163 R. A., and Key, R. M.: Global relationships of total alkalinity with salinity and temperature in surface waters of  
2164 the world's oceans. *Geophys. Res. Lett.* 33, L19605. doi10.1029/2006GL027207, 2006.  
2165  
2166 Lenton, A., Codron, F., Bopp, L., Metzl, N., Cadule, P., Tagliabue, A., and Le Sommer, J.: Stratospheric ozone  
2167 depletion reduces ocean carbon uptake and enhances ocean acidification. *Geophys. Res. Lett.*, 36, L12606, 2009.  
2168 doi:10.1029/2009GL038227, 2009  
2169  
2170 Lenton, A., Tilbrook, B., Law, R. M., Bakker, D., Doney, S. C., Gruber, N., Ishii, M., Hoppema, M.,  
2171 Lovenduski, N. S., Matear, R. J., McNeil, B. I., Metzl, N., Mikaloff Fletcher, S. E., Monteiro, P. M. S.,  
2172 Rödenbeck, C., Sweeney, C., and Takahashi, T.: Sea–air CO<sub>2</sub> fluxes in the Southern Ocean for the period 1990–  
2173 2009, *Biogeosciences*, 10, 4037–4054, <https://doi.org/10.5194/bg-10-4037-2013>, 2013.  
2174  
2175 Le Quéré, C., Rödenbeck, C., Buitenhuis, E. T., Conway, T. J., Langenfelds, R., Gomez, A., Labuschagne, C.,  
2176 Ramonet, M., Nakazawa, T., Metzl, N., Gillett, N., and Heimann, M.: Saturation of the Southern Ocean CO<sub>2</sub>  
2177 Sink Due to Recent Climate Change, *Science*, 316, 1735–1738, <https://doi.org/10.1126/science.1136188>, 2007.  
2178  
2179 Lerner, P., Romanou, A., Kelley, M., Romanski, J., Ruedy, R., and Russell, G.: Drivers of air-sea CO<sub>2</sub> flux  
2180 seasonality and its long-term changes in the NASA-GISS model CMIP6 submission. *Journal of Advances in*  
2181 *Modeling Earth Systems*, 13, e2019MS002028. <https://doi.org/10.1029/2019MS002028>, 2021.  
2182  
2183 Leseurre, C., Lo Monaco, C., Reverdin, G., Metzl, N., Fin, J., Mignon, C., and Benito, L.: Summer trends and  
2184 drivers of sea surface fCO<sub>2</sub> and pH changes observed in the southern Indian Ocean over the last two decades  
2185 (1998–2019), *Biogeosciences*, 19, 2599–2625, <https://doi.org/10.5194/bg-19-2599-2022>, 2022.  
2186  
2187 Leung, S., Cabré, A., and Marinov, I.: A latitudinally banded phytoplankton response to 21st century climate  
2188 change in the Southern Ocean across the CMIP5 model suite, *Biogeosciences*, 12, 5715–5734,  
2189 <https://doi.org/10.5194/bg-12-5715-2015>, 2015.  
2190  
2191 Lewis E., and Wallace, D. W. R.: Program developed for CO<sub>2</sub> system calculations. ORNL/CDIAC-105. Carbon  
2192 Dioxide Information Analysis Center, Oak Ridge National Laboratory, US. Dept. of Energy, Oak Ridge, TN,  
2193 1998.  
2194

2195 Lo Monaco, C., Goyet, C., Metzl, N., Poisson, A., and Touratier, F.: Distribution and inventory of anthropogenic  
2196 CO<sub>2</sub> in the Southern Ocean: Comparison of three databased methods, *J. Geophys. Res.-Oceans*, 110, C09S02,  
2197 <https://doi.org/10.1029/2004JC002571>, 2005.

2198

2199 Lo Monaco, C., Álvarez, M., Key, R. M., Lin, X., Tanhua, T., Tilbrook, B., Bakker, D. C. E., van Heuven, S.,  
2200 Hoppema, M., Metzl, N., Ríos, A. F., Sabine, C. L., and Velo, A.: Assessing the internal consistency of the  
2201 CARINA database in the Indian sector of the Southern Ocean, *Earth Syst. Sci. Data*, 2, 51–70,  
2202 <https://doi.org/10.5194/essd-2-51-2010>, 2010.

2203

2204 Lo Monaco, C., Metzl, N., D’Ovidio, F., Llort, J., and Ridame, C.: Rapid establishment of the CO<sub>2</sub> sink  
2205 associated with Kerguelen’s bloom observed during the KEOPS2/OISO20 cruise, *Biogeosciences Discuss.*, 11,  
2206 17543–17578, <https://doi.org/10.5194/bgd-11-17543-2014>, 2014.

2207

2208 ~~Lo Monaco, C.: OISO-30 cruise, RV Marion Dufresne, <https://doi.org/10.17600/18000679>, 2020.~~

2209

2210 ~~Lo Monaco, C., Jeandel, C., and Planquette, H.: OISO-31 cruise, RV Marion Dufresne,  
2211 <https://doi.org/10.17600/18001254>, 2021.~~

2212

2213 Long, M. C., Lindsay, K., Peacock, S., Moore, J. K., and Doney, S. C.: Twentieth-Century Oceanic Carbon  
2214 Uptake and Storage in CESM1(BGC), *J. Climate*, 26 (18), 6775–6800, doi:10.1175/JCLI-D-12-00184.1, 2013.

2215

2216 Long, M. C., Stephens, B. B., McKain, K., Sweeney, C., Keeling, R. F., Kort, E. A., Morgan, E. J., Bent, J. D.,  
2217 Chandra, N., Chevallier, F., Commancie, R., Daube, B. C., Krummel, P. B., Loh, Z., Luijkx, I. T., Munro, D.,  
2218 Patra, P., Peters, W., Ramonet, M., Rödenbeck, C., Stavert, A., Tans, P., and Wofsy, S. C.: Strong Southern  
2219 Ocean carbon uptake evident in airborne observations, *Science*, 374, 1275–1280,  
2220 <https://doi.org/10.1126/science.1243555>, 2021.

2221

2222 Louanchi, F., Ruiz-Pino, D., and Poisson, A.: Temporal variations of mixed layer oceanic CO<sub>2</sub> at JGOFS-  
2223 KERFIX time-series station: Physical versus biogeochemical processes. *Journal of Marine Research* 57(1): 165-  
2224 187. <https://doi.org/10.1357/002224099765038607>, 1999.

2225

2226 Louanchi, F., Ruiz-Pino, D. P., Jeandel, C., Brunet, C., Schauer, B., Masson, A., Fiala, M., and Poisson, A.:  
2227 Dissolved inorganic carbon, alkalinity, nutrient and oxygen seasonal and interannual variations at the Antarctic  
2228 Ocean JGOFS-KERFIX site. *Deep Sea Research Part I: Oceanographic Research Papers* 48(7): 1581-1603,  
2229 [https://doi.org/10.1016/S0967-0637\(00\)00086-8](https://doi.org/10.1016/S0967-0637(00)00086-8), 2001.

2230

2231 Lovenduski, N. S., and Gruber, N.: Impact of the Southern Annular Mode on Southern Ocean circulation and  
2232 biology, *Geophys. Res. Lett.*, 32, L11603, doi:10.1029/2005GL022727, 2005.

2233

2234 Lueker, T. J., Dickson, A. G., and Keeling, C. D.: Ocean pCO<sub>2</sub> calculated from dissolved inorganic carbon,  
2235 alkalinity, and equations for K-1 and K-2: validation based on laboratory measurements of CO<sub>2</sub> in gas and  
2236 seawater at equilibrium. *Marine Chemistry* 70, 105-119. [https://doi.org/10.1016/S0304-4203\(00\)00022-0](https://doi.org/10.1016/S0304-4203(00)00022-0), 2000.

2237

2238 Ma, D., Gregor, L., and Gruber, N.: Four decades of trends and drivers of global surface ocean acidification.  
2239 *Global Biogeochemical Cycles*, 37, e2023GB007765. [10.1029/2023GB007765](https://doi.org/10.1029/2023GB007765), 2023.

2240

2241 Mackay, N., Watson, A. J., Suntharalingam, P. et al.: Improved winter data coverage of the Southern Ocean CO<sub>2</sub>  
2242 sink from extrapolation of summertime observations. *Commun Earth Environ* 3, 265,  
2243 <https://doi.org/10.1038/s43247-022-00592-6>, 2022.

2244

2245 Mahieu, L., Lo Monaco, C., Metzl, N., Fin, J., and Mignon, C.: Variability and stability of anthropogenic CO<sub>2</sub> in  
2246 Antarctic Bottom Water observed in the Indian sector of the Southern Ocean, 1978–2018, *Ocean Sci.*, 16, 1559–  
2247 1576, <https://doi.org/10.5194/os-16-1559-2020>, 2020.

2248  
2249 Marshall, G. J.: Trends in the Southern Annular Mode from observations and reanalyses. *J. Clim.*, 16, 4134-  
2250 4143, doi:10.1175/1520-0442%282003%29016<4134%3ATITSAM>2.0.CO%3B2, 2003.  
2251  
2252 Mayot, N., Le Quéré, C., Rödenbeck, C., Bernardello, R., Bopp, L., Djeutchouang, L. M., Gehlen, M., Gregor,  
2253 L., Gruber, N., Hauck, J., Iida, Y., Ilyina, T., Keeling, R. F., Landschützer, P., Manning, A. C., Patara, L.,  
2254 Resplandy, L., Schwinger, J., Séférian, R., Watson, A. J., Wright, R. M. and Zeng, J.: Climate-driven variability  
2255 of the Southern Ocean CO<sub>2</sub> sink. *Phil. Trans. R. Soc. A.* 381: 20220055, <http://doi.org/10.1098/rsta.2022.0055>,  
2256 2023  
2257  
2258 Mazloff, M. R., Verdy, A., Gille, S. T., Johnson, K. S., Cornuelle, B. D., and Sarmiento, J.: Southern Ocean  
2259 acidification revealed by biogeochemical-Argo floats. *Journal of Geophysical Research: Oceans*, 128,  
2260 e2022JC019530. <https://doi.org/10.1029/2022JC019530>, 2023.  
2261  
2262 McKinley, G. A., Bennington, V. S., Meinshausen, M., and Nicholls, Z.: Modern air-sea flux distributions  
2263 reduce uncertainty in the future ocean carbon sink, *Environmental Research Letters*, 18, doi:10.1088/1748-  
2264 9326/acc195, 2023.  
2265  
2266 McNeil, B. I. and Matear, R. J.: Southern Ocean acidification: A tipping point at 450-ppm atmospheric  
2267 CO<sub>2</sub>, *P. Natl. Acad. Sci. USA*, 105, 18860–18864, <https://doi.org/10.1073/pnas.0806318105>, 2008.  
2268  
2269 McNeil, B. I. and Sasse, T. P.: Future ocean hypercapnia driven by anthropogenic amplification of the natural  
2270 CO<sub>2</sub> cycle, *Nature*, 529, 383–386, doi:10.1038/nature16156, 2016  
2271  
2272 McNeil, B. I., Metzl, N., Key, R. M., Matear, R. J. and Corbiere, A.: An empirical estimate of the Southern  
2273 Ocean air-sea CO<sub>2</sub> flux, *Global Biogeochem. Cycles*, Vol. 21, No. 3, GB3011 10.1029/2007GB002991, 2007.  
2274  
2275 Meinshausen, M., Nicholls, Z. R. J., Lewis, J., Gidden, M. J., Vogel, E., Freund, M., et al.: The shared  
2276 socioeconomic pathway (SSP) greenhouse gas concentrations and their extensions to 2500. *Geoscientific Model*  
2277 *Development*, 13(8), 3571–3605. <https://doi.org/10.5194/gmd-13-3571-2020>, 2020.  
2278  
2279 Metzl, N., and Lo Monaco, C.: OISO- Océan Indien Service d'Observation,  
2280 <https://doi.org/10.18142/228>, 1998.  
2281  
2282 Metzl, N., Brunet, C., Jabaud-Jan, A., Poisson, A., and Schauer, B.: Summer and winter air–sea CO<sub>2</sub> fluxes in  
2283 the Southern Ocean, *Deep-Sea Res.*, 53, 1548–1563, <https://doi.org/10.1016/j.dsr.2006.07.006>, 2006.  
2284  
2285 Metzl, N.: Decadal increase of oceanic carbon dioxide in Southern Indian Ocean surface waters (1991–2007),  
2286 *Deep-Sea Res. Pt. II*, 56, 607–619, <https://doi.org/10.1016/j.dsr2.2008.12.007>, 2009.  
2287  
2288 Midorikawa, T., Inoue, H. Y., Ishii, M., Sasano, D., Kosugi, N., Hashida, G., Nakaoka, S., and Suzuki, T.:  
2289 Decreasing pH trend estimated from 35-year time series of carbonate parameters in the Pacific sector of the  
2290 Southern Ocean in summer, *Deep-Sea Res.*, 61, 131–139, <https://doi.org/10.1016/j.dsr.2011.12.003>, 2012.  
2291  
2292 Millero, F. J., Lee, K., and Roche, M.: Distribution of alkalinity in the surface waters of the major oceans, *Mar.*  
2293 *Chem.*, 60, 111–130, [https://doi.org/10.1016/S0304-4203\(97\)00084-4](https://doi.org/10.1016/S0304-4203(97)00084-4), 1998.  
2294  
2295 Minas, H. J., and Minas, M.: Net community production in high nutrient-low chlorophyll waters of the tropical  
2296 and Antarctic oceans – grazing vs iron hypothesis, *Oceanol. Acta*, 15, 145–162, 1992.  
2297  
2298 Mongin, M., Nelson, D. M., Pondaven, P., and Tréguer, P.: Simulation of upper-ocean biogeochemistry with a  
2299 flexible-composition phytoplankton model: C, N and Si cycling and Fe limitation in the Southern Ocean. *Deep*

2300 Sea Research Part II: Topical Studies in Oceanography, Elsevier, 2006, 53 (5-7), pp.601-619.  
2301 10.1016/j.dsr2.2006.01.021, 2006.  
2302  
2303 Mongin, M., Nelson, D. M., Pondaven P., and Tréguer, P.: Potential phytoplankton responses to iron and  
2304 stratification changes in the Southern Ocean based on a flexible-composition phytoplankton model. *Global*  
2305 *Biogeochemical Cycles* 21 (GB4020), /<http://dx.doi.org/10.1029/2007GB002972S>, 2007.  
2306  
2307 Mongin, M., Molina, E., and Trull, T. W.: Seasonality and scale of the Kerguelen plateau phytoplankton bloom:  
2308 A remote sensing and modeling analysis of the influence of natural iron fertilization in the Southern Ocean.  
2309 *Deep Sea Research Part II: Topical Studies in Oceanography*, Vol 55, Issues 5–7, Pages 880-892,  
2310 <https://doi.org/10.1016/j.dsr2.2007.12.039>. 2008.  
2311  
2312 Mongwe, N. P., Vichi, M., and Monteiro, P. M. S.: The seasonal cycle of pCO<sub>2</sub> and CO<sub>2</sub> fluxes in the Southern  
2313 Ocean: diagnosing anomalies in CMIP5 Earth system models, *Biogeosciences*, 15, 2851–2872,  
2314 <https://doi.org/10.5194/bg-15-2851-2018>, 2018.  
2315  
2316 Mongwe, P., Gregor, L., Tjiptura, J., Hauck, J., Ito, T., Danek, C., Vichi, M., Thomalla S., and Monteiro, M. S.:  
2317 A shift in the mechanism of CO<sub>2</sub> uptake in the Southern Ocean under high emission-scenario, DOI:  
2318 10.21203/rs.3.rs-2849464/v1, 2023.  
2319  
2320 Moore, J. K. and Abbott, M. R.: Phytoplankton chlorophyll distributions and primary production in the Southern  
2321 Ocean, *J. Geophys. Res.-Oceans*, 105, 28709–28722, <https://doi.org/10.1029/1999JC000043>, 2000  
2322  
2323 Moy, A. D., Palmer, M. R., Howard, W. R., Bijma, J., Cooper, M. J., Calvo, E., Pelejero, C., Gagan M. K. and  
2324 Chalk, T. B.: Reduced calcification in modern Southern Ocean planktonic foraminifera. *Nature Geosci* 2, 276–  
2325 280. <https://doi-org.insu.bib.cnrs.fr/10.1038/ngeo460>, 2009.  
2326  
2327 Negrete-García, G., Lovenduski, N. S., Hauri, C., Krumhardt, K. M., and Lauvset, S. K.: Sudden  
2328 emergence of a shallow aragonite saturation horizon in the Southern Ocean. *Nature Climate Change*, 1758–  
2329 6798, 10.1038/s41558-019-0418-8, 2019.  
2330  
2331 Neveux, J., and Lantoiné, F.: Spectrofluorometric assay of chlorophylls and phaeopigments using the least  
2332 squares approximation technique, *Deep-Sea Res. I*, 40(9), 1747-1765, [https://doi.org/10.1016/0967-](https://doi.org/10.1016/0967-0637(93)90030-7)  
2333 [0637\(93\)90030-7](https://doi.org/10.1016/0967-0637(93)90030-7), 1993.  
2334  
2335 Nicholson S. A., Whitt, D. B., Fer, I., du Plessis, M. D., Lebéhot A. D., et al.: Storms drive outgassing of CO<sub>2</sub> in  
2336 the subpolar Southern Ocean. *Nat. Commun.* 13:158. <https://doi.org/10.1038/s41467-021-27780-w>, 2022  
2337  
2338 Olafsson, J., Olafsdottir, S. R., Benoit-Cattin, A., Danielsen, M., Arnarson, T. S., and Takahashi, T.: Rate of  
2339 Iceland Sea acidification from time series measurements. *Biogeosciences* 6, 2661–2668.  
2340 <https://doi.org/10.5194/bg-6-2661-2009>, 2009.  
2341  
2342 Olafsson, J., Olafsdottir, S. R., Benoit-Cattin, A., and Takahashi, T.: The Irminger Sea and the Iceland Sea time  
2343 series measurements of sea water carbon and nutrient chemistry 1983–2006. *Earth Syst. Sci. Data* 2, 99–104.  
2344 <https://doi.org/10.5194/essd-2-99-2010>, 2010.  
2345  
2346 Olsen, A., Key, R. M., van Heuven, S., Lauvset, S. K., Velo, A., Lin, X., Schirnick, C., Kozyr, A., Tanhua, T.,  
2347 Hoppema, M., Jutterström, S., Steinfeldt, R., Jeansson, E., Ishii, M., Pérez, F. F., and Suzuki, T.: The Global  
2348 Ocean Data Analysis Project version 2 (GLODAPv2) – an internally consistent data product for the world ocean,  
2349 *Earth Syst. Sci. Data*, 8, 297–323, <https://doi.org/10.5194/essd-8-297-2016>, 2016.  
2350  
2351 Olsen, A., Lange, N., Key, R. M., Tanhua, T., Álvarez, M., Becker, S., Bittig, H. C., Carter, B. R., Cotrim da  
2352 Cunha, L., Feely, R. A., van Heuven, S., Hoppema, M., Ishii, M., Jeansson, E., Jones, S. D., Jutterström, S.,

2353 Karlsen, M. K., Kozyr, A., Lauvset, S. K., Lo Monaco, C., Murata, A., Pérez, F. F., Pfeil, B., Schirnack, C.,  
2354 Steinfeldt, R., Suzuki, T., Telszewski, M., Tilbrook, B., Velo, A., and Wanninkhof, R.: GLODAPv2.2019 – an  
2355 update of GLODAPv2, *Earth Syst. Sci. Data*, 11, 1437–1461, <https://doi.org/10.5194/essd-11-1437-2019>, 2019.  
2356

2357 Olsen, A., Lange, N., Key, R. M., Tanhua, T., Bittig, H. C., Kozyr, A., Álvarez, M., Azetsu-Scott, K., Becker, S.,  
2358 Brown, P. J., Carter, B. R., Cotrim da Cunha, L., Feely, R. A., van Heuven, S., Hoppema, M., Ishii, M.,  
2359 Jeansson, E., Jutterström, S., Landa, C. S., Lauvset, S. K., Michaelis, P., Murata, A., Pérez, F. F., Pfeil, B.,  
2360 Schirnack, C., Steinfeldt, R., Suzuki, T., Tilbrook, B., Velo, A., Wanninkhof, R., and Woosley, R. J.: An updated  
2361 version of the global interior ocean biogeochemical data product, GLODAPv2.2020, *Earth Syst. Sci. Data*, 12,  
2362 3653–3678, <https://doi.org/10.5194/essd-12-3653-2020>, 2020.  
2363

2364 Orr, J. C., Fabry, V. J., Aumont, O., Bopp, L., Doney, S. C., Feely, R. A., Gnanadesikan, A., Gruber, N., Ishida,  
2365 A., Joos, F., Key, R. M., Lindsay, K., Maier-Reimer, E., Matear, R., Monfray, P., Mouchet, A., Najjar, R. G.,  
2366 Plattner, G.-K., Rodgers, K. B., Sabine, C. L., Sarmiento, J. L., Schlitzer, R., Slater, R. D., Totterdell, I. J.,  
2367 Weirig, M.-F., Yamanaka, Y., and Yool, A.: Anthropogenic ocean acidification over the twenty-first century and  
2368 its impact on calcifying organisms, *Nature*, 437, 681–686, <https://doi.org/10.1038/nature04095>, 2005.  
2369

2370 Orr, J. C., Epitalon, J.-M., and Gattuso, J.-P.: Comparison of ten packages that compute ocean carbonate  
2371 chemistry, *Biogeosciences*, 12(5), 1483–1510, doi:10.5194/bg-12-1483-2015, 2015.  
2372

2373 Orr, J. C., Epitalon, J.-M., Dickson, A. G., and Gattuso, J.-P.: Routine uncertainty propagation for the marine  
2374 carbon dioxide system, *Marine Chemistry*, Vol. 207, 84–107, doi:10.1016/j.marchem.2018.10.006., 2018.  
2375

2376 Oschlies, A., Brandt, P., Stramma, L., and Schmidtko, S.: Drivers and mechanisms of ocean deoxygenation. *Nat.*  
2377 *Geosci.* 11, 467–473. doi: 10.1038/s41561-018-0152-2, 2018.  
2378

2379 Pardo, P. C., Pérez, F. F., Khatiwala, S., and Ríos, A. F.: Anthropogenic CO<sub>2</sub> estimates in the Southern Ocean:  
2380 Storage partitioning in the different water masses, *Prog. Oceanogr.*, 120, 230–242,  
2381 <https://doi.org/10.1016/j.pocean.2013.09.005>, 2014.  
2382

2383 Pardo, P. C., Tilbrook, B., Langlais, C., Trull, T. W., and Rintoul, S. R.: Carbon uptake and biogeochemical  
2384 change in the Southern Ocean, south of Tasmania. *Biogeosciences*, 14(22), 5217–5237.  
2385 <https://doi.org/10.5194/bg-14-5217-2017>, 2017.  
2386

2387 Pasquer, B., Metzl, N., Grosse, H., and Lancelot, C.: What drives the seasonality of air-sea CO<sub>2</sub> fluxes in the  
2388 ice-free zone of the Southern Ocean: A 1D coupled physical-biogeochemical model approach. *Marine*  
2389 *Chemistry*, 177 (3): 554-565. doi:10.1016/j.marchem.2015.08.008, 2015.  
2390

2391 Pauthenet, E., Roquet, F., Madec, G., Guinet, C., Hindell, M., McMahon, C. R., Harcourt, R., and Nerini, D.:  
2392 Seasonal Meandering of the Polar Front Upstream of the Kerguelen Plateau, *Geophys. Res. Lett.*, 45, 9774–  
2393 9781, <https://doi.org/10.1029/2018GL079614>, 2018.  
2394

2395 Petrou, K., Baker, K. G., Nielsen, D. A., Hancock, A. M., Schulz, K. G. and Davidson, A. T.: Acidification  
2396 diminishes diatom silica production in the Southern Ocean. *Nature Climate Change*, 9, 781-786,  
2397 <https://doi.org/10.1038/s41558-019-0557-y>, 2019.  
2398

2399 Pierrot, D., Lewis, E., and Wallace, D. W. R.: MS Excel Program Developed for CO<sub>2</sub> System Calculations  
2400 ORNL/CDIAC-105, Carbon Dioxide Inf. Anal. Cent., Oak Ridge Natl. Lab., U. S. Dept. of Energy, Oak Ridge,  
2401 Tenn., [https://cdiac.ess-dive.lbl.gov/ftp/co2sys/CO2SYS\\_calc\\_XLS\\_v2.1/](https://cdiac.ess-dive.lbl.gov/ftp/co2sys/CO2SYS_calc_XLS_v2.1/) (last access: 3 March 2022), 2006.  
2402

2403 Pilcher, D. J., Brody, S. R., Johnson, L., and Bronselaer, B.: Assessing the abilities of CMIP5 models to  
2404 represent the seasonal cycle of surface ocean pCO<sub>2</sub>, *J. Geophys. Res. Oceans*, 120, 4625–4637,  
2405 doi:10.1002/2015JC010759, 2015.



2406  
2407 Pfeil, B., Olsen, A., Bakker, D. C. E., Hankin, S., Koyuk, H., Kozyr, A., Malczyk, J., Manke, A., Metzl, N.,  
2408 Sabine, C. L., Akl, J., Alin, S. R., Bates, N., Bellerby, R. G. J., Borges, A., Boutin, J., Brown, P. J., Cai, W.-J.,  
2409 Chavez, F. P., Chen, A., Cosca, C., Fassbender, A. J., Feely, R. A., González-Dávila, M., Goyet, C., Hales,  
2410 B., Hardman-Mountford, N., Heinze, C., Hood, M., Hoppema, M., Hunt, C. W., Hydes, D., Ishii, M.,  
2411 Johannessen, T., Jones, S. D., Key, R. M., Körtzinger, A., Landschützer, P., Lauvset, S. K., Lefèvre, N.,  
2412 Lenton, A., Lourantou, A., Merlivat, L., Midorikawa, T., Mintrop, L., Miyazaki, C., Murata, A., Nakadate, A.,  
2413 Nakano, Y., Nakaoka, S., Nojiri, Y., Omar, A. M., Padin, X. A., Park, G.-H., Paterson, K., Perez, F. F., Pierrot,  
2414 D., Poisson, A., Ríos, A. F., Santana-Casiano, J. M., Salisbury, J., Sarma, V. V. S. S., Schlitzer, R.,  
2415 Schneider, B., Schuster, U., Sieger, R., Skjelvan, I., Steinhoff, T., Suzuki, T., Takahashi, T., Tedesco, K.,  
2416 Telszewski, M., Thomas, H., Tilbrook, B., Tjiputra, J., Vandemark, D., Veness, T., Wanninkhof, R., Watson,  
2417 A. J., Weiss, R., Wong, C. S., and Yoshikawa-Inoue, H.: A uniform, quality controlled Surface Ocean CO<sub>2</sub> Atlas  
2418 (SOCAT), *Earth Syst. Sci. Data*, 5, 125-143, doi:10.5194/essd-5-125-2013, 2013.  
2419  
2420 Poisson, A.: INDIGO 1 - MD 43 cruise, RV Marion Dufresne, <https://doi.org/10.17600/85000111>, 1985.  
2421  
2422 Poisson, A., Schauer, B., and Brunet, C. : MD43/INDIGO 1, Cruise report; Les rapports des campagnes à la mer,  
2423 85(06). Les publications de la Mission de Recherche des Terres Australes et Antarctiques Françaises, Paris, 267  
2424 pp., 1988.  
2425  
2426 Poisson, A., Metzl, N., Brunet, C., Schauer, B., Bres, B., Ruiz-Pino, D., and Louanchi, F.: Variability of sources  
2427 and sinks of CO<sub>2</sub> in the western Indian and southern oceans during the year 1991, *J. Geophys. Res. Oceans*, 98,  
2428 22759–22778, <https://doi.org/10.1029/93JC02501>, 1993.  
2429  
2430 Pondaven, P., Fravallo, C., Ruiz-Pino, D., Tréguer, P., Quéguiner, B., and Jeandel, C.: Modelling the silica pump  
2431 in the Permanently Open Ocean Zone of the Southern Ocean, *J. Mar. Syst.*, 17, 1-4, 587–619,  
2432 [https://doi.org/10.1016/S0924-7963\(98\)00066-9](https://doi.org/10.1016/S0924-7963(98)00066-9), 1998.  
2433  
2434 Pondaven, P., Ruiz-Pino, D., Fravallo, C., Tréguer, P., and Jeandel, C.: Interannual variability of Si and N cycles  
2435 at the time-series station KERFIX between 1990 and 1995 – a 1-D modelling study, *Deep-Sea Res. Pt. I*, 47, 2,  
2436 223–257, [https://doi.org/10.1016/S0967-0637\(99\)00053-9](https://doi.org/10.1016/S0967-0637(99)00053-9), 2000.  
2437  
2438 Prend, C. J., Gray, A. R., Talley, L. D., Gille, S. T., Haumann, F. A., Johnson, K. S., et al.: Indo-Pacific sector  
2439 dominates Southern Ocean carbon outgassing. *Global Biogeochemical Cycles*, 36, e2021GB007226.  
2440 <https://doi.org/10.1029/2021GB007226>, 2022.  
2441  
2442 Racapé, V., Lo Monaco, C., Metzl, N., and Pierre, C.: Summer and winter distribution of  $\delta^{13}\text{C}_{\text{DIC}}$  in surface  
2443 waters of the South Indian Ocean (20°S-60°S). *Tellus-B*, DOI: 10.1111/j.1600-0889.2010.00504, 2010.  
2444  
2445 Reynolds, R. W., Rayner, N. A., Smith, T. M., Stokes, D. C., and Wang, W.: An improved in situ and satellite  
2446 SST analysis for climate. *J. Clim.* 15, 1609–1625. [https://doi.org/10.1175/1520-0442\(2002\)015<1609:AIISAS>2.0.CO;2](https://doi.org/10.1175/1520-0442(2002)015<1609:AIISAS>2.0.CO;2), 2002.  
2447  
2448 Rödenbeck, C., Keeling, R. F., Bakker, D. C. E., Metzl, N., Olsen, A., Sabine, C., and Heimann, M.: Global  
2449 surface-ocean pCO<sub>2</sub> and sea–air CO<sub>2</sub> flux variability from an observation-driven ocean mixed-layer scheme,  
2450 *Ocean Sci.*, 9, 193–216, <https://doi.org/10.5194/os-9-193-2013>, 2013.  
2451  
2452 Rödenbeck, C., DeVries, T., Hauck, J., Le Quéré, C., and Keeling, R. F.: Data-based estimates of  
2453 interannual sea–air CO<sub>2</sub> flux variations 1957–2020 and their relation to environmental drivers,  
2454 *Biogeosciences*, 19, 2627–2652, <https://doi.org/10.5194/bg-19-2627-2022>, 2022.  
2455  
2456

2457 Rodgers, K. B., Schwinger, J., Fassbender, A. J., Landschützer, P., Yamaguchi, R., Frenzel, H., et al.: Seasonal  
2458 variability of the surface ocean carbon cycle: A synthesis. *Global Biogeochemical Cycles*, 37, e2023GB007798.  
2459 <https://doi.org/10.1029/2023GB007798>, 2023  
2460  
2461 Rustogi, P., Landschützer, P., Brune, S. et al.: The impact of seasonality on the annual air-sea carbon flux and its  
2462 interannual variability. *Clim. Atmos. Sci.*, 6, 66, <https://doi.org/10.1038/s41612-023-00378-3>, 2023.  
2463  
2464 Sabine, C. L., Key, R. M., Johnson, K. M., Millero, F. J., Poisson, A., Sarmiento, J. L., Wallace, D. W. R., and  
2465 Winn, C. D.: Anthropogenic CO<sub>2</sub> inventory of the Indian Ocean, *Global Biogeochemical Cycles*, 13, 179-198,  
2466 <https://doi.org/10.1029/1998GB900022>, 1999.  
2467  
2468 Sabine, C. L., Feely, R. A., Gruber, N., Key, R. M., Lee, K., Bullister, J. L., Wanninkhof, R., Wong, C. S.,  
2469 Wallace, D. W. R., Tilbrook, B., Millero, F. J., Peng, T.-H., Kozyr, A., Ono, T., and Rios, A. F.: The Oceanic  
2470 Sink for Anthropogenic CO<sub>2</sub>, *Science*, 305, 367–371, <https://doi.org/10.1126/science.1097403>, 2004.  
2471  
2472 Sasse, T. P., McNeil, B. I., Matear, R. J., and Lenton, A.: Quantifying the influence of CO<sub>2</sub> seasonality on future  
2473 aragonite undersaturation onset, *Biogeosciences*, 12, 6017–6031, <https://doi.org/10.5194/bg-12-6017-2015>,  
2474 2015.  
2475  
2476 Schlitzer, R.: Ocean Data View, Ocean Data View, <http://odv.awi.de> (last access: 13 March 2019), 2018.  
2477  
2478 Schmidtko, S., Stramma, L., and Visbeck, M.: Decline in global oceanic oxygen content during the past five  
2479 decades, *Nature*, 542, 335–339, <https://doi.org/10.1038/nature21399>, 2017.  
2480  
2481 Seifert, M., Nissen, C., Rost, B., Vogt, M., Völker, C., and Hauck, J.: Interaction matters: Bottom-up driver  
2482 interdependencies alter the projected response of phytoplankton communities to climate change. *Global Change*  
2483 *Biology*, 00, 1– 25. <https://doi.org/10.1111/gcb.16799>, 2023.  
2484  
2485 Shadwick, E. H., Wynn-Edwards, C. A., Matear, R.J., Jansen, P., Schulz, E. and Sutton, A. J.: Observed  
2486 amplification of the seasonal CO<sub>2</sub> cycle at the Southern Ocean Time Series. *Front. Mar. Sci.* 10:1281854. doi:  
2487 10.3389/fmars.2023.1281854, 2023  
2488  
2489 Skjelvan, I., Lauvset, S. K., Johannessen, T., et al.: Decadal trends in Ocean Acidification from the Ocean  
2490 Weather Station M in the Norwegian Sea, *Journal of Marine Systems*,  
2491 <https://doi.org/10.1016/j.jmarsys.2022.103775>, 2022.  
2492  
2493 Smith, H. E. K., Poulton, A. J., Garley, R., Hopkins, J., Lubelczyk, L. C., Drapeau, D. T., Rauschenberg, S.,  
2494 Twining, B. S., Bates, N. R., and Balch, W. M.: The influence of environmental variability on the biogeography  
2495 of coccolithophores and diatoms in the Great Calcite Belt, *Biogeosciences*, 14, 4905–4925,  
2496 <https://doi.org/10.5194/bg-14-4905-2017>, 2017.  
2497  
2498 Strickland, J. D. H. and Parsons, T. R.: *A Practical Hand Book of Seawater Analysis*. Fisheries Research Board  
2499 of Canada Bulletin, 2nd Edition., 310 p. pp., 1972.  
2500  
2501 Sutton, A. J., Williams, N. L., and Tilbrook, B.: Constraining Southern Ocean CO<sub>2</sub> Flux Uncertainty Using  
2502 Uncrewed Surface Vehicle Observations, *Geophys. Res. Lett.*, 48, e2020GL091748,  
2503 <https://doi.org/10.1029/2020GL091748>, 2021.  
2504  
2505 Takahashi, T., Olafsson, J., Goddard, J. G., Chipman, D. W., and Sutherland, S. C.: Seasonal variation of CO<sub>2</sub>  
2506 and nutrients in the high-latitude surface oceans: A comparative study, *Global Biogeochem. Cycles*, 7(4), 843–  
2507 878, doi:10.1029/93GB02263, 1993.  
2508

2509 Takahashi, T., Sutherland, S. C., Wanninkhof, R., Sweeney, C., Feely, R. A., Chipman, D. W., Hales, B.,  
2510 Friederich, G., Chavez, F., Sabine, C., Watson, A., Bakker, D. C. E., Schuster, U., Metzl, N., Yoshikawa-Inoue,  
2511 H., Ishii, M., Midorikawa, T., Nojiri, Y., Körtzinger, A., Steinhoff, T., Hoppema, M., Olafsson, J., Arnarson, T.  
2512 S., Tilbrook, B., Johannessen, T., Olsen, A., Bellerby, R., Wong, C. S., Delille, B., Bates, N. R., and de Baar, H.  
2513 J. W.: Climatological mean and decadal change in surface ocean pCO<sub>2</sub>, and net sea–air CO<sub>2</sub> flux over the  
2514 global oceans, *Deep-Sea Res. Pt. II*, 56, 554–577, <https://doi.org/10.1016/j.dsr2.2008.12.009>, 2009a.  
2515

2516 Takahashi, T., Sutherland, S. C., Wanninkhof, R., Sweeney, C., Feely, R. A., Chipman, D. W., Hales, B.,  
2517 Friederich, G., Chavez, F., Sabine, C., Watson, A., Bakker, D. C. E., Schuster, U., Metzl, N., Yoshikawa-Inoue,  
2518 H., Ishii, M., Midorikawa, T., Nojiri, Y., Körtzinger, A., Steinhoff, T., Hoppema, M., Olafsson, J., Arnarson, T.  
2519 S., Tilbrook, B., Johannessen, T., Olsen, A., Bellerby, R., Wong, C. S., Delille, B., Bates, N. R., and de Baar, H.  
2520 J. W.: Corrigendum to “Climatological mean and decadal change in surface ocean pCO<sub>2</sub>, and net sea–air CO<sub>2</sub>  
2521 flux over the global oceans” [*Deep Sea Res. II* 56 (2009) 554–577], *Deep Sea Research Part I: Oceanographic  
2522 Research Papers*, 56, 11, 2075–2076, <https://doi.org/10.1016/j.dsr.2009.07.007>. 2009b.  
2523

2524 Takao, S., Hirawake, T., Wright, S. W., and Suzuki, K.: Variations of net primary productivity and  
2525 phytoplankton community composition in the Indian sector of the Southern Ocean as estimated from ocean color  
2526 remote sensing data, *Biogeosciences*, 9, 3875–3890, doi:10.5194/bg-9-3875-2012, 2012.  
2527

2528 Talley, L. D.: Closure of the global overturning circulation through the Indian, Pacific, and Southern Oceans:  
2529 Schematics and transports. *Oceanography*, 26(1), 80–97. <https://doi.org/10.5670/oceanog.2013.07>, 2013.  
2530

2531 Tanhua, T., Hoppema, M., Jones, E. M., Stöven, T., Hauck, J., Dávila, M. G., Santana-Casiano, M., Álvarez, M.,  
2532 and Strass, V. H.: Temporal changes in ventilation and the carbonate system in the Atlantic sector of the  
2533 Southern Ocean, *Deep Sea Res. Part II Top. Stud. Oceanogr.*, 138, 26–38,  
2534 <https://doi.org/10.1016/j.dsr2.2016.10.004>, 2017.  
2535

2536 Touratier, F., Azouzi, L. and Goyet, C.: CFC-11, Δ14C and 3H tracers as a means to assess anthropogenic CO<sub>2</sub>  
2537 concentrations in the ocean. *Tellus B*, 59(2), 318–325, doi:10.1111/j.1600-0889.2006.00247.x, 2007.  
2538

2539 Tréguer, P., and Le Corre, P.: Manuel d’analyse des sels nutritifs dans l’eau de mer (utilisation de  
2540 l’autoanalyseur II Technicon), 2nd ed., 110 pp., L.O.C.U.B.O., Brest, 1975.  
2541

2542 Uppström, L. R.: The boron/chlorinity ratio of deep-sea water from the Pacific Ocean, *Deep Sea Research and  
2543 Oceanographic Abstracts*, 21, 161–162, [https://doi.org/10.1016/0011-7471\(74\)90074-6](https://doi.org/10.1016/0011-7471(74)90074-6), 1974.  
2544

2545 van Heuven, S. M. A. C., Hoppema, M., Huhn, O., Slagter, H. A., and de Baar, H. J. W.: Direct observation of  
2546 increasing CO<sub>2</sub> in the Weddell Gyre along the Prime Meridian during 1973–2008, *Deep-Sea Res. Pt. II*, 58,  
2547 2613–2635, <https://doi.org/10.1016/j.dsr2.2011.08.007>, 2011.  
2548

2549 Vázquez-Rodríguez, M., Touratier, F., Lo Monaco, C., Waugh, D. W., Padin, X. A., Bellerby, R. G. J., Goyet,  
2550 C., Metzl, N., Ríos, A. F., and Pérez, F. F.: Anthropogenic carbon distributions in the Atlantic Ocean: data-based  
2551 estimates from the Arctic to the Antarctic, *Biogeosciences*, 6, 439–451, <https://doi.org/10.5194/bg-6-439-2009>,  
2552 2009.  
2553

2554 Wanninkhof, R., and Trinanes, J.: The impact of changing wind speeds on gas transfer and its effect on  
2555 global air–sea CO<sub>2</sub> fluxes, *Global Biogeochem. Cycles*, 31, doi:10.1002/2016GB005592, 2017.  
2556

2557 Wanninkhof, R., Barbero, L., Byrne, R., Cai, W.-J., Huang, W.-J., Zhang, J.-Z., Baringer, M., and Langdon, C.:  
2558 Ocean acidification along the Gulf Coast and East Coast of the USA, *Continental Shelf Research*, 98, 54–71,  
2559 <https://doi.org/10.1016/j.csr.2015.02.008>, 2015  
2560

2561 Weir, I., Fawcett, S., Smith, S., Walker, D., Bornman, T., and Fietz, S.: Winter biogenic silica and diatom  
2562 distributions in the Indian sector of the Southern Ocean, *Deep Sea Research Part I: Oceanographic Research*  
2563 *Papers*, Volume 166, 103421, <https://doi.org/10.1016/j.dsr.2020.103421>, 2020.  
2564  
2565 Weiss, R. F. and Price, B. A.: Nitrous oxide solubility in water and seawater. *Marine Chemistry*, 8(4), 347–359,  
2566 doi:10.1016/0304-4203(80)90024-9, 1980.  
2567  
2568 Wright, R. M., Le Quéré, C., Mayot, N., Olsen, A., and Bakker, D.: Fingerprint of climate change on Southern  
2569 Ocean carbon storage. *Global Biogeochemical Cycles*, 37, e2022GB007596. Doi: 10.1029/2022GB007596,  
2570 2023.  
2571  
2572 Xue, L., Cai, W. J., Takahashi, T. et al.: Climatic modulation of surface acidification rates through summertime  
2573 wind forcing in the Southern Ocean. *Nat. Commun.*, 9, 3240, Doi:10.1038/s41467-018-05443-7, 2018.  
2574  
2575 Yun, J., Jeong, S., Gruber, N., Gregor, L., Ho, C.-H., Piao, S., Ciais, P., Schimel, D., and Kwon, E. Y.: Enhance  
2576 seasonal amplitude of atmospheric CO<sub>2</sub> by the changing Southern Ocean carbon sink, *Science Advances*, 8, 41,  
2577 doi: 10.1126/sciadv.abq0220, 2022.  
2578